VIBRATIONAL SPECTRA OF THE AMMONIUM HALIDES AND THE ALKALI-METAL BOROHYDRIDES

by

NEIL ROBERT McQUAKER

B.Sc. (Hons.), University of British Columbia, 1965

M.Sc., University of British Columbia, 1966

A THESIS SUBMITTED IN PARTIAL FULFILLMENT OF

THE REQUIREMENTS FOR THE DEGREE OF

DOCTOR OF PHILOSOPHY

in the Department

of

CHEMISTRY

We accept this thesis as conforming to the required standard:

THE UNIVERSITY OF BRITISH COLUMBIA

October, 1970

In presenting this thesis in partial fulfilment of the requirements for an advanced degree at the University of British Columbia, I agree that the Library shall make it freely available for reference and study. I further agree that permission for extensive copying of this thesis for scholarly purposes may be granted by the Head of my Department or by his representatives. It is understood that copying or publication of this thesis for financial gain shall not be allowed without my written permission.

Department of CHEMISTRY

The University of British Columbia
Vancouver 8, Canada

Date 9 OCT 70

ABSTRACT

Using both infrared and Raman techniques the vibrational spectra of selected polymorphs of the ammonium halides; NH_4Cl, ND_4Cl, NH_4Br, ND_4Br, NH_4I and ND_4I, have been recorded in the spectral region 4000 - 50 cm^{-1}. The Raman spectra of NH_4F and ND_4F were also recorded. Although all the foregoing crystals have been the subject of previous spectroscopic investigations some important new features are observed. These include (i) Raman active longitudinal modes and (ii) previously unreported internal and external modes. In addition more meaningful assignments are made for some previously reported spectral lines. Included are assignments involving (i) the non-degenerate NH_4^+ stretching mode in combination with acoustical modes and (ii) the transverse and longitudinal components of the triply degenerate NH_4^+ bending mode in combination with the librational mode.

A study analagous to that involving the ammonium halides was made of the following alkali-metal borohydrides: $LiBH_4$, $LiBD_4$, $NaBH_4$, $NaBD_4$, KBH_4, KBD_4, $RbBH_4$ and $CsBH_4$. From the vibrational spectrum of potassium borohydride recorded at 10°K it is possible to infer that the ordered phase associated with this salt has a cubic structure compatible with the space group T_d^2. The vibrational spectrum of the ordered tetragonal phase of sodium borohydride allows the placing of the seven $BH_4^-(D_{2d})$ internal vibrational modes. In addition a mode of translatory origin is observed and a mode of rotatory origin is inferred from a line assigned as the second overtone of a librational mode. In the case of lithium borohydride seven of the nine $BH_4^-(C_s)$ modes are observed. Six modes of translatory origin

appear in the infrared and a mode of rotatory origin is inferred from a line assigned as the second overtone of a librational mode.

The structure of potassium borohydride at room temperature is discussed and evidence in support of a structure intermediate between the ordered cubic T_d^2 phase and the disordered cubic O_h^5 phase of sodium borohydride is given.

Finally, the F matrix associated with an undistorted $XY_4(T_d)$ (XY_4 = NH_4^+, BH_4^-) ion and the G matrix associated with the same ion which has undergone a slight angular distortion to give an $XY_4(D_{2d})$ ion is used to calculate the contribution of the kinetic energy to the spectrum of the $XY_4(D_{2d})$ ion. It is found that the order of appearance in the spectrum of the B_2 and E components associated with the two F_2 vibrations is correctly predicted.

TABLE OF CONTENTS

LIST OF FIGURES

FIGURES PAGE

LIST OF TABLES

CHAPTER I

INTRODUCTION

1-1 Historical Background

Ever since Ewald's (1) discovery in 1914 of an anomaly in the heat capacity of ammonium chloride the ammonium halides have continuously attracted the attention of physicists and chemists. As a result an enormous amount of information about these substances has accumulated and from this information has emerged the fact that the structures of NH_4Cl, NH_4Br and NH_4I (at one atmosphere and over the temperature interval 0°K-450°K) are distributed among four distinct crystalline phases. All three of these ammonium halides exist in the high temperature modification known as phase I.

Both x-ray and neutron diffraction data (2) indicate a face centered cubic phase I structure (Z=4) compatible with the space group $O_h^5(Fm3m)$. Under this space group a number of possible structural models are allowed. However, for each model the overall crystal symmetry must be achieved statistically by randomness involving the hydrogen atoms thus giving rise to a disordered structure. Levy and Peterson's neutron diffraction data (2) narrows the choice of models to three. One of the three models allows unaxial rotation of the NH_4^+ ion and the remaining two models, while they do not allow for either unaxial or free rotation, do allow for a NH_4^+ ion which is relatively free. Recent neutron inelastic scattering studies by Venkataraman and his co-workers (3) show no torsional peak in the scattering patterns for $NH_4I(I)$, instead a broad distribution is observed. This result is in agreement with an earlier infrared study (4) which shows a very broad

diffuse absorption arising from the combination of the torsional mode with the NH_4^+ bending mode. However, whereas Plumb and Hornig (4) interpreted their infrared result in favor of a model involving unaxial rotation the more recent work of Venkataraman and his co-workers (3) shows that form factor measurements tend to preclude the possibility of unaxial rotation - thus favoring a model in which the NH_4^+ ion is relatively free. On this basis the choice is between the two models which Levy and Peterson denote as the double approach model and the triple approach model. In the former two of the hydrogen-halide distances associated with each NH_4^+ ion are minimized and in the later three are minimized. The model maximizing the hydrogen-halide distances is excluded by the neutron diffraction data. Such a model would place 32/2 H atoms on the 3m positions under the space group $O_h^5(Fm3m)$ and, as will be indicated later, this is the structure of the phase I alkali metal borohydrides.

It is found that the second highest temperature modification of the ammonium halides is also a disordered cubic structure and that the three salts, NH_4Cl, NH_4Br and NH_4I, exist in this phase, known as phase II. The phase II structure was established by Levy and Peterson (4-6). Their neutron diffraction data gave a body centered cubic structure (Z=1), compatible with the space group $O_h^1(Pm3m)$ and having 8/2 H atoms occupying the 3m positions. Thus, the overall crystal symmetry required under the space group is achieved by a random distribution of the NH_4^+ tetrahedra between the two possible orientations in the unit cell. It is clear then, that the phase transition, II → I is of the disorder-disorder type and heat capacity data (7-9) show it to be of the first order.

The remaining two phases, III and IV are the low temperature poly-

morphs and both possess ordered structures which have been determined by X-ray (10) and neutron diffraction (2) methods. Of NH_4Cl, NH_4Br and NH_4I only NH_4Br is found to exist in both low temperature phases - the lowest temperature phase for NH_4Br being phase IV. For NH_4Cl the low temperature phase is IV and for NH_4I it is III. Phase IV has a body centered cubic structure (Z=1) under the space group $T_d^1(P\bar{4}3m)$. The 4 H atoms lie on the 3m positions. This compares with the 8/2 H atoms on the 3m positions under the space group $O_h^1(Fm3m)$ for the disordered phase II structure. These configurations for the hydrogen atoms allow for the second order phase change IV → II. The expected excess entropy of transition of R ln 2 = 1.36 e.u. for such an order-disorder phase change is indeed observed, within experimental error, for ammonium chloride (8).

The phase III structure which can be thought of as a distorted body centered arrangement has a tetragonal structure (Z=2) compatible with the space group $D_{4h}^7(P4/nmm)$. In this structure the nitrogen atoms occupy the $\bar{4}2m$ positions; (0,0,0) and (½,½,0) and the halide ions occupy the 4mm positions, (0,½,u) and (½,o,$\bar{u}$). The parameter, u, is a measure of the displacement of the halide ions from the corresponding cubic positions which would be (o,½,½) and (½,0,½). Also, in order to have a true cubic structure the condition, $a = c/\sqrt{2}$ would have to be satisfied. The 8 H atoms associated with the two nitrogen atoms in the unit cell will occupy the m(i) positions of the space group $D_{4h}^7(P4/nmm)$. This configuration for the hydrogen atoms allows for a III → II phase transformation which is of the second order. For ammonium bromide the reported excess entropy of transition (7) is in agreement with the expected value of R ln 2 for an order-disorder transformation. A corresponding experimental result is

not available for ammonium iodide.

The final phase change to be considered is the order-order transformation IV → III for ammonium bromide. Here the hydrogen atoms are also involved in the phase transformation, since in phase IV the NH_4^+ ions are arranged in parallel layers and in phase III they are in anti-parallel layers. Because there is no change in order for the transitions, the entropy change as expected is small (7,9) corresponding to a small increase in volume. It has been postulated (7) that the phase change is of the first order type.

Most of the above information is summarized in Table 1-1. Also included are recent values for lattice parameters (11-16), transition temperatures (17-19) and the percent volume changes (12-16, 19,20) experienced by the salts as they go through their respective phase transitions.

The final ammonium halide to be mentioned is ammonium fluoride. Not unexpectedly this salt is not isomorphous with any of the ammonium halides already discussed. Instead, the structure is hexagonal (Z=2) and is compatible with the space group $C_{6V}^4(P6_3mc)$ (21). Under this space group both the nitrogen atoms and fluoride ions will be on the 3m positions; (1/3, 2/3, z) and (2/3, 1/3, 1/2 + z). For the nitrogen atoms z = 0 and for the fluoride atoms z = u. If the parameter u which fixes the positions of the fluoride ions is 3/8 and if the axial ratio c/a is $(8/3)^{\frac{1}{2}}$ then the site symmetry for the NH_4^+ ions will be raised from C_{3v} to an effective symmetry of T_d and, indeed, the X-ray studies reported by Plumb and Hornig (21) do show these conditions for a tetrahedral arrangement of NH_4^+ ions to be satisfied. Only one modification

TABLE 1-1. The Phases of the Ammonium Halides

		NH_4Cl	ND_4Cl	NH_4Br	ND_4Br	NH_4I	ND_4I	REFERENCES
PHASE IV								
$T_d^1(P\bar{4}3m)$	a(A°)	$3.820^{88°}$		$4.009^{82°}$				11, 12,
IV → III	T(°K)			108.5°	166.7°			7,9
	ΔV(%)			+2.20%	+2.23%			12,12
	ΔS(e.u.)			0.3	0.3			7,9
PHASE III								
$D_{4h}^7(P4/nmm)$	a(A°)			$5.718^{157°}$		$6.105^{157°}$		12, 13
	c(A°)			4.060		4.338		
IV,III → II	T(°K)	242.2°	249.7°	234.57°	215.05°	231.0°	224°	8, 8, 7, 9, 7,19
	ΔV(%)	+0.48%	+0.39%	-0.43%	-0.73%	-0.28%	-0.21%	20,20,12,12,13,19
	ΔS(e.u.)	1.3±0.2	1.3±0.2	1.3±0.2	1.3±0.2			8, 8, 7, 9
PHASE II								
$O_h^1(Pm\bar{3}m)$	a(A°)	$3.8756^{299°}$		$4.0594^{299°}$		$4.333^{248°}$		11, 11, 13
II → I	T(°K)	456.3°	448°	410.4°	405°	257°	254°	17,18,17,18, 7,19
	ΔV(%)	+19.43%		+18.3%		+16.96%		14, 15, 16
PHASE I								
$O_h^5(Fm3m)$	a(A°)	$6.6004^{473°}$		$6.8725^{453°}$		$7.256^{282°}$		14, 15, 16

of ammonium fluoride is known to exist at one atmosphere (21).

In view of the foregoing outline of the polymorphism associated with the ammonium halides it is easy to understand why it was early recognized by spectroscopists that the ammonium halides would provide for a most interesting study, particularly if such a study involved temperature dependence so that the spectra of different phases could be compared. It was Wagner and Hornig (22,23) who were the first to undertake a comprehensive infrared study of ammonium chloride (22) and ammonium bromide (23). Their published work included spectral results for: NH_4Cl(II), ND_4Cl(II), NH_4Cl(IV), ND_4Cl(IV), NH_4Br(II), ND_4Br(II), NH_4Br(III), ND_4Br(III) and ND_4Br(IV). It was not until 1968 (24) that the infrared spectrum of NH_4Br(IV) was published. The infrared spectrum of NH_4I(III) was included in Bovey's paper (25) of 1950. Plumb and Hornig (21) in 1954 published spectra for NH_4F and ND_4F.

In the above works (21-25) it is found that the infrared spectral line showing the greatest sensitivity to the phase changes, III → II, IV → II and IV → III is the line arising from the ν_4 bending mode. In phase IV the NH_4^+ ion lies on a site of T_d symmetry and the expected singlet is observed for the triply degenerate vibration, $\nu_4(F_2)$. In phase III the degeneracy is partially lifted - here the NH_4^+ ion lies on a site of D_{2d} symmetry and as expected a doublet appears corresponding to $\nu_4(B_2)$ and $\nu_4(E)$. As we go to phase II, which has a cubic structure, ν_4 unexpectedly appears as a doublet. Wagner and Hornig (22) in their original work associated the anomalous component with the disorder in the lattice. It is now well known (26,27) that for disordered systems there can be densities of states with $\underline{K} \neq 0$ associated with the fundamental

vibrations predicted in the zero wave-vector limit and recently Garland and Schumaker (28) have shown that the anomalous phase II component of ν_4 must be attributed to a density of states with $\underline{K} \neq 0$. Disordered systems in the ammonium halides will be discussed at greater length in Chapter IV - the important point to note now is that the appearance of the ν_4 doublet at high temperatures serves to help identify phase II spectra.

Finally, the infrared spectrum of ammonium fluoride (21) shows a single sharp line for ν_4, thus supporting a tetrahedral configuration of NH_4^+ ions as indicated by the x-ray data (21).

Turning now to the Raman spectra of the ammonium halides we find that the most comprehensive studies were those carried out by Couture-Mathieu and Mathieu (29) in 1952. Earlier studies were made by Krishnan (30,31) in 1947 and 1948. Couture-Mathieu and Mathieu recorded spectra of NH_4Cl(II), NH_4Cl(IV), NH_4Br(II) and NH_4Br(III). The Raman spectrum of NH_4Br(IV) was reported by Schumaker (24) in 1968. The Raman studies are a very important complement to the infrared work because they place the infrared inactive NH_4^+ bending and stretching modes. In addition Raman spectra were the first to place crystal modes of translatory origin for the ammonium halides (29 - 31).

Consideration of the foregoing outline of previous infrared and Raman studies indicates an extensive set of spectroscopic data. However, it should be noted that the studies mentioned have not included the infrared spectrum of ND_4I(III), nor have they included Raman spectra for ND_4Cl(II), ND_4Cl(IV), ND_4Br(II), ND_4Br(III), ND_4Br(IV), NH_4I(III), ND_4I(III), NH_4F and ND_4F. Also, most of the work on the ammonium halides was carried out in the 1950's and since then there has been considerable sophistication

in instrumentation. Thus, with the recent availability of laser Raman spectrophotometers as well as grating spectrophotometers that can scan the infrared down to about 30 cm^{-1} considerable data can now be obtained which will complement that obtained by earlier workers. The study of the ammonium halides was carried out, then, with a view to placing those lattice modes of rotatory and translatory origin which had not been previously observed. It was hoped, too, that assignments for the internal fundamentals of the various salts could be made which would be more complete than those of previous workers.

Also, earlier workers (22,23,29) had observed lines in the low temperature phase spectra which were not obvious combinations or overtones of the fundamental modes. Since a clear one to one correspondence between the spectra of the protonated and deuterated samples was not established for these lines it was hoped that such a one to one correspondence could be established. This would then aid in making meaningful assignments. Finally, it was believed that it would be very worthwhile to compare a study of the ammonium halides with an analogous study of the alkali metal borohydrides - about which considerably less is known.

The high temperature modification of $NaBH_4$ and KBH_4, known as phase I (32), has a face centered cubic structure (Z=4) under the space group $O_h^5(Fm3m)$ (33-35). There are 32/2 H atoms lying on the 3m positions thus giving rise to a disordered structure. Heat capacity data (36,37) for both sodium and potassium borohydride indicate a disorder-order transformation at low temperature. For sodium borohydride this transformation results in a contraction along what becomes the c axis of a body centered tetragonal structure (38) and if a simple order-disorder transformation

involving the orientation of the borohydride ions is assumed the low temperature structure (z=2) must be compatible with the space group $D_{2d}^{9}(I\bar{4}m2)$. A tetragonal structure under the $D_{2d}^{9}(I\bar{4}m2)$ space group places 8 H atoms on the m(i) positions and allows for an order-disorder transformation analogous to that of the ammonium halides.

The heat capacity data (37) for potassium borohydride suggest that the disorder-order transformation takes place over a fairly large temperature interval finally undergoing completion at 77.2°K where there is a pronounced anomaly in the heat capacity curve. No X-ray diffraction data have been reported for potassium borohydride below 90°K. However, it is known that the structure does remain cubic down to 90°K (40) and the infrared results of this work recorded at 10°K are also compatible with a cubic structure and can hardly be interpreted on any other basis. For the infrared spectrum of KBD_4 the ν_4 half-height line width is only 3.5 cm^{-1} at 10°K and since the observed ν_4 splittings for sodium borohydride are about 20 cm^{-1} any distortion from true cubic symmetry would have to be very small indeed; especially when it is considered that the probable angular distortions from a tetrahedral configuration of BH_4^- ions in sodium borohydride are only +2.22° and -1.10° for the two different types of H-B-H angles (see section 1-2). Thus, it would appear that the disorder-order transformation for KBH_4 effectively differs from that of $NaBH_4$ in that there is no axial contraction. This gives a face centered cubic structure (Z=4) under the space group $T_d(F\bar{4}3m)$ and places 16 H atoms on the 3m positions. Since there are 32/2 H atoms on the 3m positions of phase I a second order phase transformation involving hydrogen atoms is allowed for. The heat capacity data (36) show that the anomaly

at 77.2°K accounts for 0.70 e.u. of the 1.36 e.u. expected for the excess entropy of transition. However, as previously indicated, the data suggest that the original onset of the transition is at a much higher temperature with the missing excess entropy of transition extending over a very broad temperature interval which lies above 77.2°K.

Schutte (32) has called the low temperature modification of $NaBH_4$ phase II and this designation is followed here. In addition, the low temperature phase of KBH_4 will be called phase III.

Thus far no mention has been made of $RbBH_4$ and $CsBH_4$. It has been found (38) that the high temperature modifications of these salts are also face centered cubic, so they very likely possess the phase I structure. Cooling and warming curves for rubidium and cesium borohydride respectively show breaks at 44 and 27°K (41) and it is likely that each of these temperatures represents the completion of a disorder-order phase transformation, which like that of potassium borohydride takes place over a wide temperature interval .

Most of the foregoing information relating to the alkali metal borohydrides is summarized in Table 1-2.

Finally, we come to the remaining alkali metal borohydride - $LiBH_4$, whose structure is not isomorphous with any of the phases common to the other alkali metal borohydrides. The structure for lithium borohydride given by the sole reference in the literature (42) is compatible with the space group D_{2h}^{16}(Pcmn). Since there are four molecules per unit cell the boron atoms must lie on m positions giving a BH_4^- ion of C_s site symmetry. The lithium ions must also lie on m positions if they are to be surrounded by the distorted tetrahedron of H atoms suggested in reference 42. There

TABLE 1-2. Phases of the Alkali Metal Borohydrides

		$NaBH_4$	KBH_4	$RbBH_4$	$CsBH_4$	REFS.
Phase III						
$T_d^2(F\bar{4}3m)$	a(A°)		$6.636^{90°}$			39
III → 1	T(°K)		77.2°	44	27	36,41
	ΔS(e.u.)		0.70			
Phase II						
$D_{2d}^9(I\bar{4}m2)$	a(A°)	$4.354^{78°}$				37
	c(A°)	5.907				
II → 1	T(°K)	189.9°				35
Phase I						
$O_h^5(Fm3m)$	a(A°)	$6.1635^{298°}$	$6.7272^{298°}$	7.029	7.419	37

will be 8 H atoms on two different m positions and the remaining 8 H atoms will lie on the general positions. Heat capacity data (43) indicates that lithium borohydride undergoes no transitions in the temperature interval 15-300°K.

Consideration of the foregoing structural information relating to the alkali metal borohydrides suggests some very worthwhile studies for vibrational spectroscopists. However, in actual fact, very few of these studies appear to have been pursued. No reported Raman studies have been made of any of the crystalline phases of the borohydrides and the only infrared studies that have been previously reported are the infrared studies of $NaBH_4$(I) and $NaBH_4$(II) by Schutte (32). The present work includes both infrared and Raman spectra of $LiBH_4$, $LiBD_4$, $NaBH_4$(I), $NaBH_4$(II), $NaBD_4$(I), $NaBD_4$(II), KBH_4(I), KBH_4(III), KBD_4(I) and KBD_4(III). Raman and infrared spectra of $RbBH_4$ and $CsBH_4$ were also recorded. The studies were carried out with the following objectives; (i) the placing of crystal modes of translatory and rotatory origin, (ii) assigning for both $NaBH_4$(II) and $NaBD_4$(II) the 7 internal fundamentals predicted by the BH_4^- D_{2d} site symmetry, (iii) assigning for both $LiBH_4$ and $LiBD_4$ the 9 non-degenerate fundamentals predicted by the BH_4^- C_s site symmetry, and deducing, if possible, the structure of the low temperature phase of potassium borohydride. The result of this final objective has already been given. This allows for a more ordered presentation of the detailed crystallographic information which follows. In keeping with the order of the discussion thus far the information relating to the ammonium halides is presented first.

1-2 Crystallographic Data

Table 1-3, 1-4 and 1-5 respectively, give detailed crystallographic data for phases II, III and IV of the ammonium halides. In all cases an N-H bond length of 1.03 A° determined by Levy and Peterson (2,5,6,44) was used to fix the hydrogen positions.

Particular attention should be paid to phase III. This structure is compatible with the space group D_{4h}^{7}(P4/nmm) and has the hydrogen atoms lying on the m(i) positions. Under the symmetry requirements of the space group the (X,0,Z) nitrogen atom associated with the (0,0,0) nitrogen atom may be placed anywhere in the XZ plane bounded by the unit cell edges. Once this (X,0,Z) hydrogen atom has been placed the symmetry elements of the space group will generate the remaining hydrogen atoms. Levy and Peterson (2) carried out a neutron diffraction study of an ammonium bromide powder in 1952. Their results were compatible with the hydrogen atoms lying on the face diagonals. However, their results do not meaningfully exclude the possibility that the hydrogen atoms are slightly removed from these X = Z positions. Since the H/2 atoms point toward the nearest bromide ions in phase II, the possibility that the phase III H atoms point directly toward the nearest bromide ions should also be considered.

The above two configurations for the NH_4^+ ions give two different situations for the angular distortion of the NH_4^+ ions. If the hydrogen atoms are on the face diagonals then the angular distortion from a tetrahedral configuration for the NH_4^+ ions will result in two H-N-H angles less than the tetrahedral angle (-0.23°) and four H-N-H angles greater

than the tetrahedral angle (+0.11°). If the hydrogen atoms are pointing directly toward the nearest bromide ions the reverse situation will hold; i.e. there will be two H-N-H angles greater than the tetrahedral angle (+3.09°) and four H-N-H angles less than the tetrahedral angle (-1.52°). It is this last situation for the angular distortion which the BH_4^- ions in $NaBH_4$(II) almost certainly experience. (This is discussed later on in this section).

Now, the spectral results of this work (see sections 4-2 and 5-2) show that the ν_3/ν_4 splitting patterns for NH_4Br(III) and $NaBH_4$(II) are of the same type; i.e. the following results are obtained:

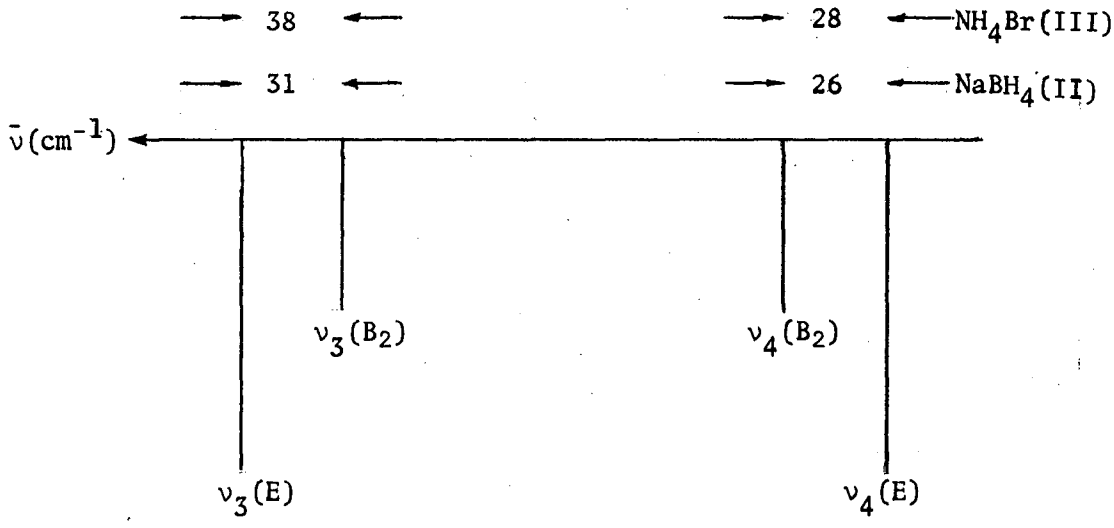

Therefore, it is very likely that the situation for the D_{2d} distortions are also of the same type and the implication is that in NH_4Br(III) the hydrogen atoms are probably pointed directly toward the nearest bromide ions. This means that the parameter, u, which fixes the positions of the halide ions will effectively determine the angular distortions for the NH_4^+ ions. Ketalaar (10) has determined these parameters for NH_4Br(III)

TABLE 1-3. Crystal Structure of Phase II Ammonium Halides

Space Group: O_h^1 (Pm3m)

Atomic Positions

1 X Atom at $(\frac{1}{2},\frac{1}{2},\frac{1}{2})$

1 N Atom at (0,0,0)

8/2 H Atoms at (X,X,X), $(X,\bar{X},\bar{X})$, $(\bar{X},X,\bar{X})$, $(\bar{X},\bar{X},X)$
$(\bar{X},\bar{X},\bar{X})$, $(\bar{X},X,X)$, $(X,\bar{X},X)$, $(X,X,\bar{X})$

(i) NH_4Cl a = 3.8756 A°

X = 0.153

(ii) NH_4Br a = 4.0594 A°

X = 0.146

(iii) NH_4I a = 4.333 A°

X = 0.137

Ammonium Ion Parameters - NH_4^+ (T_d)

$\angle$(H-N-H) = 109.47°, r(N-H) = 1.03 A°

TABLE 1-4. Crystal Structure of Phase III Ammonium Halides

Space Group: $D_{4h}^{7}(P4/nmm)$

Atomic Positions

2 X Atoms at $(0,\frac{1}{2},u)$, $(\frac{1}{2},0,\bar{u})$

2 N Atoms at $(0,0,0)$, $(\frac{1}{2},\frac{1}{2},0)$

8 H Atoms at $(0,x,z)$, $(X,0,\bar{Z})$, $(\frac{1}{2},\frac{1}{2}+X,\bar{Z})$, $(\frac{1}{2}+X,\frac{1}{2},\bar{Z})$
$(0,\bar{X},Z)$, $(\bar{X},0,Z)$, $(\frac{1}{2},\frac{1}{2}-X,\bar{Z})$, $(\frac{1}{2}-X,\frac{1}{2},Z)$

(i) NH_4Br $a = 5.718$ A° $c = 4.060$ A°

$u = 0.47$, $X = 0.150$, $Z = 0.141$

(ii) NH_4I $a = 6.105$ A° $c = 4.338$ A°

$u = 0.49$, $X = 0.138$, $Z = 0.137$

Ammonium Ion Parameters - $NH_4^+(D_{2d})$

(i) $4\angle(H\text{-}N\text{-}H) = 107.95°$, $2\angle(H\text{-}N\text{-}H) = 112.56°$,

$r(N\text{-}H) = 1.03$ A°

(ii) $4\angle(H\text{-}N\text{-}H) = 109.06°$, $2\angle(H\text{-}N\text{-}H) = 110.30°$,

$r(N\text{-}H) = 1.03$ A°

TABLE 1-5. Crystal Structures of Phase IV Ammonium Halides

Space Group: $T_d^1(P\bar{4}3m)$

Atomic Positions

1 X Atom at $(\frac{1}{2},\frac{1}{2},\frac{1}{2})$

1 N Atom at (0,0,0)

4 H Atoms at (X,X,X), $(X,\bar{X},\bar{X})$, $(\bar{X},X,\bar{X})$, $(\bar{X},\bar{X},X)$

(i)	NH_4Cl	a = 3.820 A°
		X = 0.156
(ii)	NH_4Br	a = 4.009
		X = 0.148

Ammonium Ion Parameters - $NH_4^+(T_d)$

$\angle$(H-N-H) = 109.47°, r(N-H) = 1.03 A°

FIGURE I—I

THE CRYSTAL STRUCTURE OF THE PHASE IV AND PHASE III AMMONIUM HALIDES PROJECTION ON (001) PLANE

PHASE IV

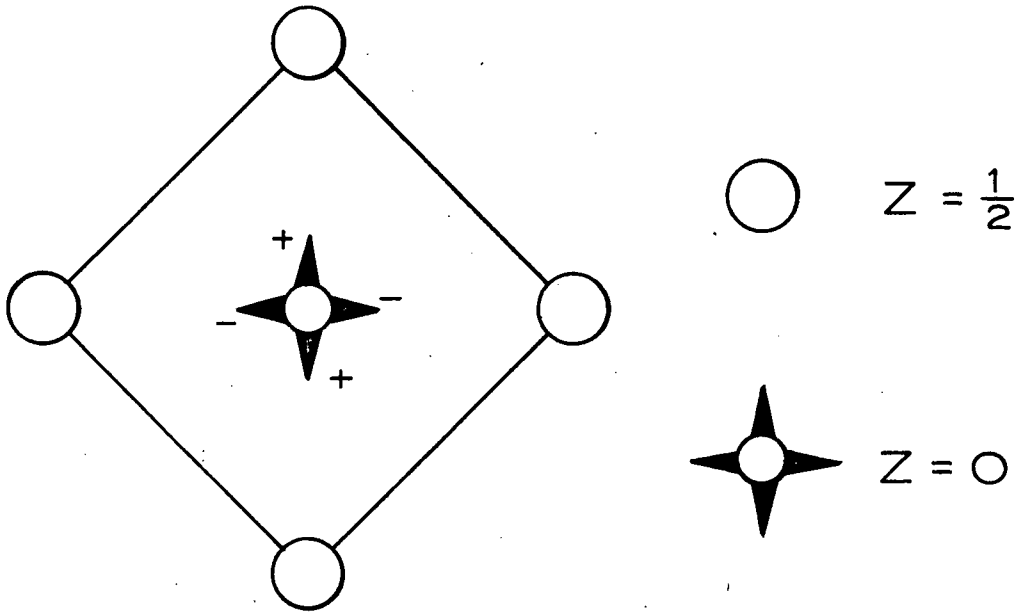

PHASE III

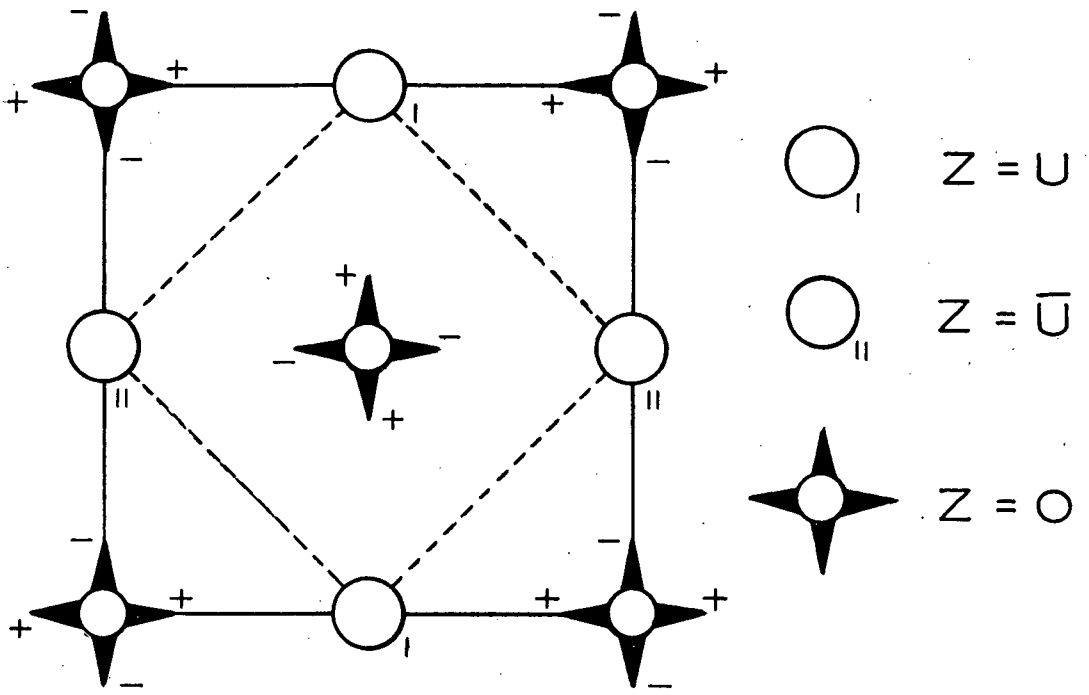

and NH_4I(III) to be 0.47 and 0.49 respectively. The value of 0.47 for ammonium bromide was subsequently confirmed by Levy and Peterson (2).

Figure 1-1 shows the ordered structures for both phases III and IV and thus complements the structural data given in Tables 1-4 and 1-5.

We turn now to the alkali-metal borohydrides. Tables 1-6, 1-7 and 1-8 respectively give detailed crystallographic data for phases I, II and III. In all cases a B-H bond distance of 1.26 A° determined by Peterson (34) was used to fix the hydrogen positions.

Special attention should be given to phase II which has a tetragonal structure under the space group $D_{2d}^{9}(I\bar{4}m2)$. The hydrogen atoms lie on the m(i) positions. In direct analogy to the case of the phase III ammonium halides, the symmetry requirements of the space group allow the (X,0,Z) hydrogen atom associated with the (0,0,0) boron atom to be placed anywhere in the XZ plane bounded by the unit cell edges. Again, once this (X,0,Z) hydrogen atom has been placed, the symmetry elements of the space group will generate the remaining hydrogen atoms. Neutron diffraction studies could aid in placing the hydrogen atoms; however, these studies have not been carried out. One possibility is that the hydrogen atoms are pointed toward the second nearest neighbour sodium ions. This possibility is seen to be reasonable when we consider the phase change which yields the low temperature tetragonal modification of sodium borohydride.

In the high temperature disordered cubic structure the H/2 atoms point toward the second nearest neighbour sodium ions. The ordering

process results in a contraction along what becomes the c axis of the tetragonal structure. This contraction could very conceivably result in a flattening of the BH_4^- tetrahedra with the H atoms still pointed toward the second nearest neighbour sodium ions. Such a situation gives the two angles lying in the XZ and XY mirror planes a positive distortion of +2.22°. The remaining four angles have a negative angular distortion of -1.10°.*

Figures 1-2 and 1-3 which respectively show the phase II and phase III structures complement the data contained in Tables 1-7 and 1-8.

---

* When the contraction along the C axis is considered for $NaBH_4$ any distortion of the BH_4^- ions will almost certainly result in two angles greater than 109.47° and four angles less than 109.47°. The situation cited here is probably the most likely.

TABLE 1-6. Crystal Structure of Phase I Alkali Metal Borohydrides

Space Group: $O_h^5(Fm3m)$

Atomic Positions

4 X Atoms at $(\frac{1}{2},\frac{1}{2},\frac{1}{2})$

4 B Atoms at (0,0,0)

32/2 H Atoms at (X,X,X), $(X,\bar{X},\bar{X})$, $(\bar{X},X,\bar{X})$, $(\bar{X},\bar{X},X)$
$(\bar{X},\bar{X},\bar{X})$, $(\bar{X},X,X)$, $(X,\bar{X},X)$, $(X,X,\bar{X})$

(i) $NaBH_4$ a = 6.1635 A°

X = 0.118

(ii) KBH_4 a = 6.7272 A°

X = 0.108

(iii) $RbBH_4$ a = 7.029 A°

X = 0.103

(iv) $CsBH_4$ a = 7.419 A°

X = 0.098

Borohydride Ion Parameters - $BH_4^-(T_d)$

$\angle$(H-B-H) = 109.47°, r(B-H) = 1.26 A°

TABLE 1-7. Crystal Structure of Phase II Alkali Metal Borohydrides

Space Group: $D_{2d}^{9}(I\bar{4}m2)$

Atomic Positions

2 Na Atoms at $(0,0,\frac{1}{2})$

2 B Atoms at (0,0,0)

8 H Atoms at (X,0,Z), (X,0,Z), (0,X,Z), (0,X,Z)

a = 4.353 A° c = 5.907 A°

X = 0.240, Z = 0.120

Borohydride Ion Parameters - $BH_4^-(D_{2d})$

$4\angle$(H-B-H) = 108.37°, $2\angle$(H-B-H) = 111.69°,

r(B-H) = 1.26 A°

FIGURE 1—2

THE CRYSTAL STRUCTURE OF $NaBH_4$ – PHASE II
PROJECTION ON (001) PLANE

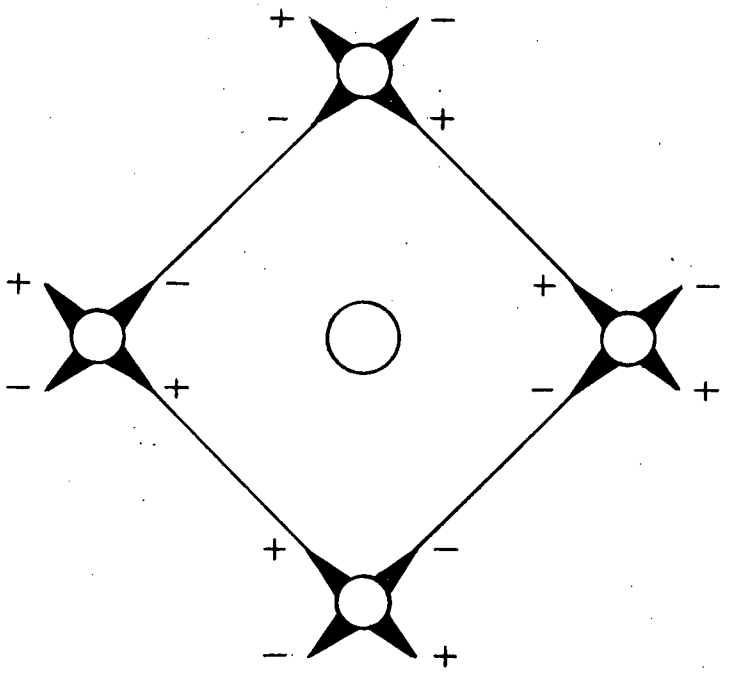

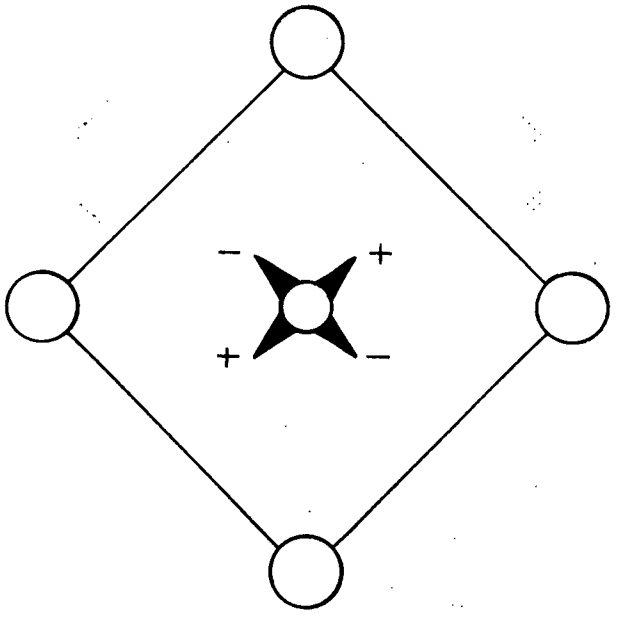

TABLE 1-8. Crystal Structure of Phase III Alkali Metal Borohydrides

Space Group: $T_d^2(F\bar{4}3m)$

Atomic Positions

4 K Atoms at $(\frac{1}{2},\frac{1}{2},\frac{1}{2})$

4 B Atoms at $(0,0,0)$

16 H Atoms at (X,X,X), $(X,\bar{X},\bar{X},)$, $(\bar{X},X,\bar{X})$, $(\bar{X},\bar{X},X)$

$a = 6.636$ A°

$X = 0.110$

Borohydride Ion Parameters - $BH_4^-(T_d)$

$\angle$(H-B-H) = 109.47°, r(N-H) = 1.26 A°

FIGURE 1—3

THE CRYSTAL STRUCTURE OF KBH_4 – PHASE III
PROJECTION ON (001) PLANE

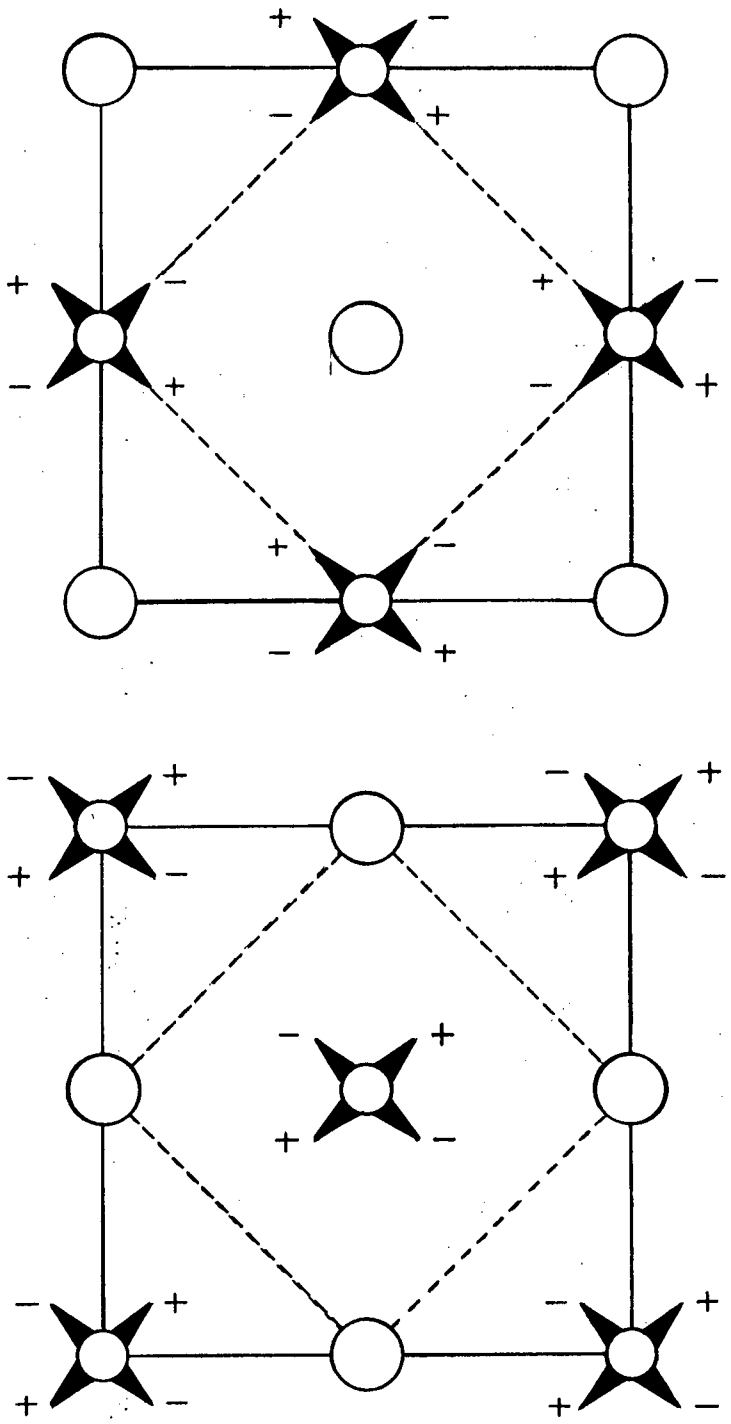

CHAPTER II

EXPERIMENTAL

2-1 Materials

All compounds used in this work, with the exception of ND_4I and ND_4F, were obtained commercially. The alkali-metal borohydrides, $LiBH_4$, $NaBH_4$ and KBH_4 were obtained from Metal Hydrides Inc. and the remaining two salts in this series, $RbBH_4$ and $CsBH_4$ were obtained from Gallard Schlesinger Ltd.. British Drug Houses Ltd. supplied the ammonium halides - this included the fluoride, chloride, bromide and iodide. The fully deuterated salts; $LiBD_4$, $NaBD_4$, KBD_4, ND_4Cl and ND_4Br were obtained from Merck, Sharpe and Dohme (Canada) Ltd.. All of the above salts were of reagent grade, with an assay of not less than 98%. The fully deuterated analogs of NH_4I and NH_4F were prepared by five successive recrystallizations of the appropriate protonated compound from D_2O. The isotopic purities of the resulting salts were estimated spectroscopically to be in the range 90 $\sim$ 95%.

2-2 Technique

The preparation of samples for the infrared studies involved three different techniques; the choice of technique depended on the compound under study and also on the region of the infrared to be scanned. The first technique consisted of mulling finely divided crystalline powder with nujol and then mechanically depositing a thin uniform layer of the resulting slurry on a suitable support. For our work the supports used with this technique were either cesium iodide or polyethylene.

The second technique allowed for mechanically depositing a thin uniform film of crystalline powder on either a sodium chloride or potassium bromide support. This was accomplished by first grinding one surface of the polished support with a very fine emery paper (Carbimet 600 Grit). A small mound of very finely divided crystalline powder was then placed on the surface of a ground glass plate. Carbon tetrachloride was then added to the surface of this ground glass plate in such a manner so as to completely surround and moisten the mound of crystalline powder without dispersing it. The ground side of the support was then placed directly on top of the mound of moistened crystalline powder and then rubbed, using small circular motions, against the surface of the ground glass plate. The support was slid off the ground glass plate before a sufficient amount of the carbon tetrachloride had evaporated to cause "sticking". After sliding the support off the ground glass plate and also allowing for sufficient "drying time" the excess crystal powder was carefully brushed off the ground surface of the support; a small, fine, hair brush was used for this purpose. Depending on the salt the above procedure was repeated up to three successive times in order to obtain a sufficiently thick film. It was found that films prepared in such a manner can give excellent crystal spectra.

The final technique involved the preparation of a polyethylene pellet. The first step, in the preparation of the pellet, was to intimately mix a small amount of very finely divided crystalline powder with a larger amount of polyethylene powder. (The optimum ratios of crystalline powder and polyethylene powder for the different salts

could only be found by trial and error). After the mixing process was complete an optimum portion of the mixture was placed on the surface of a 1½" x 1½" x ¼" glass plate and then spread evenly over the surface so as to give a thin, roughly circular, layer. The glass plate supporting the mixture and a second glass plate of equal dimensions were then placed on a hot plate heated to about 300°C. As soon as the polyethylene was observed to melt enough to flow slightly the second glass plate was placed directly on top of the glass plate supporting the sample. The two plates were then firmly pressed together by hand and then immediately transferred to a mechanical press which allowed a uniform pressure to be maintained until the sample had cooled. Pellets prepared in this manner were of uniform opaqueness and gave good crystal spectra. They were, however, useful for only room temperature work as the thinness of the pellets did not allow for good thermal contact in our low temperature cells.

It should be noted that for all three techniques, the handling of the crystalline compounds was carried out in a dry box containing a dry nitrogen atmosphere.

All spectra, with the exception of the polyethylene pellet spectra, were recorded with the samples mounted either in a liquid nitrogen, Hornig type, cell or a liquid helium cell. In each of these cells provision was made for the sample supports to be fitted tightly into a cold block which was in direct contact with the coolant. A copper-constantan thermocouple attached to the cold blocks allowed for monitoring the temperature of the cold blocks. When using the liquid nitrogen cell it was possible to bring the cell into the dry box and thus mount

the samples in a dry atmosphere. However, because of its size this was not possible with the liquid helium cell. In this case the sample was removed from the dry box in a sealed container. Once this container was opened the sample was fitted, under a stream of dry nitrogen, as quickly as possible and evacuation of the cell started.

The spectra of the ammonium halides recorded in the spectral region, 4000-500 cm^{-1} were recorded using the liquid nitrogen cell and samples prepared using the thin film technique. With the exception of the lithium salt all the spectra taken of the alkali-metal borohydrides in the spectral region 4000-500 cm^{-1} were also recorded using samples prepared as thin crystalline films. However, for these studies the liquid helium cell was used. The spectra taken of lithium borohydride were recorded using nujol mull samples mounted in the liquid nitrogen cell. Finally, for spectra recorded in the 600-50 cm^{-1} region polyethylene pellets were used at room temperature and for lower temperatures samples prepared by the nujol mull technique were mounted in either the liquid nitrogen or liquid helium cell.

Thus far, the discussion of sampling techniques has related to the infrared experiments. We turn now to the preparation of samples for Raman experiments. In order to prepare the sample all that was necessary was to tightly compress finely divided crystalline powder into a conical cavity at the end of a brass rod. Once the sample had been prepared in this way, the brass rod could then be fitted into a specially designed low temperature cell. (The cell used was a modification of the one described by G.L. Carlson (45) which was designed for coaxial viewing using the Cary 81 spectrophotometer fitted with a He-Ne laser). In the

cell which was used for this work the non sample end of the brass rod fitted precisely into a cylindrical cavity in the cold block and in so doing butted against a spring placed in this cavity. When the cell was fitted together this spring caused the sample end of the brass rod to butt tightly against one end of a pyrex light pipe. When the cell was correctly positioned the opposite end of the pyrex light pipe was in optical contact with the hemispherical lens of the spectrophotometer.

Again, the samples were prepared and the cell assembled in a dry box containing a dry nitrogen atmosphere.

2-3 Instrumentation

The infrared spectra were recorded on two complementary double beam grating spectrophotometers, the Perkin Elmer 421 and the Perkin Elmer 301. The 421 was used in the spectral region, 4000-500 cm^{-1} and the 301 in the region 600-50 cm^{-1}. The wave number scale of both these spectrophotometers was calibrated with the atmospheric water vapor spectrum and the uncertainty in the measured frequencies is $\pm$ 2 cm^{-1}. All spectra recorded on both instruments were recorded with the optical paths sealed from the atmosphere. This allowed for the use of an air dryer and also allowed for the purging of atmospheric CO_2 with dry nitrogen.

The Raman spectra were recorded with the Cary 81 Raman spectrophotometer equipped with the Spectra-Physics He-Ne laser. The instrument was calibrated with emission lines from a neon lamp over the spectral range 0 - 4000 cm^{-1} and the uncertainty in the measured frequencies is $\pm$ 2 cm^{-1}.

CHAPTER III

THEORY

3-1 The Vibrations of Molecules

The classical treatment of molecular vibrational motion, yielding solutions for the vibrational frequencies, is well known (46). However, since both computed vibrational frequencies and force constants form an important part of the discussion in both Chapters IV and V - it will be helpful to give an outline of the classical treatment leading to the formation of the vibrational secular equations. The solution of these equations will then be briefly discussed according to the method of Green and Harvey (47).

Classically, the molecular model that is used to describe vibrational motion is that of N elastically coupled point masses (or nuclei). Such a system of N nuclei has 3N degrees of freedom of which six (only the non-linear case is considered) account for the translations and rotations of the molecule as a whole. If the 3N mass weighted Cartesian displacement co-ordinates, {q}, are introduced, where,

$$q_i = (m_i)^{\frac{1}{2}} \cdot \Delta x_i, \quad (i = 1,3N) \tag{1}$$

then the kinetic energy T, of the molecule in matrix notation is given by:

$$2T = \dot{\underline{q}}^{t} \dot{\underline{q}} \tag{2}$$

The potential energy, V, can be expressed as a Taylor series expanded about the displacement co-ordinates {q} giving:

$$2V = 2V_o + 2\sum_i \left(\frac{\partial V}{\partial q_i}\right)_o q_i + \sum_{i,j} \left(\frac{\partial^2 V}{\partial q_i dq_j}\right)_o q_i q_j + \ldots\ldots \quad (3)$$

where the sums are over the 3N co-ordinates. Now, the equilibrium configuration is associated with a minimum in the potential energy surface and when it is defined to have zero energy the first two terms in the above expression vanish. Thus, neglecting higher order terms we have:

$$2V = \sum_{i,j} \left(\frac{\partial^2 V}{\partial q_i \partial q_j}\right)_o q_i q_j = \sum_{i,j} f_{ij} q_i q_j, \quad \text{or} \quad (4)$$

$$2V = \underline{q}^t \underline{\underline{F}}\, \underline{q} \quad (5)$$

The dependence of the potential energy only on second order terms implies harmonic motions of the atoms; if the displacements are large this approximation is not valid and higher order terms begin to become important.

The motions of the system are governed by Newton's equations of motion, which are, in the mass weighted Cartesian system and in Lagrangian form:

$$\frac{d}{dt}\frac{\partial L}{\partial \dot{q}_i} - \frac{\partial L}{\partial q_i} = 0, \quad (i = 1,3N) \quad (6)$$

where, L, the Lagrangian function is given by L = T-V. Since T is a function of the $\dot{q}_i$ and V of the q_i, substitution of equations 1 and 4 into equation 6 gives the set of 3N homogeneous differential equations:

$$\ddot{q} + \sum_j f_{ij} q_j = 0, \quad (i = 1,3N) \quad (7)$$

One possible solution is:

$$q_i = q_i^{\circ} \sin (t\lambda^{\frac{1}{2}} + \delta) \quad (8)$$

where q_i° is the amplitude of the motion, δ is a phase factor and λ is related to the vibrational frequency. Substitution of equation 8 into equation 7 gives rise to a set of 3N linear homogeneous equations which have a non-trivial solution only if the secular determinant equals zero; i.e.

$$\left| f_{ij} - \lambda \delta_{ij} \right| = 0 \qquad (9)$$

Six of the 3N values of λ satisfying equation 9 are always found to be zero; these correspond to the three molecular rotations and to the three translations. The remaining 3N-6 values of λ are related to the normal frequencies of vibration, $\bar{\nu}$, (in cm^{-1}) by $\lambda = 4\pi^2\bar{\nu}^2c^2$; substitution of these values of λ back into equation 8 shows how each of the co-ordinates q_i varies with time. The motion of the nuclei corresponding to each normal frequency is known as a normal mode of vibration. The normal frequencies and the normal modes of vibration are, of course, independent of the co-ordinate system used.

The analysis of the vibrational problem would be simplified if a co-ordinate system could be found for which all cross terms between co-ordinates in both the potential and kinetic energy expressions were zero; (the mass weighted Cartesians have this property for only the kinetic energy). It is found, though, that such a co-ordinate system can be defined and that a single displacement co-ordinate in this system describes the motion executed by all the atoms when the molecule undergoes a normal vibration. If the orthogonal transformation relating the 3N Cartesian displacement co-ordinates and the 3N normal co-ordinates,

{Q}, is written as:

$$\underline{q} = \underline{\underline{X}}\ \underline{Q} \tag{10}$$

where $\underline{\underline{X}}$ is the transformation matrix; then the expressions for the kinetic and potential energies may be written as:

$$2T = \underline{\dot{Q}}^{t}\ \underline{\dot{Q}}, \quad \text{and} \tag{11}$$

$$2V = \underline{Q}^{t}\ \underline{\underline{\Lambda}}\ \underline{Q} \tag{12}$$

respectively. The diagonal matrix $\underline{\underline{\Lambda}}$ is defined by:

$$\underline{\underline{\Lambda}} = \underline{\underline{X}}^{t}\ \underline{\underline{F}}\ \underline{\underline{X}} \tag{13}$$

Since it is usual to treat the kinetic energy in terms of internal co-ordinates a further transformation must be introduced. It is:

$$\underline{q} = \underline{\underline{T}}\ \underline{S} \tag{14}$$

Where $\underline{\underline{T}}$ is the matrix relating the 3N Cartesian co-ordinates, {q}, with the internal co-ordinates, {S}. (In the absence of redundancy there will be 3N-6 internal co-ordinates) Now, the matrix $\underline{\underline{T}}$ is not readily available from the molecular geometry and it is convenient to introduce the $\underline{\underline{G}}$ matrix elements of Wilson (36). From the molecular geometry the matrix $\underline{\underline{B}}$ for the inverse transformation

$$\underline{S} = \underline{\underline{B}}\ \underline{q} \tag{15}$$

can be calculated. Since {S}and {q} generally have different dimension, $\underline{\underline{B}}$ is not square and thus cannot be inverted to give $\underline{\underline{T}}$. However, $\underline{\underline{B}}\underline{\underline{B}}^{t}$ is square and if the matrix $\underline{\underline{G}}$ is defined as:

$$\underline{\underline{G}} = \underline{\underline{B}}\underline{\underline{B}}^{t} \tag{16}$$

then it can be shown (reference 46, appendix 7) that the kinetic energy is given by:

$$2T = \dot{\underline{S}}^t \underline{\underline{G}}^{-1} \dot{\underline{S}} \tag{17}$$

Also, in terms of internal co-ordinates the potential energy may be written:

$$2V = \underline{S}^t \underline{\underline{F}} \underline{S} \tag{18}$$

where $\underline{\underline{F}}$ is the force constant matrix for the internal co-ordinates. The normal co-ordinates are linearly related to the internal co-ordinates by the transformation:

$$\underline{S} = \underline{\underline{L}} \underline{Q} \tag{19}$$

Substituting equation 19 into 17 and 18 yields:

$$2T = \dot{\underline{Q}}^t \underline{\underline{L}}^t \underline{\underline{G}}^{-1} \underline{\underline{L}} \dot{\underline{Q}} = \dot{\underline{Q}}^t \underline{\underline{I}} \dot{\underline{Q}} \text{ , and} \tag{20}$$

$$2V = \underline{Q}^t \underline{\underline{L}}^t \underline{\underline{F}} \underline{\underline{L}} \underline{Q} = \underline{Q}^t \underline{\underline{\Lambda}} \underline{Q} \tag{21}$$

From the equations 20 and 21 we obtain the vibrational secular equations:

$$\underline{\underline{L}}^t \underline{\underline{F}} \underline{\underline{L}} = \underline{\underline{\Lambda}} \text{ , and} \tag{22}$$

$$\underline{\underline{L}}^{-1} \underline{\underline{G}} \underline{\underline{L}}^{-t} = \underline{\underline{I}} \tag{23}$$

By substituting equations 17 and 18 into equation 6 the vibrational secular equations can be cast into the form:

$$|\underline{\underline{G}}\ \underline{\underline{F}} - \lambda_i\ \underline{\underline{I}}| = 0 \tag{24}$$

However, $\underline{\underline{G}}\ \underline{\underline{F}}$ is not symmetrical and a symmetric matrix formulation of the vibrational secular equation is clearly desirable since the eigenvalues and eigenvectors of a symmetric matrix are more easily evaluated than those of a non-symmetric matrix.

Green and Harvey (47) have recently cast the vibrational secular equations into a symmetric matrix formulation. In their treatment they set

$$\underline{\underline{L}} = \underline{\underline{U}}\ \underline{\underline{\Gamma}}^{\frac{1}{2}}\ \underline{\underline{P}} \tag{25}$$

where the matrices $\underline{\underline{U}}$ and $\underline{\underline{P}}$ are orthogonal. Thus, we have the set of relations:

$$\underline{\underline{L}} = \underline{\underline{U}}\ \underline{\underline{\Gamma}}^{\frac{1}{2}}\ \underline{\underline{P}}$$

$$\underline{\underline{L}}^{-1} = \underline{\underline{P}}^{t}\ \underline{\underline{\Gamma}}^{-\frac{1}{2}}\ \underline{\underline{U}}^{t},$$

$$\underline{\underline{L}}^{-t} = \underline{\underline{U}}\ \underline{\underline{\Gamma}}^{-\frac{1}{2}}\ \underline{\underline{P}}, \text{ and}$$

$$\underline{\underline{L}}^{t} = \underline{\underline{P}}^{t}\ \underline{\underline{\Gamma}}^{\frac{1}{2}}\ \underline{\underline{U}}^{t}.$$

Substitution of equation 25 into 23 gives

$$\underline{\underline{P}}^{t}\ \underline{\underline{\Gamma}}^{-\frac{1}{2}}\ \underline{\underline{U}}^{t}\ \underline{\underline{G}}\ \underline{\underline{U}}\ \underline{\underline{\Gamma}}^{-\frac{1}{2}}\ \underline{\underline{P}} = \underline{\underline{I}} \tag{26}$$

The matrix $\underline{\underline{U}}$ is now defined as the orthogonal matrix diagonalizing the $\underline{\underline{G}}$ matrix, according to:

$$\underline{\underline{U}}^{t}\ \underline{\underline{G}}\ \underline{\underline{U}} = \underline{\underline{\Gamma}} \tag{27}$$

and $\underline{\underline{\Gamma}}$ becomes the diagonal matrix giving the eigenvalues of $\underline{\underline{G}}$. The orthogonal matrix $\underline{\underline{U}}$ is then composed of the eigenvectors of $\underline{\underline{G}}$. Thus, $\underline{\underline{L}} = \underline{\underline{U}}\ \Gamma^{\frac{1}{2}}\ \underline{\underline{P}}$, satisfies $\underline{\underline{L}}^{-1}\ \underline{\underline{G}}\ \underline{\underline{L}}^{-t} = \underline{\underline{I}}$ and also retains the appropriate freedom to satisfy $\underline{\underline{L}}^{t}\ \underline{\underline{F}}\ \underline{\underline{L}} = \underline{\underline{\Lambda}}$ i.e, we can write:

$$\underline{\underline{P}}^{t}\ \underline{\underline{\Gamma}}^{\frac{1}{2}}\ \underline{\underline{U}}^{t}\ \underline{\underline{F}}\ \underline{\underline{U}}\ \underline{\underline{\Gamma}}^{\frac{1}{2}}\ \underline{\underline{P}} = \underline{\underline{\Lambda}} \tag{28}$$

The matrix $\underline{\underline{\Gamma}}^{\frac{1}{2}}\ \underline{\underline{U}}^{t}\ \underline{\underline{F}}\ \underline{\underline{U}}\ \Gamma^{\frac{1}{2}}$ is symmetric and its eigenvalues are shown by Green and Harvey to be the same as those of $\underline{\underline{G}}\ \underline{\underline{F}}$; its eigenvectors are orthogonal and thus comprise the orthogonal matrix $\underline{\underline{P}}$.

Equation 28 can be rearranged to give an expression for the force constants which is

$$\underline{\underline{F}} = \underline{\underline{U}}\ \underline{\underline{\Gamma}}^{-\frac{1}{2}}\ \underline{\underline{P}}\ \underline{\underline{\Lambda}}\ \underline{\underline{P}}^{t}\ \underline{\underline{\Gamma}}^{-\frac{1}{2}}\ \underline{\underline{U}}^{t} \tag{29}$$

It is shown by Green and Harvey (47) that $\underline{\underline{P}}$ possesses the important property that the elements P_{ij} of $\underline{\underline{P}}$ equal zero unless the λ_i belong to the same symmetry class. This arises from the fact that the orthogonal matrix $\underline{\underline{U}}$ can be written as:

$$\underline{\underline{U}} = \underline{\underline{\$}}\ \underline{\underline{\mathbb{U}}} \tag{30}$$

where $\underline{\underline{\$}}$ is the usual orthogonal matrix relating internal and symmetry co-ordinates. $\underline{\underline{\mathbb{U}}}$ is an orthogonal matrix defined by equation 30. It should

be noted that the symmetry co-ordinates are just the linear combinations of the internal co-ordinates formed by projecting one member of each symmetrically equivalent set of internal co-ordinates into the point group of the molecule. This allows for maximum symmetry factorization since no interaction terms in the $\underline{\underline{F}}$ or $\underline{\underline{G}}$ matrices will occur between two co-ordinates of different symmetry. The force constants calculated using symmetry co-ordinates are known as symmetry force constants.

3-2 Symmetry and Selection Rules

By the use of group theory it is possible to show how the 3N normal modes of vibration (including translations and rotations) are distributed among the symmetry types associated with the molecular point group appropriate to the molecule being considered (46). The result is summarized by the equation:

$$n^{\gamma} = \frac{1}{N} \sum_j h_j \chi_j(R) \chi_j^{\gamma}(R) \qquad (1)$$

where n^{γ} is the number of times the irreducible representation Γ_j is contained in the reducible representation Γ_j^{γ} ; $\chi_j(R)$ and $\chi_j^{\gamma}(R)$ are the characters under the operation R of Γ_j and Γ_j^{γ} respectively; N is the order of the group and h_j is the number of group operations falling under the j^{th} class. All terms in equation 1 with the exception of $\chi^{\gamma}{}_j(R)$ may be obtained from the appropriate point group. The expression for $\chi_j^{\gamma}(R)$ is:

$$\chi_j^{\gamma}(R) = \omega_R(\pm 1 + \cos \phi_R) \qquad (2)$$

where ω_R is the number of atoms invariant under the operation R and ϕ_R is the angle of rotation associated with the operation R. The +ve signs are taken for proper rotations and the -ve signs for improper rotations.

Group theory may also be used to derive the transition moment selection rules for both infrared and Raman experiments. For a fundamental transition to occur by absorption of infrared radiation the integral, $< \psi_i | \underset{\sim}{\mu} | \psi_j >$, must have a non-zero value. In the integral ψ_i is the totally symmetric vibrationless ground state, ψ_j is the excited state and $\underset{\sim}{\mu}$ is the dipole moment operator. Now, the Cartesian components of $\underset{\sim}{\mu}$ will transform like the Cartesian displacement co-ordinates; T_x, T_y and T_z. Therefore, ψ_j must transform like either T_x, T_y or T_z in order that the integrand for the above integral have a totally symmetric component and so be non-zero.

For a transition to be Raman active one of the elements of the three by three symmetric tensor, $[< \psi_i | \underset{\approx}{\alpha} | \psi_j >]$ must have a non-zero value. Again ψ_i is the totally symmetric ground state and ψ_j is the excited state; $\underset{\approx}{\alpha}$ represents the polarizability tensor. If the transition is to appear in the Raman effect, ψ_j must transform like at least one of the nine elements of the polarizability tensor. Methods for determining the transformation properties of the polarizability tensor under the various point groups are discussed by Herzberg (48).

3-3 Crystal Symmetry and Solid State Spectra

It is found that all of the symmetry operations of a crystal form

what is known as the finite space group for the crystal. The space group consists of two subgroups: the translation operations form one subgroup and the remaining operations form the second subgroup called the factor group. The factor group or unit cell group is isomorphous with one of the 32 point groups possible for crystals. It is convenient also to mention the site group - this group is the group of all symmetry operations acting through any point, or site, in the crystal. When the site coincides with a molecular position in the crystal, the site is then a subgroup of the molecular point group as well as the factor group.

We have already seen that the vibrational analysis for free molecules analyzes the molecular motion under the appropriate molecular point group. In crystals the motion of the unit cell is analysed under the appropriate factor group. If there are N atoms in the primitive unit cell then there will be 3N crystal or lattice vibrations. Three of these, known as acoustical modes, correspond to pure translations and in the zero wavevector limit will have zero frequency. The remaining 3N-3 vibrations are known as optical modes. The three acoustical and 3N-3 optical modes may be further classified as either internal or external modes. The external modes always include the three acoustical modes and arise from translatory or rotatory motions of the molecules in the unit cell. The internal vibrations are those which arise from motions of the atoms associated with the individual molecules in the unit cell.

By considering the group of N non-equivalent points corresponding to the N non-equivalent atoms contained in the primitive unit cell and

applying the principles of group theory it is possible to obtain an expression for n^{γ}; the number of times a particular irreducible representation Γ_j is contained in the reducible representation, Γ_j^{γ}. The desired expression corresponds to equation 1 of section 3-2.

Again, $\chi_j(R)$ and $\chi_j(R)$ are the characters under the operation R of Γ_j and Γ_j^{γ} respectively; N is the order of the group and h_j is the number of the group operations falling under the j^{th} class. All terms except $\chi_j^{\gamma}(R)$ can be obtained from the appropriate factor group. Analytical expressions for the $\chi_j^{\gamma}(R)$ have been devised by Bhagavantam and Venkatarayudu (49).

By a suitable choice of the reducible representation Γ_j^{γ} and by utilizing the characters, $\chi_j^{\gamma}(R)$, appropriate to it, it is possible to determine how the internal, external translatory, external rotatory and acoustical modes are distributed among the various symmetry species of the factor group. It is to be emphasized that the factor group analysis considers only a single unit cell and the assumption is made that all equivalent atoms in adjacent unit cells move in phase. In the following sections it will be seen that this assumption may fail in certain cases.

3-4 Phonons and Lattice Vibrations

The energy in a lattice vibration or elastic wave is quantized - giving rise to quanta of energy known as phonons. This is analogous to the case of electromagnetic waves, where the quanta are known as photons. It is found that phonons of wavevector, $\underline{K}_{phonon}$ $\{|\underline{K}| = 2\pi/\lambda\}$, and photons of wavevector, $\underline{K}_{photon}$ $\{|\underline{K}| = 2\pi/\lambda\}$, interact

as if they possessed momenta $h\underline{K}_{phonon}$ and $h\underline{K}_{photon}$. The momentum conservation law for crystals, which acts as a selection rule for optical and acoustical transitions, may therefore be expressed in terms of wavevectors and for this reason the wavevector is of significant physical importance.

A photon-phonon interaction may result in either the creation or absorption of a phonon, with the photon being scattered in the process; as a result both the photon wavevector and frequency will change. For the creation of a phonon the conservation of wavevector requires that:

$$\underline{K}_i = \underline{K}_s + \underline{K} \tag{1}$$

where $\underline{K}_i$, $\underline{K}_s$ and $\underline{K}$ are the wavevectors of the incident light, scattered light and phonon respectively. Similarly by conservation of energy

$$\omega_i = \omega_s + \omega_o \tag{2}$$

where ω_i, ω_s and ω_o respectively are the angular frequencies of the incident light, scattered light and phonon. Equation 2 may be rewritten as:

$$c|\underline{K}_i| = c|\underline{K}_s| + v|\underline{K}| \tag{3}$$

where, v, the velocity of the phonon (soundwave) is much less than, c, the velocity of the photon (light wave). If $\underline{K}$ (phonon) and $\underline{K}_i$ (photon) are of comparable magnitude ω_i (photon) will be much greater than ω_o (phonon). Thus, the percentage difference between ω_i and ω_s is small and it follows that $|\underline{K}_i|$ and $|\underline{K}_s|$ are not very different. In a vector momentum diagram with $|\underline{K}_i| = |\underline{K}_s|$, $|\underline{K}|$, will form the base of an isoceles triangle and we can write:

$$K \cong 2\, K_i \sin\tfrac{1}{2}\phi \qquad (4)$$

where ϕ is the scattering angle. For Raman experiments using right angle viewing ($\phi = 90°$) the phonon wavevector will be $2\, K_i$; so if the incident Raman exciting light has a wavelength of about 6000 Å the phonon wavevector will be of order 1.5×10^5 cm^{-1}.

In the case of infrared absorption experiments wavevector and energy conservation lead to:

$$\omega_i = \omega_o \qquad (5)$$

$$\underline{K}_i = \underline{K} \qquad (6)$$

where ω_i and $\underline{K}_i$ are angular frequency and wavevector respectively for the incident light and ω_o and $\underline{K}$ are the angular frequency and wavevector of the phonon. For absorption at about 1000 cm^{-1} the phonon wavevector will be of order 6×10^3 cm^{-1}.

Since it is possible for the phonon wavevector to take on any value lying in the Brillouin zone - the maximum value being of order π/a where a is the lattice constant - it is evident that the phonon wavevectors associated with both Raman scattering and infrared absorption experiments are small compared to the maximum order of about 10^8 cm^{-1}. The relative smallness of the phonon wavevectors has important consequences since this implies that the phonons will have wavelenghts very long compared to the lattice constant. In the case of <u>infrared inactive phonons</u> the frequencies are determined mainly by short range forces in the lattice;

phonons with wavelength long compared to the lattice constant are not significantly influenced by the dispersive effects of these forces and have essentially the same frequency as infinite wavelength phonons. The Raman shifts thus measure the phonon frequencies at $\underline{K} = 0$.

The infrared active phonons produce an electric dipole moment in the lattice and the accompanying long range (macroscopic) electric fields may extend over many lattice cells. Thus the motion of the dipoles may be influenced by these long range electric forces; i.e. the motion of the vibrating dipoles through the presence of the macroscopic electric field may couple with the motion of the electromagnetic radiation in the lattice. The result is that for each infrared active phonon there will be a frequency difference between different directions of phonon propagation relative to the electric field, $\underline{E}$. For non cubic crystals where the polarization, $\underline{P}$, is no longer parallel to $\underline{E}$, the magnitude of the frequency difference between transverse ($\underline{P} \perp \underline{K}$) and longitudinal ($\underline{P} \parallel \underline{K}$) phonons will depend on the orientation of the crystal with respect to the electric field.

In order to see how the above results are arrived at the motion of both the electromagnetic radiation and the vibrating dipoles will be considered in a classical context.

Maxwell's equations can be used to describe the propagation of the electromagnetic waves in homogeneous media. Four vector quantities are involved. These are, $\underline{E}$, the electric field, $\underline{H}$, the magnetic field, $\underline{D}$, the electric displacement and, $\underline{B}$, the magnetic induction. They are related by the two equations:

$$\underline{D} = \underline{\underline{\varepsilon}}\,\underline{E} \tag{7}$$

$$\underline{B} = \underline{\underline{\mu}}\,\underline{H} \tag{8}$$

where $\underline{\underline{\varepsilon}}$ and $\underline{\underline{\mu}}$ are real symmetric tensors of second order. Since magnetic effects can usually be ignored, most crystals will behave as if $\underline{\underline{\mu}}$ was a unit tensor and so $\underline{B} = \underline{H}$. For a particular crystal the elements of $\underline{\underline{\varepsilon}}$ are determined by measuring its dielectric properties. The polarization, $\underline{P}$, which represents the dipole moment per unit volume is related to $\underline{E}$ and $\underline{D}$ by the equation

$$\underline{D} = \underline{E} + 4\pi\underline{P} \tag{9}$$

According to the theory of Maxwell the above vector quantities are related by the following four fundamental equations:

$$\underline{\nabla} \cdot \underline{H} = 0 \tag{10}$$

$$\underline{\nabla} \cdot \underline{D} = 0 \tag{11}$$

$$\underline{\nabla} \times \underline{H} = \frac{1}{c}\dot{\underline{D}} \tag{12}$$

$$\underline{\nabla} \times \underline{E} = -\frac{1}{c}\dot{\underline{H}} \tag{13}$$

If the electromagnetic waves as they propagate in the lattice are assumed to have plane form with spatial and time dependence exp i $(\underline{K}\cdot\underline{r} - \omega t)$ then Maxwell's equations impose the requirement (50) that

$$\underline{E} = \frac{-4\pi\underline{K}\,(\underline{K}\cdot\underline{P}) - \omega^2/c^2\,\underline{P}}{K^2 - \omega^2/c^2} \tag{14}$$

If $K >> \omega/c$ for the phonons which is the case in Raman experiments then equation 14 becomes

$$\underline{E} = -4\pi\left(\frac{\underline{K}}{K}\right)\left(\frac{\underline{K}\cdot\underline{P}}{K}\right) \tag{15}$$

The above result for $\underline{E}$ is identical to that obtained when Maxwell's equations are replaced by the equations of electrostatics:

$$\underline{\nabla}\cdot\underline{D} = \underline{\nabla}\times\underline{E} = 0 \tag{16}$$

Thus, equation 15 is the solution of:

$$\underline{K}\cdot\underline{D} = 0 \tag{17}$$

$$\underline{K}\times\underline{E} = 0 \tag{18}$$

Born and Huang (51) have shown that in the harmonic and adiabatic approximation the potential energy density for a crystal may be expressed as follows:

$$\phi = \tfrac{1}{2}\underline{U}^t\underline{\underline{L}}\,\underline{U} - \underline{U}^t\,\underline{\underline{Q}}\,\underline{E} - \tfrac{1}{2}\underline{E}^t\underline{\underline{\chi}}\,\underline{E} \tag{19}$$

Here $\underline{U}$ is a 3n dimensional vector whose components represent the displacements of the n different types of atoms, identified by k = 1,2,....n. The displacements are represented by a super position of travelling waves so that in a wave of wavevector $\underline{K}$ and frequency ω the displacement of the

atoms at a point $\underline{r}$ will be $\underline{U}$ exp i ($\underline{K} \cdot \underline{r} - \omega t$) and the field will be $\underline{E}$ exp i ($\underline{K} \cdot \underline{r} - \omega t$). The 3n x 3n matrix $\underline{\underline{L}}$ has elements $L_{\alpha\beta}(k, k')$ which depend on the force constants between atoms of type k and k' (α,β, and γ are Cartesian co-ordinates). $\underline{\underline{Q}}$ is a 3n x 3 matrix and has elements $Q_{\alpha\beta}(k)$ which depend on the charges residing in atoms of type k. Finally the elements, $\chi_{\alpha\beta}$, of the matrix $\underline{\underline{\chi}}$ are the components of what is known as the electronic susceptibility tensor.

According to equation 19 the potential energy density, ϕ, arises from (i) the displacement of the 3n atoms from their equilibrium positions, (ii) the relative displacement of the atoms due to the presence of a macroscopic electric field and (iii) the displacement of the electrons in the atoms relative to the nuclei.

The equations of motion for atoms moving in such a potential are:

$$\underline{\underline{\rho}}\, \ddot{\underline{U}} = - \underline{\underline{L}}\, \underline{U} + \underline{\underline{Q}}\, \underline{E} \qquad (20)$$

where $\underline{\underline{\rho}}$ is the diagonal 3n x 3n mass density matrix for which the elements $m_{\alpha\alpha}(k\ k) = m_k$ for all α. When the periodic solutions for $\underline{E}$ and $\underline{U}$ are substituted into equation 20 it yields:

$$\omega^2\, \underline{\underline{\rho}}\, \underline{U} = \underline{\underline{L}}\, \underline{U} - \underline{\underline{Q}}\, \underline{E} \qquad (21)$$

We see that in equation 21 two terms contribute to the restoring forces. These are the local elastic restoring forces and the long range electric forces.

The polarization, $\underline{P} = - \partial\phi/\partial\underline{E}$, (Reference 51 - Appendix 5) is given by:

$$\underline{P} = \underline{\underline{Q}}^{t}\underline{U} + \underline{\underline{\chi}}\,\underline{E} \tag{22}$$

If the matrix $\underline{\underline{\rho}}$ is eliminated by defining:

$$W_{\alpha}(k) = (\rho_k)^{\frac{1}{2}} U_{\alpha}(k) \tag{23}$$

$$N_{\alpha\beta}(k\ k') = L_{\alpha\beta}(k\ k')/(\rho_k \rho_{k'})^{\frac{1}{2}} \tag{24}$$

$$Z_{\alpha\beta}(k) = Q_{\alpha\beta}(k)/(\rho_k)^{\frac{1}{2}} \tag{25}$$

then equations 21 and 22 become:

$$\omega^2 \underline{W} = \underline{\underline{N}}\,\underline{W} - \underline{\underline{Z}}\,\underline{E} \tag{26}$$

$$\underline{P} = \underline{\underline{Z}}^{t}\underline{W} + \underline{\underline{\chi}}\,\underline{E} \tag{27}$$

and we recall that for $K > > \omega/c$ the macroscopic electric field is given by equation 15; i.e.

$$\underline{E} = -4\Pi\left(\frac{\underline{K}}{K}\right)\left(\frac{\underline{K}\cdot\underline{P}}{K}\right)$$

Equations 26 and 27 completely define the motion of the vibrating dipoles in the presence of a macroscopic field and so are applicable whenever conditions are uniform over regions containing many lattice cells. The expression for the macroscopic field, $\underline{E}$, has been obtained by considering the motion of electromagnetic radiation in homogeneous media. Since the solutions of equation 26 are dependent on $\underline{E}$, these solutions will relate

the motion of the dipoles to the motion of the electromagnetic radiation.

Using the above three equations we will consider two cases after Cochran and Cowley (52).

Case I; $\underline{E} = 0$

In this case the macroscopic electric field is suppressed and the 3n eigen frequencies, Ω_j (j = 1,2,...3n), will be given by the secular equations:

$$|\underline{\underline{N}} - \Omega_j^2 \underline{\underline{I}}| = 0 \tag{28}$$

Three of these frequencies will correspond to acoustical modes for which $\Omega_j = 0$, say j = 1,2,3. If the rows and columns of the singular matrix $\underline{\underline{N}}$ which involve the k^{th} atom are deleted, then the resulting minor, $\bar{\underline{\underline{N}}}$, is non singular and of order 3n-3. Its determinant is independent of the choice of k and

$$\text{Det } \bar{\underline{\underline{N}}} = \prod_{j=4}^{3n} \Omega_j^2 \tag{29}$$

An effective inverse $\underline{\underline{N}}^{-1}$ may be formed by taking the inverse of $\bar{\underline{\underline{N}}}$ and adding zeros in those rows and columns which are eliminated from $\underline{\underline{N}}$ to give $\bar{\underline{\underline{N}}}$. The matrix $\underline{\underline{N}}^{-1}$ is of importance in the next case.

Case II, $\underline{E} \neq 0$

When the crystal is in equilibrium in a static field $\partial\phi/\partial\underline{U} = 0$ and thus $\underline{\underline{N}}\underline{W} = \underline{\underline{Z}}\underline{E}$. Using this result to eliminate $\underline{W}$ from equation 27 gives a relation between $\underline{P}$ and $\underline{E}$ which, with the help of equations 7 and 9, leads to the following expression for the static dielectric constant.

$$\varepsilon^{(o)}_{\alpha\beta} = \delta_{\alpha\beta} + 4\pi(\underline{\underline{Z}}^t \underline{\underline{N}}^{-1} \underline{\underline{Z}} + \underline{\underline{\chi}})_{\alpha\beta} \tag{30}$$

The optical dielectric constant is then:

$$\varepsilon^{(\infty)}_{\alpha\beta} = \delta_{\alpha\beta} + 4\pi(\underline{\underline{\chi}})_{\alpha\beta} \tag{31}$$

The elements of $\underline{\underline{\varepsilon}}^{(o)}$ and $\underline{\underline{\varepsilon}}^{(\infty)}$ may be determined experimentally. Those of $\underline{\underline{\varepsilon}}^{(\infty)}$ are determined at a relatively high frequency such that the inertia of the atoms eliminates the contribution due to their relative displacement.

In considering the eigenvalue problem it is convenient to choose axes so that $\underline{K}$ is parallel to a direction $\underline{\alpha}$, which may be taken as being completely arbitrary. Thus, from equations 15 and 17; $E_\alpha = -4\pi P$ with $E_\beta = E_\gamma = 0$ and $P_\beta = P_\gamma = 0$. This result can be used to eliminate $\underline{E}$ from equation 26. The secular equations for long wavelength vibrations with $\underline{K}$ in the $\underline{\alpha}$ direction then become:

$$\left|\underline{\underline{N}} + \frac{4\pi}{\varepsilon^{(\infty)}_{\alpha\alpha}} \underline{\underline{Z}}\, \underline{\underline{X}}\, \underline{\underline{Z}}^t - \omega_j(\alpha)\underline{\underline{I}}\right| = 0 \tag{32}$$

where $\underline{\underline{X}} = \begin{bmatrix} 1 & 0 & 0 \\ 0 & 0 & 0 \\ 0 & 0 & 0 \end{bmatrix}$

Cochran and Cowley (52) show that for the 3n-3 optical modes:

$$\prod_{j=4}^{3n} \omega_j(\alpha) = \text{Det}\ \bar{N} \left[1 + \frac{4\pi}{\varepsilon^{(\infty)}_{\alpha\alpha}} (\underline{\underline{Z}}^t \underline{\underline{N}}^{-1} \underline{\underline{Z}})_{\alpha\alpha}\right] \tag{33}$$

The important result from cases I and II is that equations 29,30,31 and 33 lead to:

$$\prod_{j=4}^{3n} \left(\frac{\omega_j(\alpha)}{\Omega_j} \right)^2 = \frac{\varepsilon_{\alpha\alpha}^{(o)}}{\varepsilon_{\alpha\alpha}^{(\infty)}} \tag{34}$$

Equation 34 can be simplified if some of the frequencies $\omega_j(\alpha)$ are the same as the frequencies Ω_j. This can be so only if the polarization in the $\underline{\alpha}$ direction vanishes and the macroscopic field, $\underline{E}$, vanishes. (When all the Maxwell equations are considered (51) the macroscopic field will be suppressed but $\underline{E}$ cannot vanish identically). It can be shown (52) that the polarization of each of the modes whose frequencies are the Ω_j is along one of the crystallographic axes for crystals of orthorhombic or higher symmetry. Therefore from equation 17 we can say that for modes satisfying $\omega_j(\alpha) = \Omega_j$, where $\underline{\alpha}$ specifies the direction of a crystallographic axes we will have $\underline{K} \perp (\underline{P} \parallel \underline{\alpha})$. Such modes are known as transverse modes.

The other solutions are the longitudinal modes of case II for which $\underline{K}$ is parallel to $\underline{\alpha}$. Here $\underline{\alpha}$ instead of specifying a general crystal direction will now be taken to be the $\underline{\alpha}$ associated with the transverse modes. In this case $\underline{K} \parallel (\underline{P} \parallel \underline{\alpha})$. Remembering that there will be n-1 modes associated with each crystallographic axis we can rewrite equation 32 as:

$$\prod_{n-1} \left(\frac{\omega_L(\alpha)}{\omega_T(\alpha)} \right)^2 = \frac{\varepsilon_{\alpha\alpha}^{(o)}}{\varepsilon_{\alpha\alpha}^{(\infty)}} \tag{35}$$

where the ω_L and the ω_T are respectively the frequencies of modes of longitudinal and transverse polarization. For a particular dipole the frequency of the transverse mode will lie lower than the longitudinal frequency since in a transverse mode $\underline{E}$ vanishes and the vibrational frequency is determined solely by the local elastic restoring forces (see equation 26). For a longitudinal mode there is an electric field, $\underline{E}$, which through the $\underline{\underline{Q}}$ matrix contributes an additional restoring force. If a mode has no polarization associated with it (i.e. if it is infrared inactive) then ω_L and ω_T will be equal for that particular mode.

Equation 35 is a generalized form of the LST relation which was first derived for diatomic cubic crystals by Lyddane, Sachs and Teller (53).

It should be emphasised that equation 35 holds for long waves. Thus, $\underline{K}$ is small. However, in order for these longitudinal and transverse waves to propagate in the lattice they must be of wavelength smaller than the dimension, d, of the crystal (i.e. it is necessary to have $K^{-1} << d$). The difference, then, between a mode for which $\underline{K} = 0$ and a mode for which $\underline{K} \to 0$ lies not in the value of $\underline{K}$ but in the absence of a macroscopic field in the first case and its possible presence in the second.

Born and Huang show that the ω_T will be the infrared absorption frequencies. It may be noted also that the infrared active phonons must be those for which $\underline{K} = 0$ since the polarization associated with the modes will vanish otherwise (51). Alternately, conservation of wavevector (equation 6) tells us that the phonon wavevector will be small compared to the dimensions of the Bullouin zone and therefore an infrared absorption

measures the phonon frequency at $\underline{K} = 0$.

From the foregoing discussion we see that the first order Raman and infrared spectra give information about the phonon dispersions only where $\underline{K}$ is effectively zero. More complete phonon spectra may be obtained from neutron inelastic scattering experiments. Recently Brockhouse and his co-workers (54) have used neutron inelastic scattering techniques to obtain the phonon dispersions for the translatory external modes of a crystal of interest in this work - ND_4Cl(IV). Below is a sketch of their spectra of the longitudinal optical (LO), transverse optical (TO), longitudinal acoustical (LA) and transverse acoustical (TA) phonons; $\underline{K}$ is in the $(\frac{1}{2},0,0)$ direction. (The dispersions will, of course, be different when $\underline{K}$ is in other (symmetry) directions such as $(\frac{1}{2},\frac{1}{2},0)$ or $(\frac{1}{2},\frac{1}{2},\frac{1}{2})$).

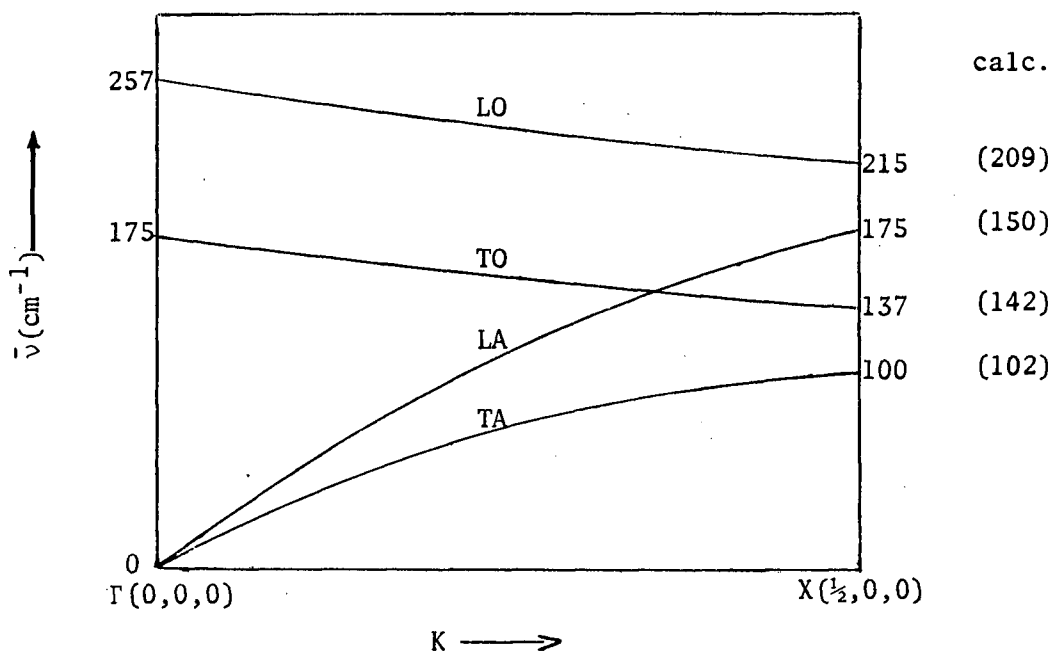

ND_4Cl(IV) phonon dispersions - ref. 54

The symbols $\Gamma(0,0,0)$ and $X(\frac{1}{2},0,0)$ appearing in the foregoing diagram represent symmetry points in the reciprocal lattice. They occur at the zone edges and their number is determined by lattice symmetry.

The simplest model which we may use to predict optical and acoustical phonon dispersions is the linear diatomic chain - only nearest neighbour interactions are considered. Such a model may be related to a simple cubic lattice (55) where atoms of mass M_1 lie on the odd numbered planes and atoms of mass M_2 lie on the even numbered planes. The spacing between the planes is a and the lattice constant is 2a. If f is the force constant connecting nearest neighbour planes (e.g. planes 2s and 2s + 1) then the equations of motion become:

$$M_1 \frac{d^2X_{2s+1}}{dt^2} = f\{(X_{2s+2} - X_{2s+1}) - (X_{2s+1} - X_{2s})\}$$

$$M_2 \frac{d^2X_{2s}}{dt^2} = f\{(X_{2s+1} - X_{2s}) - (X_{2s} - X_{2s-1})\} \qquad (36)$$

Convenient trial solutions in the form of travelling waves are:

$$X_{2s+1} = A \exp i\{(2s+1)Ka - \omega t\}$$

$$X_{2s} = B \exp i\{2s\ Ka - \omega t\} \qquad (37)$$

New equations of motion are obtained by substituting equations 37 into equations 36. They are found to be:

$$-\omega^2 M_1 A = (2f\cos Ka)B - 2fA$$

$$-\omega^2 M_2 B = (2f\cos Ka)A - 2fB \qquad (38)$$

There will be a non trivial solution only if the determinant of the coefficients of the two unknown amplitudes, A and B, vanishes. This requirement leads to the dispersion relations:

$$\omega^2(\text{optical}) = f\left[\frac{1}{M_1} + \frac{1}{M_2}\right] + f\left[\left(\frac{1}{M_1} + \frac{1}{M_2}\right)^2 - \frac{4\sin^2 Ka}{M_1 M_2}\right]^{\frac{1}{2}}$$

$$\omega^2(\text{acoustical}) = f\left[\frac{1}{M_1} + \frac{1}{M_2}\right] - f\left[\left(\frac{1}{M_1} + \frac{1}{M_2}\right)^2 - \frac{4\sin^2 Ka}{M_1 M_2}\right]^{\frac{1}{2}} \qquad (39)$$

The force constant f may be related to either transverse or longitudinal polarizations. It will, in general, be different in each case. Substituting equations 39 into equations 38 gives (at $\underline{K} = 0$) $A/B = 1$ for the acoustical branch and $A/B = -M_2/M_1$ for the optical branch. These relations show that in the $\underline{K} = 0$ limit adjacent atoms move together for acoustical modes and that for the optical modes they vibrate against each other with their center of mass fixed.

At $\underline{K} = 0$ the roots of the dispersion relations 39 are; $\omega^2(\text{optical}) = 2f(1/M_1 + 1/M_2)$ and $\omega^2(\text{acoustical}) = 0$. At the zone edge $\underline{K}_{max} = \pm\Pi/2a$. Here the roots of equation 39 ($M_1 > M_2$) are $\omega^2(\text{optical}) = 2f(1/M_2)$ and $\omega^2(\text{acoustical}) = 2f(1/M_1)$. In the case of ND_4Cl(IV) we can use this simple model to estimate the zone edge LO, TO, LA and TA frequencies (We associate the mass of the ammonium ion with M_2 and the mass of the chloride ion with M_1). The results are shown on the diagram on page 53. Considering the simplicity of the model the agreement is remarkable.

A knowledge of phonon dispersions throughout the Brillouin zone (and particularly at the symmetry points where the densities of states

possess critical points) is helpful in interpreting the second order Raman and infrared spectra. This is because the phonon wavevectors may range throughout the entire Brillouin zone. The only requirement imposed by conservation of wavevector is that the wavevectors of the two phonons should effectively be equal and opposite. That this is so is seen by considering the conservation relations

$$\underline{K}_i = \underline{K}_s + \underline{K}_1 + \underline{K}_2 \qquad \text{(Raman)}$$

$$\underline{K}_i = \underline{K}_1 + \underline{K}_2 \qquad \text{(infrared)} \tag{40}$$

In these relations the symbols have their usual meaning and the subscripts 1 and 2 refer to the phonons giving rise to either a combination or overtone mode. In the case of both infrared and Raman experiments the photon wavevectors are negligible compared to the Brillouin zone dimensions and hence wavevector conservation requires that the phonon wavevectors are effectively equal and opposite. The frequency distribution for two phonon processes is thus proportional to a weighted density of lattice states in which two phonons of equal and opposite wavevectors are present. It is found that there are particular values for the $\underline{K}$ vector (e.g. at the symmetry points) where there will be discontinuities in the frequency distribution. Therefore it is important to know the selection rules at particular $\underline{K}$ vectors for the pairs of phonon branches which can contribute to the second order spectrum.

The selection rules are simplest to calculate for processes due to

phonons with zero wavevector. In this case the requisite group theory and its application are well known (49). Selection rules for two phonon processes due to phonons with non zero wavevector are in principle calculated the same way as for phonons with $\underline{K} = 0$. However, even though the mechanics of the calculations are basically the same as for $\underline{K} = 0$ phonons, the actual manipulations are more complex due to the higher dimensionality of the representations involved. Because of the complexity involved, detailed selection rules have been worked out for only a very few simple crystals. These include the rock salt, zinc blend and diamond structures (56,57).

It is interesting to note that acoustical phonons may take part in two phonon processes. This, of course, is not the case for first order spectra where the selection rules forbid their appearance.

CHAPTER IV

VIBRATIONS OF THE AMMONIUM HALIDES

4-1 The Phase IV Ammonium Halides

The phase IV ammonium halides possess an ordered cubic structure under the space group $T_d^1(P\bar{4}3m)$. The factor group analysis is carried out under the T_d factor group and the irreducible representations for the internal, optical translatory (OT), optical librational (OL) and acoustical-translatory (AT) vibrational modes are:

$$\Gamma(\text{internal}) = A_1 + E + 2F_2$$

$$\Gamma(\text{OT}) = F_2$$

$$\Gamma(\text{OL}) = F_1$$

$$\Gamma(\text{AT}) = F_2$$

In the infrared only the triply degenerate modes of F_2 symmetry may appear, whereas in the Raman effect modes of A_1 and E as well as F_2 symmetries may be active. We recall from section 3-4 that for dipole allowed vibrational modes - in the present case modes of F_2 symmetry type - there will be both transverse and longitudinal components. Since the phase IV ammonium halides are not centrosymmetric the transverse modes may be both infrared and Raman active. The longitudinal modes can appear only in the Raman effect. Turning now to the NH_4Cl(IV) results obtained by earlier workers (3,22,29,30) we find that the fundamental modes $\nu_1(A_1)$, $\nu_2(E)$, $\nu_3(F_2)$ transverse, $\nu_4(F_2)$ transverse, $T_1(F_2)$ transverse and $L_1(F_1)$ have all been observed and assigned. The translatory mode, $T_1(F_2)$, has been observed in the Raman spectrum (29,30) and the libratory mode, $L_1(F_1)$, which is both infrared

and Raman inactive has been observed using neutron inelastic scattering techniques (3). From the results of this work assignments have been made for ν_3 (longitudinal) and ν_4 (longitudinal). Reference to the Raman spectrum of NH_4Cl(IV) (see Figure 4-2) shows a distinct doublet associated with $\nu_4(F_2)$. The low and high wave number components appear at 1401 and 1421 cm^{-1} respectively. The low wave number component compares with the infrared absorption at 1400 cm^{-1} and can be assigned as ν_4(transverse). The high wave number component can reasonably be assigned as ν_4(longitudinal) since; (i) there are no obvious combinations or overtones to which it may be assigned and (ii) it satisfies the requirement that the longitudinal component will be at higher frequency than the transverse component. There are two Raman scatterings which appear at higher wave number than the ν_3 (transverse) scattering at 3127 cm^{-1}. They are found at 3141 and 3164 cm^{-1}. Since the 3141 cm^{-1} scattering can be satisfactorily assigned as a combination mode (this assignment is discussed later) we assign the 3164 cm^{-1} scattering as ν_3(longitudinal). Unfortunately the longitudinal component of $T_1(F_2)$ is not observed. However, recent infrared reflection measurements by Lowdnes and Perry (58) have placed T_1(longitudinal) at 275 cm^{-1} and T_1(transverse) at 188 cm^{-1}. The later frequency compares with the Raman value of 183 cm^{-1}.

The first order Raman spectra of the remaining phase IV ammonium halides; i.e. NH_4Br(IV), ND_4Cl(IV) and ND_4Br(IV) very closely parallel the spectrum observed for NH_4Cl(IV). For NH_4Br(IV) Schumaker (24) does not report a line corresponding to ν_3(longitudinal); he does however report a line which may be assigned as ν_4(longitudinal) (see Table 4-2). The Raman

spectra of the two deuterated salts (see Figure 4-4) clearly show the appearance of the transverse and longitudinal components for both ν_3 and ν_4; i.e. in each case there is only one higher wave number scattering in the near vicinity of the transverse components. Infrared reflection measurements (58) have placed T_1(longitudinal) for NH_4Br(IV) and neutron inelastic scattering results (54) have placed this mode in the case of ND_4Cl(IV).

The results for the transverse and longitudinal splittings are summarized below (dielectric constant data (58) are also included).

	NH_4Cl(IV)	ND_4Cl(IV)	NH_4Br(IV)	ND_4Br(IV)
ν_3(L)	3164	2371	(3140)	2370
ν_3(T)	3127	2333.5	3126	2332
ν_4(L)	1421	1069.5	1418	1065
ν_4(T)	1401	1063.5	1402	1061
T_1(L)	275	257	215	(197)
T_1(T)	188	175	160	147
$\varepsilon(o)$	6.0		5.4	
$\varepsilon(\infty)$	2.7		2.9	

The bracketted frequencies have been computed using the product rule:

$$\prod_{n-1}\left(\frac{\omega_L}{\omega_T}\right)^2 = \frac{\varepsilon(o)}{\varepsilon(\infty)}$$

Since there is a complete set of splittings for the ammonium chlorides the ratios $\varepsilon(o)/\varepsilon(\infty)$ can be calculated using the product rule. The results are:

	NH_4Cl(IV)	ND_4Cl(IV)
$\varepsilon^{(o)}/\varepsilon^{(\infty)}$ (calc.)	2.25	2.25
$\varepsilon^{(o)}/\varepsilon^{(\infty)}$ (expt.)	2.22	2.22

The agreement is seen to be excellent. Since the internal fundamentals are at much higher frequencies than the components of $T_1(F_2)$ their small splittings have little effect on the calculated $\varepsilon^{(o)}/\varepsilon^{(\infty)}$ ratios. This is seen from calculations below where only the splitting of the translatory mode has been considered. We note, however, that the agreement between calculated and experimental ratios does improve when the frequencies of the internal modes are included.

	NH_4Cl(IV)	ND_4Cl(IV)	NH_4Br(IV)	ND_4Br(IV)
$\varepsilon^{(o)}/\varepsilon^{(\infty)}$ (calc.) (external modes only)	2.14	2.16	1.81	1.80
$\varepsilon^{(o)}/\varepsilon^{(\infty)}$ (expt.)	2.22	2.22	1.86	1.86

In addition to the product rule there are sum rules which may be derived from the eigenvalue problem of section 3-4. When the polarization is along a crystallographic axis ($\underline{\alpha}$) of a crystal of orthorhombic symmetry or higher the eigenvalue matrix for the longitudinal modes may be written as:

$$\begin{aligned}
\underline{\underline{\omega}}_L^2 &= \underline{\underline{W}}^t\left(\underline{\underline{N}} + \frac{4\Pi}{\varepsilon_{\alpha\alpha}^{(\infty)}}\,\underline{\underline{Z}}\;\underline{\underline{X}}\;\underline{\underline{Z}}^t\right)\underline{\underline{W}} \\
&= \underline{\underline{W}}^t\underline{\underline{N}}\underline{\underline{W}} + \frac{4\Pi}{\varepsilon_{\alpha\alpha}^{(\infty)}}\,\underline{\underline{W}}^t\,\underline{\underline{Z}}\;\underline{\underline{X}}\;\underline{\underline{Z}}^t\underline{\underline{W}} \\
&= \underline{\underline{\omega}}_T^2 + \frac{4\Pi}{\varepsilon_{\alpha\alpha}^{(\infty)}}\;\underline{\underline{W}}^t\;\underline{\underline{Z}}\;\underline{\underline{X}}\;\underline{\underline{Z}}^t\;\underline{\underline{W}}
\end{aligned} \qquad (1)$$

which leads to

$$\underline{\underline{\omega}}_L^2 - \underline{\underline{\omega}}_T^2 = \frac{4\Pi}{\varepsilon_{\alpha\alpha}^{(\infty)}} \underline{\underline{W}}^t \underline{\underline{Z}} \underline{\underline{X}} \underline{\underline{Z}}^t \underline{\underline{W}} \tag{2}$$

We note that there may be no more than n-1 non-vanishing elements associated with the diagonal 3n x 3n matrix $\{\underline{\underline{\omega}}_L^2 - \underline{\underline{\omega}}_T^2\}$. This is because we have taken the polarization to be along a crystallographic axis. If we take the trace of the matrices on both sides of equation 2 we have:

$$\text{Trace } \{\underline{\underline{\omega}}_L^2 - \underline{\underline{\omega}}_T^2\} = \frac{4\Pi}{\varepsilon_{\alpha\alpha}^{(\infty)}} \text{ Trace } \{\underline{\underline{W}}^t \underline{\underline{Z}} \underline{\underline{X}} \underline{\underline{Z}}^t \underline{\underline{W}}\} \tag{3}$$

which gives the sum rule:

$$\frac{\varepsilon_{\alpha\alpha}^{(\infty)}}{4\Pi} = \sum_{n-1} \frac{P_\alpha^2}{\omega_L^2 - \omega_T^2} \tag{4}$$

where P_α is the polarization experienced by a transverse mode of frequency ω_T. (If ω_L and ω_T coincide the polarization vanishes). Since P_α^2 is proportional to the (infrared) intensity of the transverse mode, the sum rule tells us that the sum of the ratios, intensity/$(\omega_L^2 - \omega_T^2)$ is an isotopic invariant. We may note that Haas and Hornig (59) have incorrectly used the equivalent of equation 4 with n-1 = 1 to compute absolute intensities for a number of crystals having n > 2. In the case of the ammonium halides it would be necessary to experimentally obtain a complete set of relative intensities before the sum rule could be used to compute absolute intensities.

Remembering that $\underline{\underline{W}}^t \underline{\underline{W}} = \underline{\underline{I}}$ and that $Z_{\alpha\beta}(k) = Q_{\alpha\beta}(k)/(\rho_k)^{\frac{1}{2}}$ we can write a second sum rule:

$$N \frac{4\Pi}{\varepsilon_{\alpha\alpha}^{(\infty)}} \sum_{k=1}^{n} \frac{q_{\alpha\alpha}^2(k)}{m_k} = \sum_{n-1} \omega_L^2 - \omega_T^2 \qquad (5)$$

The $q_{\alpha\alpha}(k)$ are related to the charges on atoms of mass m_k and N is the number of unit cells in a unit volume. (When the polarization is along a crystallographic axis the elements $Q_{\alpha\beta}(k)$ with $\alpha \neq \beta$ vanish). Because the phase IV ammonium halides are isotropic there are only three unknown $q_{\alpha\alpha}(k)$. These are $q_{\alpha\alpha}(H)$, $q_{\alpha\alpha}(N)$ and $q_{\alpha\alpha}(X)$. Isotopic data will give us two equations in three unknowns. This can be reduced to two unknowns by remembering that $\Sigma Q_{\alpha\beta}(k) = 0$. The results for ammonium chloride are:

$$q_H = +1.92e \quad q_N = +8.63e \quad q_{Cl} = -16.31e$$

These calculated charges appear to be unreasonably high - results of similar calculations could not be found for purposes of comparison. However, it is to be remembered that the charges are those associated with the atoms in the presence of a transverse wave. When the distortion of the electronic charge distribution due to such a perturbation is removed, the new effective charges may be lower. This is found to be the case for diatomic cubic crystals (60). Szigeti (60) has calculated the effective charge for atoms in a diatomic cubic lattice. When the external field is removed, $\underline{E}$ is determined by the depolarization field. In the case of atoms lying on cubic sites in a spherical crystal the depolarization field according to the Lorentz relation is $-\frac{4\Pi}{3}\underline{P}$. Substituting this result into:

$$\underline{P}_\alpha = (\underline{\underline{Z}}^t \underline{W})_\alpha + \chi_{\alpha\alpha}\underline{E}_\alpha \qquad (6)$$

gives the polarization of a spherically shaped sample in the absence of an external field as:

$$\underline{P}_\alpha = \frac{3}{\varepsilon^{(\infty)} + 2} \left\{ \underline{\underline{Z}}^t \underline{W} \right\}_\alpha \qquad (7)$$

This result can be interpreted as giving effective charges of $3/(\varepsilon^{(\infty)}+2)\ q_{\alpha\alpha}(k)$ The atoms, however, must be on cubic sites. This means that this result cannot be applied in a rigorous sense to the phase IV ammonium halides since the hydrogen atoms occupy C_{3v} sites. It can only be applied if we associate mass m_1 with the NH_4^+ ions and mass m_2 with the halide ions. Since n is now effectively two the sum on the right hand side of equation 6 has only one term. This will correspond to the external lattice vibration. The calculated values of q and $\left\{3/(\varepsilon^{(\infty)} + 2)\right\} q$ for the ions of ammonium chloride and ammonium bromide are:

	NH_4Cl(IV)	ND_4Cl(IV)	NH_4Br(IV)	ND_4Br(IV)
q	1.21e	1.21e	1.06e	1.07_5e
$\left\{3/(\varepsilon^{(\circ)}+2)\right\} q$	0.77e	0.77e	0.65e	0.66e

For a completely ionic salt it is expected that $\left\{3/(\varepsilon^{(\infty)}+2)\right\} q/e$ will be unity. Deviations from unity have been attributed to overlap of neighbouring ions (60).

Tables 4-1 and 4-2 include assignments for the fundamental modes of all the phase IV ammonium halides. The corresponding phase IV spectra are found in Figures 4-1, 4-2, 4-3 and 4-4.

In regard to the phase IV spectra and also to the phase III and II spectra which are presented later it is to be emphasized that a large

TABLE 4-1. Assignments for NH_4Cl(IV) and ND_4Cl(IV); cm^{-1}

Assignment	NH_4Cl(IV) - THIS WORK See also refs.		ND_4Cl(IV) - THIS WORK See also refs.	
	29,30 R.	22,24 I.R.	R.	22,24 I.R.
ν_1	3049		2215	
ν_2	1719		1227	
$\nu_3(t)$	3127	3126	2333.5	2332
$\nu_3(\ell)$	3164		2371	
$\nu_4(t)$	1401	1400	1063.5	1061
$\nu_4(\ell)$	1421		1069.5	
L_1	(390)*		(280)	
T_1	183		175	
$\nu_A(K\neq 0)$	(92)		—	
$\nu_A(K\neq 0)$	(51)		(62)	
$\nu_A(K\neq 0)$	(25)		(33)	
ν_1+T_1		3223		—
$\nu_1+\nu_A$	3141			
$\nu_1+\nu_A$	3100	3098	2277	2275
$\nu_1+\nu_A$	3074		2248	2247
$\nu_2+\nu_4(F_2)$	—	3050	2260	2259
$2\nu_4(F_2)$	2840	2828	2145	2139
$2\nu_4(A_1)$	—		2119	
ν_2+L_1	2022	2025	1458	1460
$\nu_4(\ell)+L_1$	1813	1813	1344	1348
$\nu_4(t)+L_1$	1791	1791		
$2L_1$		748		546

* the bracketed frequencies have been inferred from Raman active combinations; the ν_A frequencies are inferred assuming relatively flat ν_1 phonon dispersion.

TABLE 4-2. Assignments for NH_4Br(IV) and ND_4Br(IV); cm^{-1}

Assignment	NH_4Br(IV) - SCHUMAKER See Ref. 24		ND_4Br(IV) - THIS WORK See also refs. 23,24	
	R.	I.R.	R.	I.R.
ν_1	3047		2211	
ν_2	1699		1211	
$\nu_3(t)$	3126	3124	2332	2330
$\nu_3(\ell)$	—		2370	
$\nu_4(t)$	1402	1398	1061	1060
$\nu_4(\ell)$	1418		1065(sh)	
L_1	(349)*		(251)	
T_1	160		146	
$\nu_A(K\neq0)$	—		—	
$\nu_A(K\neq0)$	—		(48)	
$\nu_A(K\neq0)$	(28)		(23)	
ν_1+T_1		3200		—
$\nu_1+\nu_A$	—			
$\nu_1+\nu_A$	—		2259	2258
$\nu_1+\nu_A$	—	3075	2234	2232
$\nu_2+\nu_4(F_2)$		3040	2246	2246
$2\nu_4(F_2)$		2805	2131	2127
$2\nu_4(A_1)$			2110	
ν_2+L_1		1970	1415	1413
$\nu_4(\ell)+L_1$		1765	1312	1312
$\nu_4(t)+L_1$		1747		
$2L_1$		672		488

* the bracketed frequencies have been inferred from Raman active combinations; the ν_A frequencies are inferred assuming relatively flat ν_1 phonon dispersions.

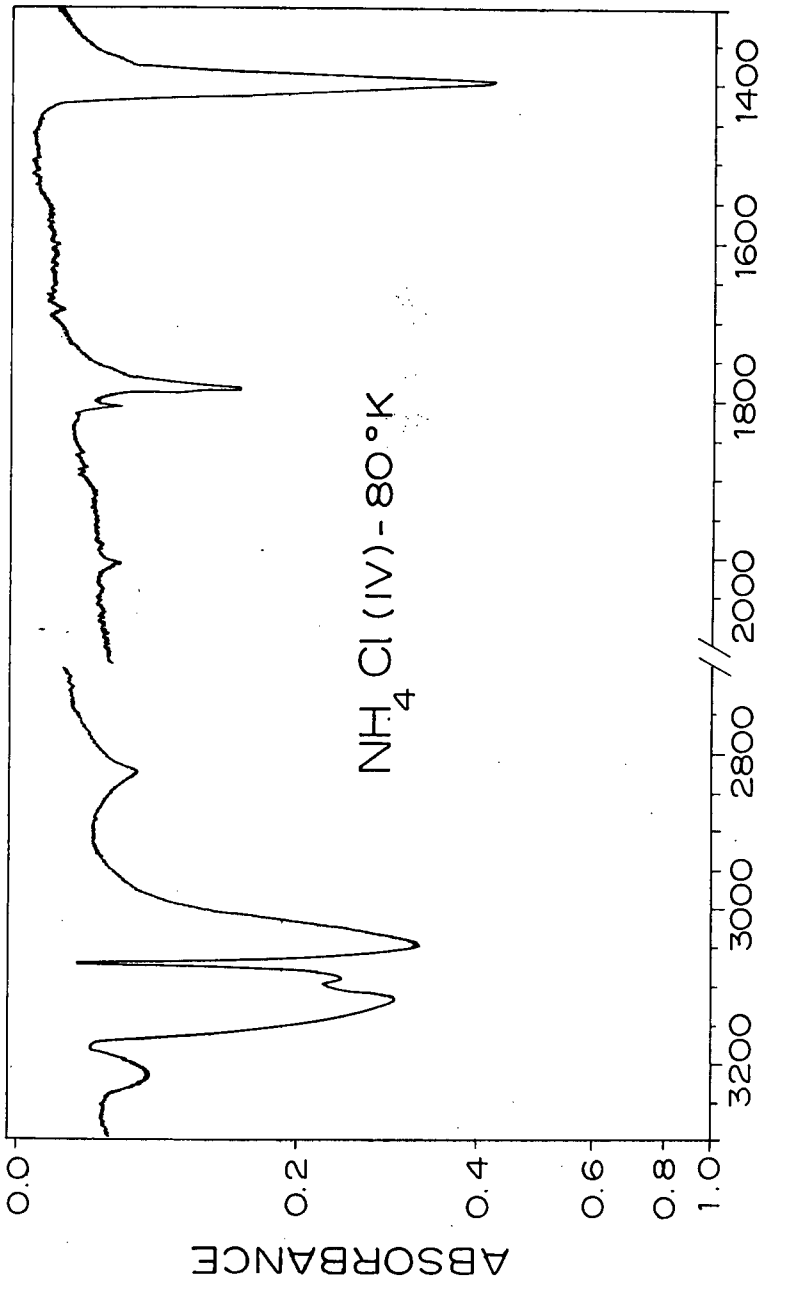

Figure 4-1 The I.R. spectrum of NH_4Cl (IV)

Figure 4-2 The Raman Spectrum of NH_4Cl (IV)

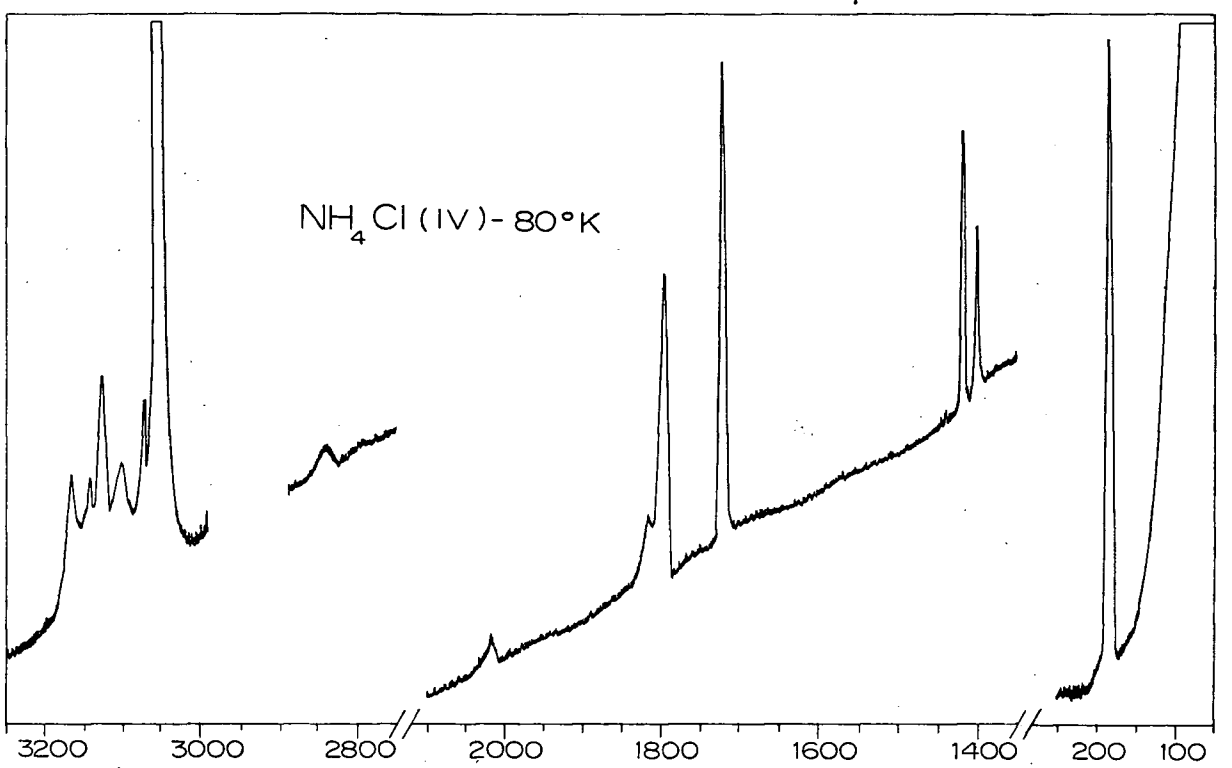

Figure 4-3 The I.R. spectra of ND_4Cl (IV) and ND_4Br (IV)

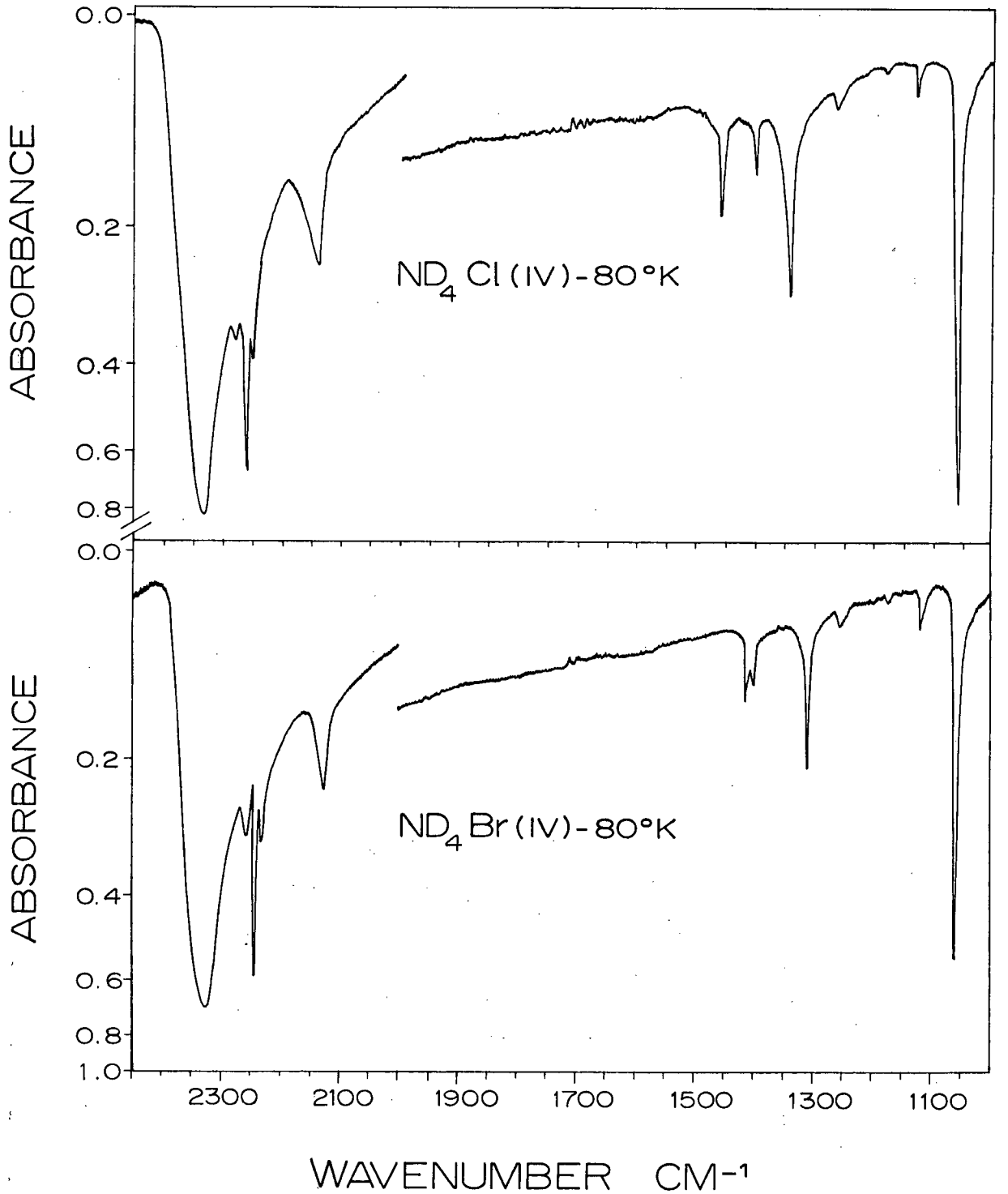

Figure 4—4 The Raman Spectra of ND_4Cl(IV) and ND_4Br(IV)

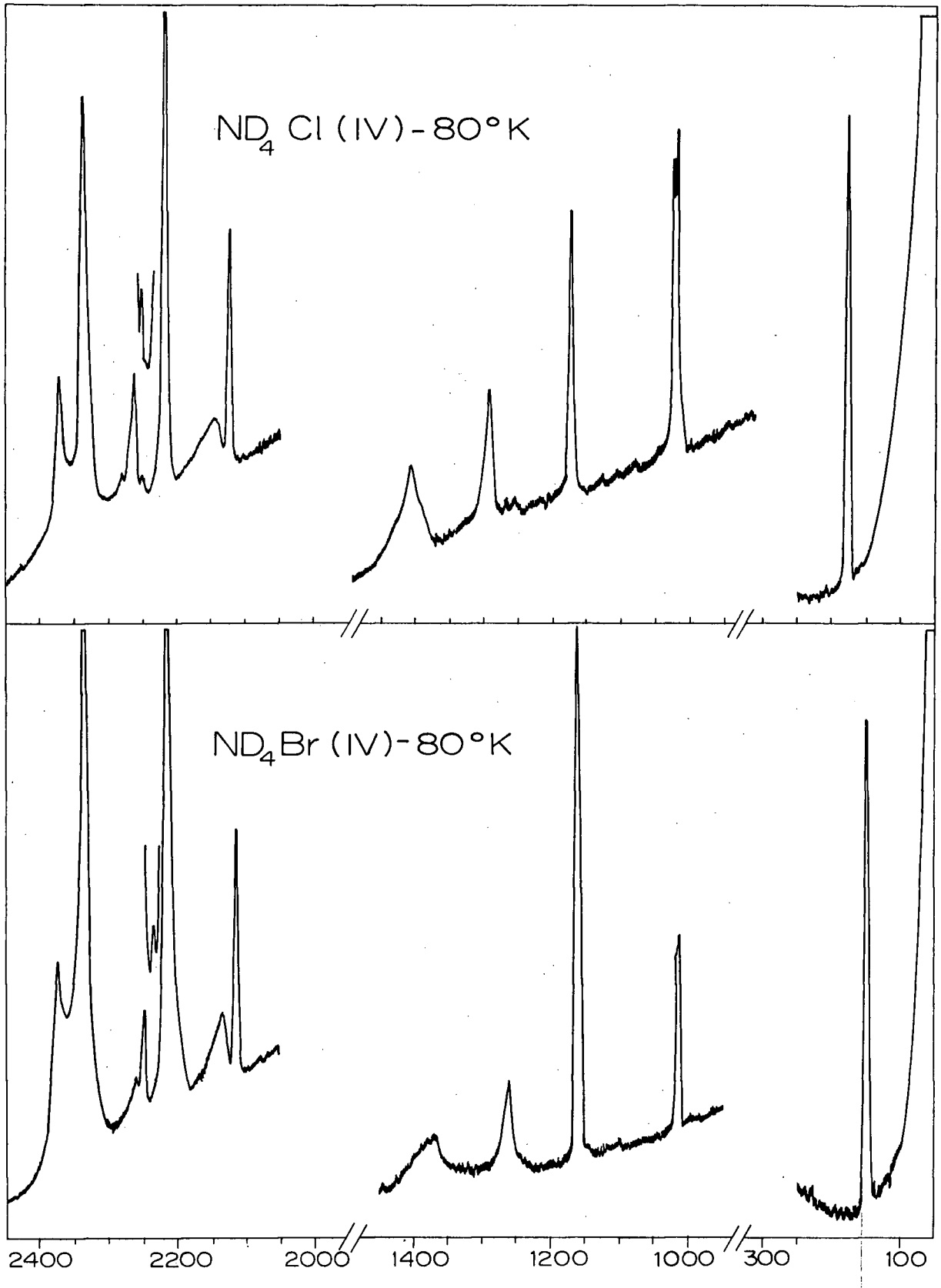

portion of the work undertaken, particularly where the infrared work is concerned, is not original and, indeed, for the most part serves only to verify the findings of earlier workers. When results are presented which duplicate those of earlier workers this is indicated in the tables and reference is made to the original work.

There are five combinations and overtones appearing in the vibrational spectra of the phase IV ammonium halides which are readily assigned. These are, in order of increasing frequency, $2L_1(A + E + F_2)$, $\nu_4 + L_1(A_2 + E + F_1 + F_2)$, $2\nu_4(A_1 + E + F_2)$, $\nu_2 + \nu_4(F_1 + F_2)$ and $\nu_1 + T_1(F_2)$. Of these five, $2L_1$ and $\nu_1 + T_1$ are not seen in the Raman effect; all the rest appear in both the Raman and infrared spectra.

Perhaps the most important combination is $\nu_4 + L_1$ (or $\nu_4 + \nu_R$). Its importance arises from the fact that historically (22) it has been used to place ν_R and, indeed, the ν_R frequencies obtained from the Raman observed $\nu_4 + \nu_R$ scatterings for all the ammonium halides are found to differ by only ± 2 cm^{-1} from the corresponding frequencies obtained from neutron inelastic scattering measurements (3) (see also Table 4-8). In both the infrared and Raman spectra of NH_4Cl(IV) and NH_4Br(IV) $\nu_4 + L_1$ appears as a doublet. In all cases the observed splitting is comparable to the splitting associated with the transverse and longitudinal components of ν_4. This suggests that the previously anomalous component (22) of $\nu_4 + L_1$ be assigned as $\nu_4(\ell) + L_1$. The low wave number component will be $\nu_4(t) + L_1$. The deuterated analogs do not show a $\nu_4 + L_1$ splitting - this is not unexpected, however, since in their case the splitting associated with the transverse and longitudinal components of ν_4 is about 5 cm^{-1} compared

to about 20 cm^{-1} for NH_4Cl(IV) and NH_4Br(IV).

For ND_4Cl(IV) and ND_4Br(IV) the overtone of ν_4, $2\nu_4(A_1 + E + F_2)$, is split into two distinct components in the Raman spectra. This is most likely due to the appearance of a component of A_1 symmetry type and also a component containing both E and F_2 symmetry types. The $\nu_1(A_1)$ fundamental lies near $2\nu_4$ at higher wave number (see Tables 4-1 and 4-2) and if $\nu_1(A_1)$ undergoes Fermiresonance with $2\nu_4(A_1 + E + F_2)$ the $2\nu_4(A_1)$ component is expected to appear on the low wave number side of $2\nu_4(E + F_2)$. On this basis, then, the sharp symmetric line appearing at 2119 cm^{-1} in the Raman spectrum of ND_4Cl(IV) becomes $2\nu_4(A_1)$ and the broader asymmetric line at 2144 cm^{-1} becomes $2\nu_4(E + F_2)$ (see Figure 4-4). This later line compares with the line $2\nu_4(F_2)$ which appears in the infrared spectrum at 2139 cm^{-1}. Similar $2\nu_4$ lines are observed for ND_4Br(IV). The Raman spectra of the protonated phase IV salts do not show a splitting for $2\nu_4$ - most likely because, in this case, $2\nu_4$ is about 200 wave numbers removed from ν_1 as compared to about 100 wave numbers for the deuterated salts.

There is one final point to be noted in relation to $2\nu_4$ for the phase IV ammonium halides, and this is that the observed infrared frequencies, $2\nu_4(F_2)$, and the observed Raman frequencies, $2\nu_4(E + F_2)$, are consistently higher than those predicted from about 10 to 40 cm^{-1}. Fermi resonance cannot be invoked to explain this situation since there are no lines of F_2 symmetry type lying nearby at lower wave number. Since the predicted frequencies are those predicted in the zero wavevector limit it would appear that for the two phonon process giving rise to $2\nu_4$ that the phonons involved must originate from points in $\underline{K}$ space where $\underline{K} \neq 0$. Such a

situation would explain the discrepancy between the observed and predicted $2\nu_4$ frequencies.

For the phase IV ammonium halides $\nu_2 + \nu_4(F_1 + F_2)$ lies some 75 cm^{-1} below $\nu_3(F)$ and can therefore be expected to undergo Fermi resonance with $\nu_3(F_2)$. The enhanced intensity observed for $\nu_2 + \nu_4(F_2)$ especially in the infrared indicatesthat Fermi resonance does, indeed, take place. A further indication of Fermi resonance is that the observed $\nu_2 + \nu_4$ frequencies are considerably lower than those predicted; for NH_4Cl(IV), NH_4Br(IV), ND_4Cl(IV) and ND_4Br(IV) the $\nu_2 + \nu_4$ frequency discrepancies are 69,57,29 and 25 cm^{-1} respectively.

Evidently $\nu_1 + T_1(F_1)$ which appears only in the infrared spectra of the protonated salts where it lies some 75-100 cm^{-1} above $\nu_3(F_2)$ does not undergo Fermi resonance since the observed frequencies are about 8 cm^{-1} lower than those predicted. In the infrared spectra of the deuterated salts the presence of $\nu_1 + T_1$ is very likely masked by the intense ν_3 absorptions.

The final line appearing in the second order spectra which is readily assigned is $2L_1(A_1 + E + F_2)$. This line appears only in the infrared spectra. For the series of salts; NH_4Cl(IV), NH_4Br(IV), ND_4Cl(IV) and ND_4Br(IV) the respective anharmonicities are 16, 13, 7 and 7 cm^{-1}.

In addition to the five combinations and overtones discussed above there are four lines appearing in the vibrational spectrum of the phase IV ammonium halides which are not obvious combinations or overtones of

the fundamentals. With reference to NH_4Cl(IV) the first of these we shall discuss is the line appearing at 2025 cm^{-1} in the infrared. Historically (22) this line has been assigned to $\nu_2 + L_1(F_1 + F_2)$. As the following discussion will show it turns out that this is the most acceptable assignment but not for obvious reasons. Assuming $\nu_2 + L_1$ is the correct assignment it is found that the frequencies predicted for $\nu_2 + L_1$ in the NH_4Cl(IV) spectrum and its counterparts in the spectra of NH_4Br(IV), NH_4Br(III) and NH_4I(III) are respectively 84, 78, 55 and 37 cm^{-1} higher than those observed. For the same series of deuterated salts these values are 47, 49, 31 and 20 cm^{-1}. This situation cannot arise from Fermi resonance since there are no lines of F_2 symmetry lying nearby at higher wave number. Also, recent studies (24) by Schumaker involving thin single crystal slices have shown that the absorption in question is structured for both NH_4Cl(IV) and NH_4Br(IV) and possesses four distinct maxima. These appear at 2015, 2040, 2085 and 2100 cm^{-1} for NH_4Cl(IV) and at 1970, 1985, 2020 and 2040 cm^{-1} for NH_4Br(IV). Since the observations mentioned above are not compatible with the observations for the $\nu_4 + L_1$ (or $\nu_4 + \nu_R$) which indicate unstructured lines whose frequencies coincide (within experimental error) with those predicted, the assignments $\nu_2 + L_1$ (or $\nu_2 + \nu_R$) may be supposed to be incorrect. However, there are no other obvious combinations or overtones which will place these lines in the desired spectral region. Also, the frequency ratios of the lines appearing in the spectra of the deuterated and protonated salts for the series NH_4Cl(IV), NH_4Br(IV), NH_4Br(III) and NH_4I(III) are compatible with the assignment $\nu_2 + \nu_R$; i.e. the frequency ratios are 0.719 ± 0.002. (This value corresponds to corresponding

ν_2 and ν_R ratios of 0.715 ± 0.002 and 0.717 ± 0.002.) Furthermore, Schumaker found the temperature dependence of the $\nu_2 + \nu_R$ lines to be very similar to that of the $\nu_4 + \nu_R$ lines. Therefore, we have frequency ratio and temperature dependence results which are compatible with the assignment $\nu_2 + L_1$ and predicted frequency and band contour results which seemingly are not. If the assignment $\nu_2 + L_1(F_1 + F_2)$ is made only a line of F_2 symmetry type can contribute to the observed intensity in both the infrared and Raman spectra. This means that the anomalous components (i.e. the four maxima observed for NH_4Cl(IV) and NH_4Br(IV)) must involve phonons with $\underline{K} \neq 0$. Such a situation could also account for the discrepancies between the observed and predicted frequencies. On this basis the assignment $\nu_2 + L_1$ is not an unreasonable choice.

The remaining three lines which are not obvious overtones or combinations of the fundamentals will be discussed as a group. In the case of NH_4Cl(IV) these lines, as observed in the Raman spectrum, appear at 3141, 3100 and 3074 cm^{-1} (see Table 4-1). Of these three lines only the 3100 cm^{-1} line appears in the infrared; the appearance of the 3141 and 3074 cm^{-1} lines in the infrared is probably masked by the intense ν_3 and $\nu_2 + \nu_4$ absorptions which appear at 3126 and 3050 cm^{-1} respectively. Schumaker (24) does not report the corresponding lines for the Raman spectrum of NH_4Br(IV). However, the NH_4Br(III) Raman lines of similar origin appear at 3123, 3098 and 3068 cm^{-1} (see Table 4-3). Of these three lines only the 3068 cm^{-1} line is observed in the infrared. The remaining two lines are very likely hidden by the intense ν_3 absorption at 3115 cm^{-1}. In the spectrum of ND_4Cl(IV) there are anomalous Raman lines at 2277 and

2248 cm^{-1}. The corresponding infrared lines appear at 2275 and 2247 cm^{-1}. For ND_4Br(IV) the same set of lines appears at 2259 and 2234 cm^{-1} in the Raman and at 2258 and 2232 cm^{-1} in the infrared. The spectra of the fully deuterated salts do not give evidence for the third high wave number line which is observed for NH_4Cl(IV). However, its appearance could easily be masked by the very intense lines observed for ν_3.

The only fundamentals that these heretofore unassigned lines can be satisfactorily related to is ν_1 in combination with acoustical modes. This means that these lines like those for both $\nu_2 + L_1$ and $2\nu_4$ must involve phonons with $\underline{K} \neq 0$. If we assume a one dimensional type lattice as discussed in section 3-4, the calculated zone edge transverse acoustical modes for NH_4Cl(IV), ND_4Cl(IV), NH_4Br(IV) and ND_4Br(IV) lie at 104, 102, 71 and 70 cm^{-1} respectively. Providing we assume relatively flat ν_1 phonon despersions, the assignment ν_1 + acoustical modes ($\nu_1 + \nu_A$) for the lines under discussion gives acoustical modes at 92, 51 and 25 cm^{-1} for NH_4Cl(IV); 62 and 33 cm^{-1} for ND_4Cl(IV); 85, 60 and 30 cm^{-1} for NH_4Br(III) and 48 and 28 cm^{-1} for ND_4Br(IV). The experimentally inferred acoustical mode at 92 cm^{-1} for NH_4Cl(IV) compares with the calculated zone edge frequency of 104 cm^{-1}. In the case of NH_4Br(III) we can compare the inferred acoustical modes at 85 and 60 cm^{-1} with the predicted NH_4Br(IV) zone edge frequency of 71 cm^{-1}. It is to be emphasized that the calculated zone edge frequencies are only a rough estimate of the upper frequency limits (i.e. at maximum wavevector) for the acoustical modes. However, since the inferred frequencies do tend to fall within these limits the most meaningful assignment for these previously unassigned

lines is ν_1 in combination with acoustical modes.

A complete set of assignments for the phase IV combinations and overtones which have been discussed above are included in Tables 4-1 and 4-2.

4-2 The Phase III Ammonium Halides

For the phase III ammonium halides we have the space group, $D_{4h}^7(P_4/nmm)$. Under the factor group analysis the four fundamental modes associated with the free ammonium ion become the precursors of 14 crystal modes; i.e.

Vibrational Mode	Free Ion Symmetry - T_d		Site Group Symmetry - D_{2d}		Factor Group Symmetry - D_{4h}
ν_1	A_1	→	A_1	→	A_{1g}, B_{1u}
ν_2	E	→	A_1, B_1	→	A_{1g}, B_{1u}, B_{1g}, A_{1u}
ν_3	F_2	→	B_2, E	→	B_{2g}, A_{2u}, E_g, E_u
ν_4	F_2	→	B_2, E	→	B_{2g}, A_{2u}, E_g, E_u

From the above correlation diagram it is seen that the 14 crystal modes arise from a splitting of the degenerate bending and stretching modes by the static field (site group) and also from a further splitting by the correlation field (factor group). This latter splitting arises from the fact that there are two molecules per unit cell and hence they may execute the same normal vibration either in phase or out of phase to give rise to crystal modes of g and u symmetries. Summarizing the irreducible representation for the 14 internal fundamentals gives:

$$\Gamma(\text{internal}) = 2A_{1g} + B_{1g} + 2B_{2g} + 2E_g + A_{1u} + 2A_{2u} + 2B_{1u} + 2E_u$$

Under the D_{4h} factor group all of the above gerade symmetry species contain elements of the polarizability tensor and hence are associated with Raman active vibrations, whereas only the A_{2u} and E_u vibrations are infrared active.

The irreducible representations for the three types of external modes are:

$$\Gamma(\text{OT}) + A_{1g} + B_{2g} + 2E_g + A_{2u} + E_u$$

$$\Gamma(\text{OL}) = A_{2g} + E_g + B_{2u} + E_u$$

$$\Gamma(\text{AT}) = A_{2u} + E_u$$

We may note that the 7 infrared active modes can be expected to possess longitudinal components which will be Raman active.

The only free ion fundamental mode for which site group components have been assigned is ν_4 (23,29). In the case of NH_4Br(III) both the infrared ($\nu_4(A_{2u})$, $\nu_4(E_u)$) and the Raman ($\nu_4(B_{2g})$, $\nu_4(E_g)$) assignments have been made. From the results obtained in this work the NH_4Br(III) ν_4 frequencies are:

infrared	Raman
1405 cm^{-1}	1402 cm^{-1}
1433	1422

We see that the magnitude of the infrared splitting is 28 cm^{-1} and that

of the Raman splitting only 20 cm^{-1}. For ND_4Br(III) the infrared spectrum gives a ν_4 splitting of 23 cm^{-1}. Unexpectedly no Raman splitting is observed. There are two possibilities: (i) the high wave number NH_4Br(III) scattering is indeed due to $\nu_4(B_{2g})$ and in the case of ND_4Br(III) it just does not appear with observable intensity or (ii) the assignment $\nu_4(B_{2g})$ of previous workers is incorrect and the high wave number ν_4 scattering is an expected longitudinal component. If we assume this latter situation there is a ν_4 longitudinal-transverse splitting of 17 cm^{-1}. This compares with the 16 cm^{-1} NH_4Br(IV) splitting of similar origin. The corresponding ND_4Br(IV) splitting is only 4 cm^{-1}. Since it is determined by assigning a shoulder it is not unexpected that a ν_4 ND_4Br(III) Raman splitting would not be resolved. Of the two possibilities for the assignment of the ν_4 high wave number scattering ν_4 (longitudinal) is the most acceptable since it is compatible with the observed NH_4Br(III) ν_4 splittings and also suggests that the ND_4Br(III) ν_4 Raman splitting will not be resolved. The ν_4 results obtained for the ammonium iodides are similar to those obtained for the ammonium bromides (see Table 4-4).

With respect to the phase III ν_3 assignments previous workers (23,29) have only been able to identify the more intense doubly degenerate components. In this work it is found that there is one exception. The Raman spectrum of NH_4Br(III) allows us to place $\nu_3(B_{2g})$ at 3079 cm^{-1}; $\nu_3(E_g)$ is placed at 3117 cm^{-1}. (This latter frequency compares with the $\nu_3(E_u)$ infrared frequency of 3115 cm^{-1}.) The Raman ν_3 splitting and the infrared ν_4 splitting thus give effective ν_3/ν_4 site group splittings of

38 and 28 cm^{-1}. The corresponding splittings for $NaBH_4$(II) which has a comparable angular distortion are 31 and 26 cm^{-1} (see Table 5-3). None of the Raman spectra of the phase III ammonium halides possessed scatterings which could be identified with a ν_3 longitudinal component.

Unexpectedly no ν_2 site group splitting was found in the Raman spectra of the phase III ammonium halides. This has also been the finding of previous workers (29,30). Without exception the ν_2 Raman lines are very sharp. They are found to have a half-height width of about 5 cm^{-1} and give no evidence of the presence of a second component. It is interesting to note here that the Raman spectra of phase II sodium borohydride (see Table 5-3) shows a distinct doublet for ν_2 and only one component for ν_3. This is just the reverse of the situation observed for phase III ammonium bromide.

One of the interesting features of phase III spectra is that the partial lifting of the degeneracy associated with the $L_1(F_1)$ librational mode of the phase IV ammonium halides allows for the appearance of an E_g librational mode in the Raman and an E_u librational mode in the infrared. Altogether there are four possible librational modes which may be distinguished according to the scheme: $L_1(A_{2g})$, $L_2(E_g)$, $L_3(B_{2u})$ and $L_4(E_u)$. The $L_1(A_{2g})$ and $L_3(B_{2u})$ modes are neither Raman nor infrared active. It is found that the $L_2(E_g)$ modes do appear, albeit weakly, in the Raman spectra of NH_4Br(III) and NH_4I(III). The infrared active mode, $L_4(E_u)$, does not appear with observable intensity in phase III spectra.

The remaining external fundamentals to be discussed are those of translatory origin. There are six such fundamental modes and they may

be distinguished according to the following scheme: $T_1(B_{2g})$, $T_2(E_g)$, $T_3(A_{2u})$, $T_4(E_u)$, $T_5(A_{1g})$ and $T_6(E_g)$. The vibrations T_1, T_2, T_3 and T_4 arise from translational motions in which the motions of the halide and ammonium ions are out of phase. The T_5 and T_6 vibrations involve halide and ammonium ion motions which are in phase.

Of the four translatory modes predicted to be Raman active only $T_1(B_{2g})$ and $T_2(E_g)$ were observed in the phase III spectra. In the Raman spectrum of NH_4Br(III) these lines which arise from the two non-equivalent N-Br distances of 2.41 and 2.55 Å are found at 183 and 137 cm^{-1}. The early single crystal studies of Couture-Mathieu and Mathieu (29) suggest the respective assignments $T_1(B_{2g})$ and $T_2(E_g)$ for the low and high wave number scatterings. The infrared spectrum of NH_4Br(III) shows only a single intense absorption at 172 cm^{-1} which almost certainly derives its maximum intensity from $T_4(E_u)$. In the case of NH_4I(III) where the two non-equivalent N-I distances are 2.69 and 2.74 Å the $T_1(B_{2g})$ and $T_2(E_g)$ modes are observed at 124 and 158 cm^{-1}. The $T_4(E_u)$ mode appears in the infrared at 151 cm^{-1}.

At this point it is to be noted that very recently two papers (58,61) appeared simultaneously which report the results of independent studies of the external vibrations of the ammonium halides. In general, the results of these studies are in good agreement with the results of this work (see Table 4-5). One very interesting feature of both studies is the assignment of the Raman active $T_5(A_{1g})$ and $T_6(E_g)$ vibrations associated

TABLE 4-3. Assignments for NH_4Br(III) and ND_4Br(III); cm^{-1}

	NH_4Br(III) - THIS WORK See also refs.		ND_4Br(III) - THIS WORK See also refs.	
Assignment	29,32	23		23
	R.	I.R.	R.	I.R.
$\nu_1(A_{1g})$	3037.5		2209	
$\nu_2(A_{1g}/B_{1g})$	1694		1209.5	
$\nu_3(B_{2g},A_{2u})$	3079		—	
$\nu_3(E_g,E_u)$	3117	3115	2339	2336
$\nu_4(B_{2g},A_{2u})$	—	1433	—	1089
$\nu_4(E_g,E_u)$	1402	1405	1063	1066
$\nu_4(E_u)\ell$	1422		—	
$L_2(E_g),L_4(E_u)$	336		(241)	
$T_1(B_{1g}),T_3(A_{2u})$	137		124.5	
$T_2(E_g),T_4(E_u)$	187	172	164	
$\nu_A(K\neq0)$	(85)*		—	
$\nu_A(K\neq0)$	(60)		—	
$\nu_A(K\neq0)$	(30)		—	
$\nu_1+\nu_T$		3195		
$\nu_1+\nu_A$	3123			
$\nu_1+\nu_A$	3098			
$\nu_1+\nu_A$	3068	3068		
$\nu_2+\nu_4(E_g,E_u)$	—	3037	—	2243
$2\nu_4(E_g,E_u)$	2817	2805	2127	2122
$2\nu_4(A_{1g})$	—		2105	
$\nu_2+\nu_R$	1975	1959	1420	—
$\nu_4+\nu_R$	1737		1302	1296
$2\nu_R$		648		470

* the bracketed frequencies have been inferred from Raman active combinations; the ν_A frequencies are inferred assuming ν_1 phonon dispersions which are relatively flat.

TABLE 4-4. Assignments for NH_4I(III) and ND_4I(III); cm^{-1}

Assignment	NH_4I(III) - THIS WORK See also refs.		ND_4I(III) - THIS WORK	
		25		
	R.	I.R.	R.	I.R.
$\nu_1(A_{1g})$	3035		2202	
$\nu_2(A_{1g}/B_{1g})$	1667		1194.5	
$\nu_3(B_{2g},A_{2u})$				
$\nu_3(E_g,E_u)$	3105	3105	2320	2316
$\nu_4(B_{2g},A_{2u})$	—	1421	—	1077
$\nu_4(E_g,E_u)$	1398	1401	1059	1062
$\nu_4(E_u)\ell$	1409		—	
$L_2(E_g),L_4(E_u)$	291		208	
$T_1(B_{1g}),T_3(A_{2u})$	124		113	
$T_2(E_g),T_4(E_u)$	158	151	146	
$\nu_1+\nu_T$		3166		—
$\nu_2+\nu_4(E_g,E_u)$	3025.5	3023	2233	2229.5
$2\nu_4(E_g,E_u)$	2798	2791	2121.5	2118
$2\nu_4(A_{1g})$			2101.5	
$\nu_2+\nu_R$	1921	1912	1385	1383
$\nu_4+\nu_R$	1686	1681	1268	1265
$2\nu_R$		568		410

Figure 4-5 The I.R. spectra of NH_4Br (III) and NH_4I (III)

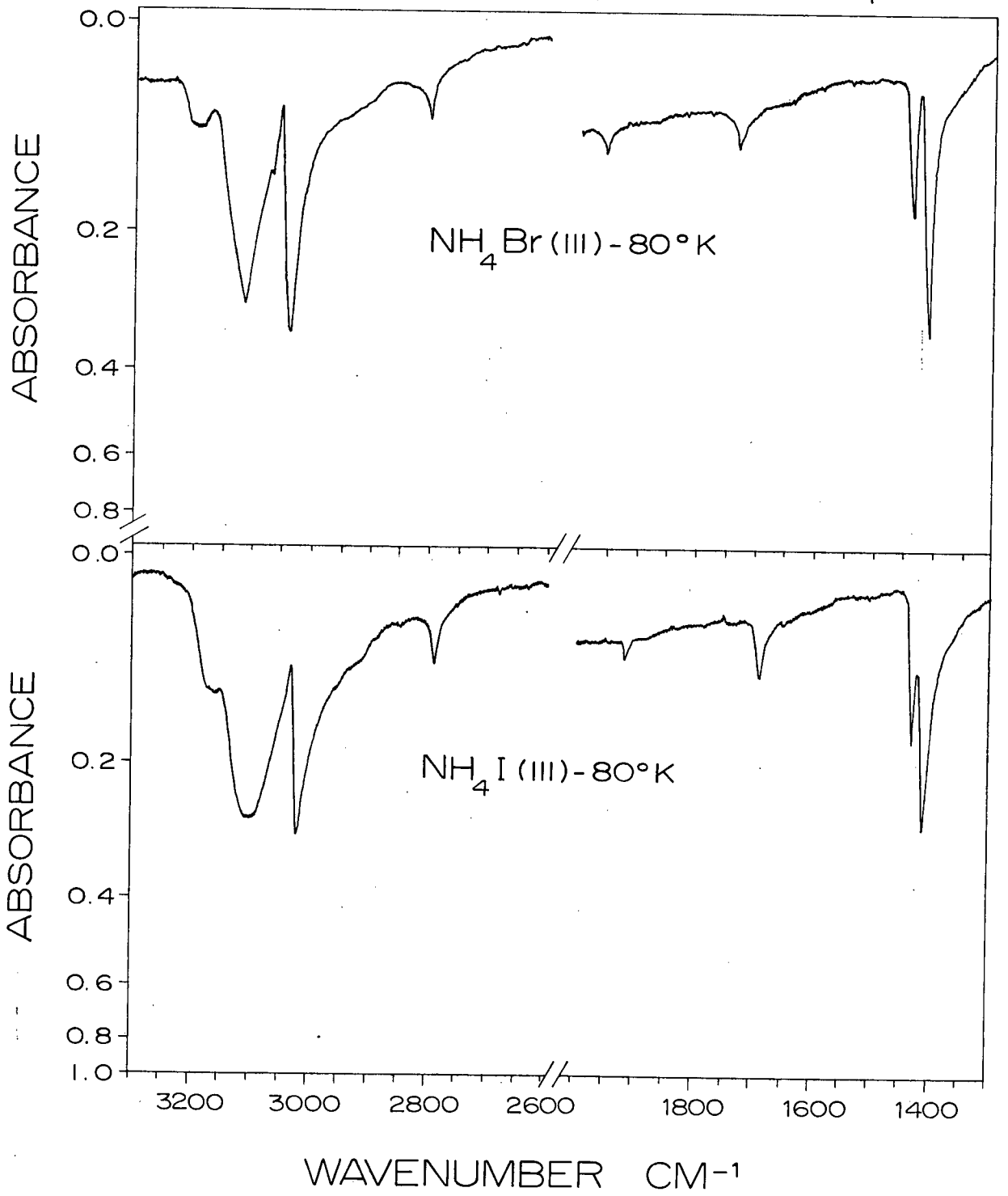

Figure 4-6 The Raman Spectra of NH_4Br(III) and NH_4I(III)

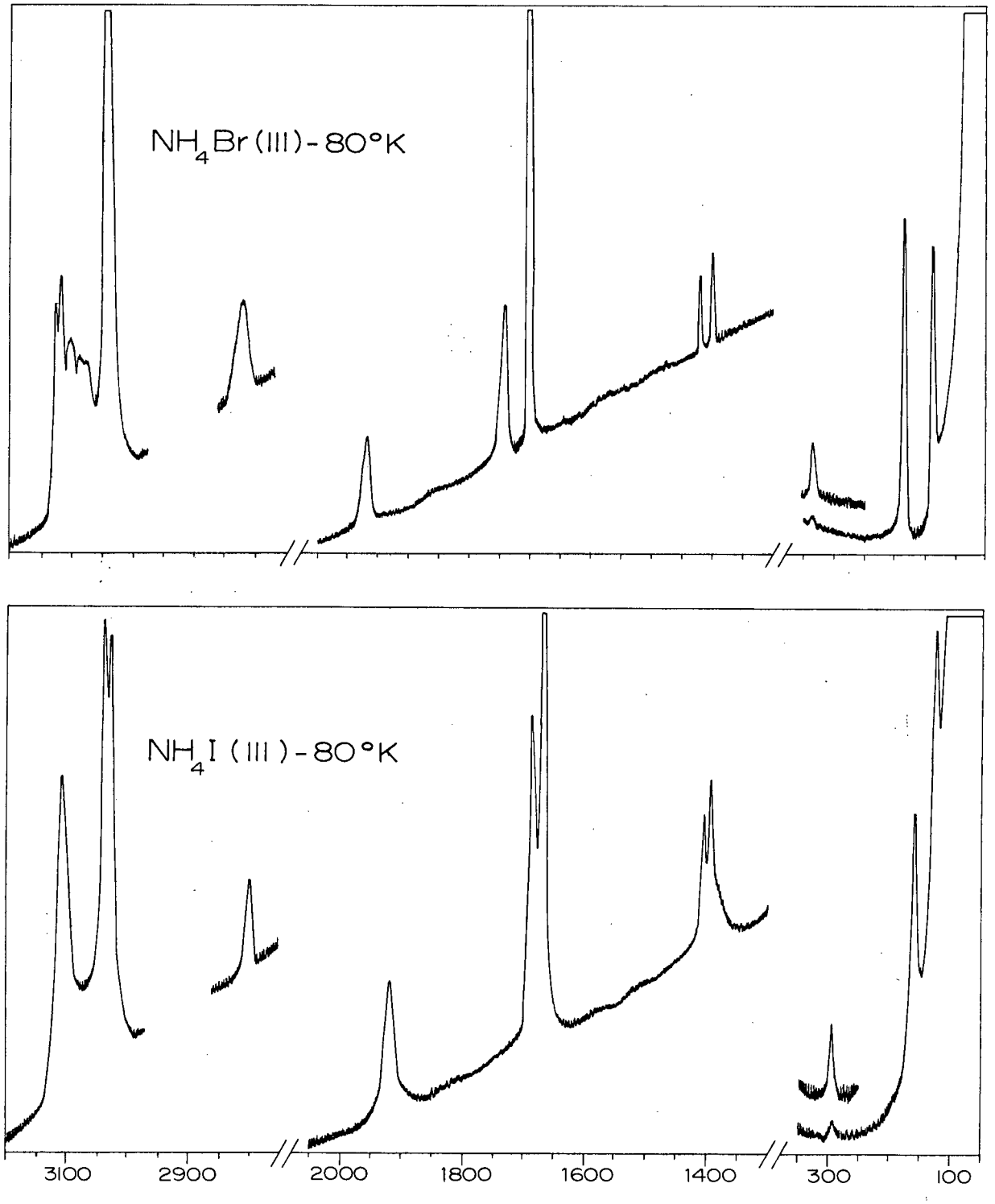

Figure 4-7 The I.R. spectra of ND_4Br (III) and ND_4I (III)

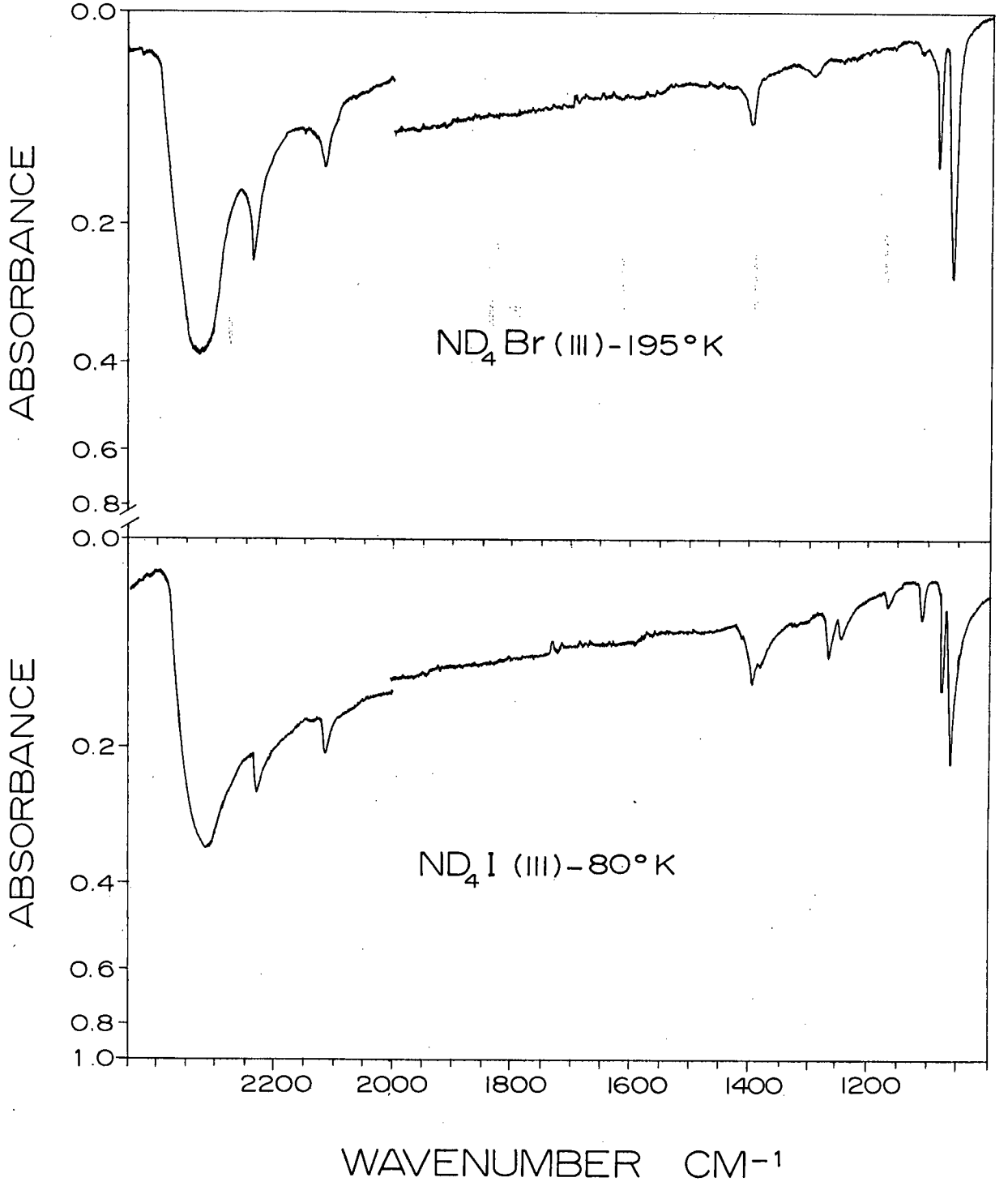

Figure 4-8 The Raman Spectra of ND_4Br(III) and ND_4I(III)

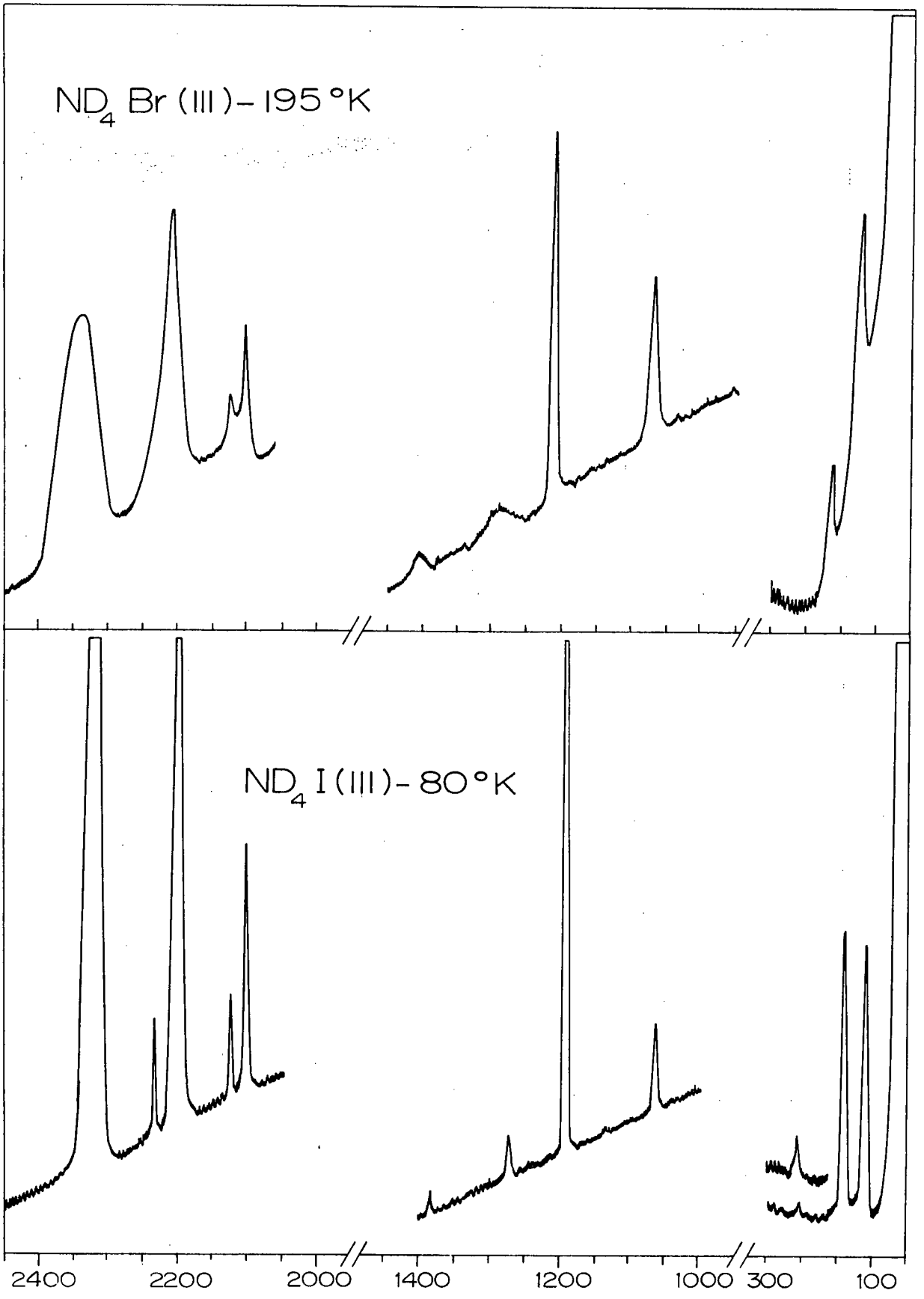

TABLE 4-5 The External Vibrations of the Ammonium Halides; cm^{-1}

	PHASE IV			PHASE II	
	THIS WORK R	REF. 58 R	REF. 58 I.R.	THIS WORK I.R.	REF. 58 I.R.
$NH_4Cl(T_1)$	183	185	188	177	172
$ND_4Cl(T_1)$	175	177	177	170	166
$NH_4Br(T_1)$	___	159	157	154	147
$ND_4Br(T_1)$	146	147	149	139	138

	THIS WORK	REF. 58	REF. 61
$NH_4Br(III)$			
$L_2(E_g)$	336	300	331
$T_1(B_{1g})$	137	133	132
$T_2(E_g)$	183	179	179
$T_4(Eu)$	172	153	-
$T_5(A_{1g})$		62	63
$T_6(E_g)$		75	76.5
$ND_4Br(III)$			
$L_2(E_g)$	-	-	-
$T_1(B_{1g})$	124.5	122	119
$T_2(E_g)$	164	165	163
$T_4(Eu)$	-	145	-
$T_5(A_{1g})$		63	62
$T_6(E_g)$		75	72

TABLE 4-5: continued

	THIS WORK	REF. 58	REF. 61
NH_4I(III)			
$L_2(E_g)$	291	285	287
$T_1(B_{1g})$	124	123	123
$T_2(E_g)$	158	155	155
T_4(Eu)	151	151	147
$T_5(A_{1g})$		45	45
$T_6(E_g)$		57	56
ND_4I(III)			
$L_2(E_g)$	208		-
$T_1(B_{1g})$	113		115
$T_2(E_g)$	146		145
T_4(Eu)	-		-
$T_5(A_{1g})$			43
$T_6(E_g)$			55

with the phase III ammonium halides. In the Raman spectrum of NH_4Br(III) Durig and Antion (61) placed $T_5(A_{1g})$ at 63 cm^{-1} and $T_6(E_g)$ at 76.5 cm^{-1}. The corresponding frequencies as observed by Perry and Lowndes (58) are 62 and 75 cm^{-1}. The reason these Raman active lines were not observed in this work is apparently due to failure to scan sufficiently close to the exciting line.

The combinations and overtones observed in the spectra of the phase III ammonium halides are similar in origin to those observed for the phase IV salts. Thus, we have the following "combinations" and "overtones": $2\nu_R$, $\nu_4 + \nu_R$, $\nu_2 + \nu_R$, $2\nu_4$, $\nu_2 + \nu_4$, $\nu_1 + \nu_T$ and $\nu_1 + \nu_A$, where the subscripts associated with ν_R, ν_T and ν_A refer to rotatory (librational), translatory and acoustical modes respectively. Clearly each of the above "overtones" and "combinations" may have a number of components contributing to its intensity. However, it is convenient to initially make only the gross distinctions between the various combinations and overtones which have been indicated. As the discussion progresses more explicit assignments can be made as they are needed.

The only phase III ammonium halide for which acoustical modes in combination with ν_1 appear is NH_4Br(III). These lines which lie at 3074, 3100 and 3141 cm^{-1} have previously been discussed. For the remaining phase III salts it is likely that band overlapping and/or insufficient intensity obscures appearance of the lines $\nu_1 + \nu_A$. In both the infrared and Raman spectra of the phase III salts bands with single maxima are observed for both $\nu_4 + \nu_R$ and $\nu_2 + \nu_R$ (see Tables 4-3 and 4-4). These bands may however contain contributions from several nearly accidentally

degenerate components. It is to be noted that there is a significant infrared -Raman frequency discrepancy for both $\nu_4 + \nu_R$ and $\nu_2 + \nu_R$. For example for NH_4Br(III) $\nu_4 + \nu_R$ appears at 1737 cm^{-1} in the Raman and at 1728 cm^{-1} in the infrared. For $\nu_2 + \nu_R$ the corresponding frequencies are 1975 and 1959 cm^{-1}. The most likely explanation for this type of behaviour is a significant g-u type splitting.

The lines associated with both $2\nu_R$ and $\nu_1 + \nu_T$ appear only in the infrared. The phase III assignments for the $2\nu_R$ infrared lines are:

$$L_2(E_g) + L_4(E_u) = 2\nu_R(A_{2u})$$

$$L_1(A_g) + L_4(E_u) = 2\nu_R(E_u)$$

$$L_2(E_g) + L_3(B_{2u}) = 2\nu_R(E_u)$$

Since $2\nu_R$ shows only one maximum it is likely that the three allowed components are all contained in the one band envelope. A similar situation occurs for $\nu_1 + \nu_T$ where the four infrared active components;

$$\nu_1(A_{1g}) + T_3(A_{2u}) = \nu_1 + \nu_T(A_{2u})$$

$$\nu_1(A_{1g}) + T_4(E_u) = \nu_1 + \nu_T(E_u)$$

$$\nu_1(B_{1u}) + T_1(B_{2g}) = \nu_1 + \nu_T(A_{2u})$$

$$\nu_1(B_{1u}) + T_2(E_g) = \nu_1 + \nu_T(E_u)$$

give only a single maximum. If it is assumed that the maximum intensity is due to the combination $\nu_1(A_{1g}) + T_4(E_u)$ then the observed frequencies for both NH_4Br(III) and NH_4I(III) are about 30 cm^{-1} lower than those

predicted.

The overtone $2\nu_4$ for the phase III salts appears in the infrared as an absorption with a single maximum. The predicted components of this absorption are:

$$\nu_4(E_g) + \nu_4(A_{2u}) = 2\nu_4(E_u)$$

$$\nu_4(B_{2g}) + \nu_4(E_u) = 2\nu_4(E_u)$$

$$\nu_4(E_g) + \nu_4(E_u) = 2\nu_4(A_{2u})$$

In the zero wavevector limit the $2\nu_4(A_{2u})$ components for all the phase III spectra have predicted frequencies which are higher than those observed. Therefore the maximum intensity of $2\nu_4$ in the infrared is most likely derived from the two combinations of E_u symmetry type. In the Raman spectra only components of gerade symmetry type may appear - there are six such $2\nu_4$ components. For the protonated salts only one Raman peak for $2\nu_4$ appears and on the basis of frequencies predicted in the zero wavevector limit the most reasonable assignments are:

$$\nu_4(B_{2g}) + \nu_4(E_g) = 2\nu_4(E_g)$$

$$\nu_4(A_{2u}) + \nu_4(E_u) = 2\nu_4(E_g)$$

The deuterated phase III salts show two distinct $2\nu_4$ Raman peaks. The principal components of the high frequency peak are very likely the two E_g components and the principal components of the low frequency peak will then be the overtones of the E_u and E_g modes which are both of symmetry $2\nu_4(A_{1g} + B_{1g} + B_{2g})$. Since these components

contain the symmetry type A_{1g} it may well be that they undergo Fermi resonance with $\nu_1(A_{1g})$.

The final combination to be discussed is $\nu_2 + \nu_4$. In phase III spectra $\nu_2 + \nu_4$ appears at essentially the same frequency and without any observable splitting in both the infrared and Raman. Also, $\nu_2 + \nu_4$ shows enhanced intensity. This may be attributed to Fermi resonance with $\nu_3(E_u)$ and $\nu_3(E_g)$ in the infrared and Raman respectively. Thus, it is very likely that the lines observed for $\nu_2 + \nu_4$ arise from a combination of one particular component of ν_2 with $\nu_4(E_g)$ and $\nu_4(E_u)$. If the ν_2 component involved is the one observed in the Raman spectra the observed $\nu_2 + \nu_4(E_u)$ frequencies for NH_4Br(III) and NH_4I(III) are 62 and 42 cm^{-1} lower than those predicted. These values for the corresponding deuterated salts are 33 and 34 cm^{-1}. The large differences between the observed and predicted frequencies are a further indication of the effects of Fermi resonance.

A complete set of assignments for the fundamental, combination and overtone modes observed for the phase III ammonium halides is found in Tables 4-3 and 4-4. The corresponding spectra are reproduced in Figures 4-5, 4-6, 4-7 and 4-8.

4-3 The Phase II Ammonium Halides

The vibrational analysis for the phase II ammonium halides is complicated by the disorder introduced into the lattice via the randomness associated with the hydrogen atoms. Both Lifshitz (26,62) and more recently Whalley and Bertie (27) have shown that when translational periodicity

in a lattice is destroyed the wavevector selection rules breakdown. Lifshitz considers the optical behaviour in the infrared of a cubic crystal containing a random mixture of two isotopes. For this simple model three important results are obtained; (i) for a particular polarization whether longitudinal or transverse transitions with $\underline{K} \neq 0$ will become allowed, (ii) the absorption band due to the transitions having $\underline{K} \neq 0$ will be shifted in frequency relative to the $\underline{K} = 0$ absorption and (iii) the intensity of the $\underline{K} \neq 0$ band is proportional to c(1-c) where c is the mole fraction of the impurity isotope.

The treatment by Whalley and Bertie considers a crystal having molecules arranged on a regular lattice. Disorder is introduced into the lattice by allowing the molecules (or dipoles) to take up random orientations. The result is that all external translational lattice vibrations whether optical, acoustical, transverse or longitudinal will become active in both the infrared and Raman spectra. In each case there will be densities of states having $\underline{K} \neq 0$.

Whalley and Bertie preface their treatment of a three dimensional crystal by considering the simple case of a monatomic chain which has masses, M. The equation of motion for the s^{th} member of the chain may be written as:

$$M\frac{d^2X_s}{dt^2} = \sum_p f_p(X_{s+p} - X_s) \qquad (1)$$

In the summation p runs over all positive and negative integers such that all interactions of the s^{th} atom with its neighbours are considered; f_p is the force constant connecting the s^{th} atom to its p^{th} neighbour.

If we associate the integers s and p with planes in a monatomic lattice we may have longitudinal or transverse polarizations (55). The f_p will, in general, be different in each case.

We look for solutions of equation 1 in the form of travelling waves. Convenient trial solutions are:

$$X_s = A \exp i\{ska - \omega t\}$$

$$X_{s+p} = A \exp i\{(s+p)ka - \omega t\} \qquad (2)$$

where a is the lattice constant. When the trial solutions are substituted into equation 1 we have the new equation of motion:

$$\omega_k^2 = \frac{2}{M} \sum_{p>0} f_p(1-\cos pka) \qquad (3)$$

The displacement $X_{s,k}$ of the s^{th} plane during the vibration k will be:

$$X_{s,k} = A \exp\{i\, ska\} \cdot \exp\{-i\, \omega_k t\}$$

$$= L_{s,k}\, Q_k \qquad (4)$$

where Q_k is the normal co-ordinate for the k^{th} vibration.

The displacements $X_{s,k}$ and $X_{s+p,k}$ are related to the dipole moment derivative for the lattice; i.e. we may write the dipole moment derivative as:

$$\frac{\partial \underset{\sim}{u}}{\partial Q_k} = \sum_{s,p} \frac{\partial \underset{\sim}{u}}{\partial (X_{s+p} - X_s)} \cdot \frac{\partial (X_{s+p} - X_s)}{\partial Q_k} \qquad (5)$$

This sum is identically zero unless $\underline{K} = 0$ and for our monatomic lattice it is always zero since the $\underline{K} = 0$ vibration is a pure translation. Disorder may be introduced into the lattice by randomly placing positive or negative charges on the atoms. Thus, the $\partial\underset{\sim}{u}/\partial(X_{s+p} - X_s) = q_p$ will be randomly positive or negative for all pairs of atoms. Whalley and Bertie show that under these conditions the most probable value of $(\partial\underset{\sim}{u}/\partial Q_k)^2$ is non-vanishing and we have:

$$(\partial\underset{\sim}{u}/\partial Q_k)^2 = \sum_{s,p} q_p^2 (L_{s+p,k} - L_{s,k})^2 \qquad (6)$$

The infrared absorption intensity is proportional to $(\partial\underset{\sim}{u}/\partial Q_k)^2$ and the implication is that for the acoustical modes, whether transverse or longitudinal, absorption bands may appear with densities of states having $\underline{K} \neq 0$ present. The intensity of Raman scattering is given by a similar treatment except that the derivatives of the polarizability with respect to the normal co-ordinate replace the derivative of the dipole moment. If a diatomic chain is considered the results may be extended to include optical modes.

The two different treatments of disorder; i.e. by Lifshitz and by Whalley and Bertie are really complementary. In the Lifshitz model the force constants between the atoms are assumed to remain fixed and only the masses of the atoms are allowed to change; whereas in Whalley and Bertie's model the masses of the atoms remain the same and only the orientations of neighbouring dipoles change - this orientational disorder may be associated with a change in force constants. Lifshitz has

shown (27) that when these two complementary treatments are considered in a quantum mechanical context they will lead to perturbations which are completely analogous.

Since the phase II ammonium halides possess orientational disorder (i.e. the NH_4^+ ions may randomly take up two alternate orientations) the results we have discussed will apply. If one assumes that only interactions between nearest neighbour NH_4^+ ions change the prediction of the Lifshitz theory for NH_4Cl is that the intensities of $\underline{K} \neq 0$ bands will be proportional to $p(1-p)$ where p is the probability that a given nearest neighbour NH_4^+ - NH_4^+ pair are oriented "parallel" to each other. In the case of NH_4Br p will be the probability that a given nearest neighbour NH_4^+ - NH_4^+ pair are oriented "antiparallel" to each other. The qualifications of "parallel" or "antiparallel" correspond to the arrangement of the NH_4^+ ions in the ordered phase IV and phase III structures. For the completely disordered state $p = \frac{1}{2}$ and for the ordered state $p = 1$.

Among the translational vibrations of the ammonium halides the only evidence for bands appearing as a result of disorder is in the Raman spectra of NH_4Cl(II) and NH_4Br(II). The low wavenumber scatterings of interest have been observed by Couture-Mathieu and Mathieu (1952) and by Perry and Lowndes (1969). In the earlier work assignments were not made and in the more recent work of Perry and Lowndes attempts to assign the scatterings to two phonon sum or difference bands were inconclusive. Evidently the effects of disorder were not considered. If disorder is considered the observed scatterings may all be accounted for. Below are the frequencies of the low wave number phase II scatterings

observed by previous workers. The assignments belong to this work.

	NH_4Cl(II)		NH_4Br(II)	
	REF. 58	REF. 29	REF. 58	REF. 29
TA($K \neq 0$)	95	88	55	56
LA($K \neq 0$)	140	143	135	136
TO($K = 0$)	170 (172)	170	- (147)	147
TO($K \neq 0$)	195	197	185	~190

The bracketted frequencies are observed in the infrared and are associated with the $\underline{K} = 0$ phonons. In the case of NH_4Cl(II) the 170 cm^{-1} $\underline{K} = 0$ scattering shifts on cooling to the phase IV 183 cm^{-1} $\underline{K} = 0$ scattering. The highest wave number scatterings may be associated with TO($K \neq 0$) phonons since the Lifshitz theory predicts that they may be shifted in frequency relative to the allowed $\underline{K} = 0$ mode. In the case of the TA($\underline{K} \neq 0$) and LA($\underline{K} \neq 0$) scatterings the frequency separation is about 50 cm^{-1} for NH_4Cl(II) and about 80 cm^{-1} for NH_4Br(II). This compares with a zone edge frequency separation of about 75 cm^{-1} for ND_4Cl(IV). The ND_4Cl(IV) zone edge TA phonon lies at 100 cm^{-1} and compares with the NH_4Cl(II) scattering at 95 cm^{-1}.

Recently Garland and Schumaker (28) have applied the predictions of the Lifshitz theory to the anomalous high wave number component of ν_4. This anomalous component is present in all infrared phase II spectra (see for example Figure 4-9). Garland and Schumaker have considered ammonium chloride in particular. By using an Ising model to approximate the disorder-order transition they were able to relate the heat capacity

FIGURE 4—9

THE TEMPERATURE DEPENDENCE OF ν_4 — NH_4Cl AND ND_4Cl

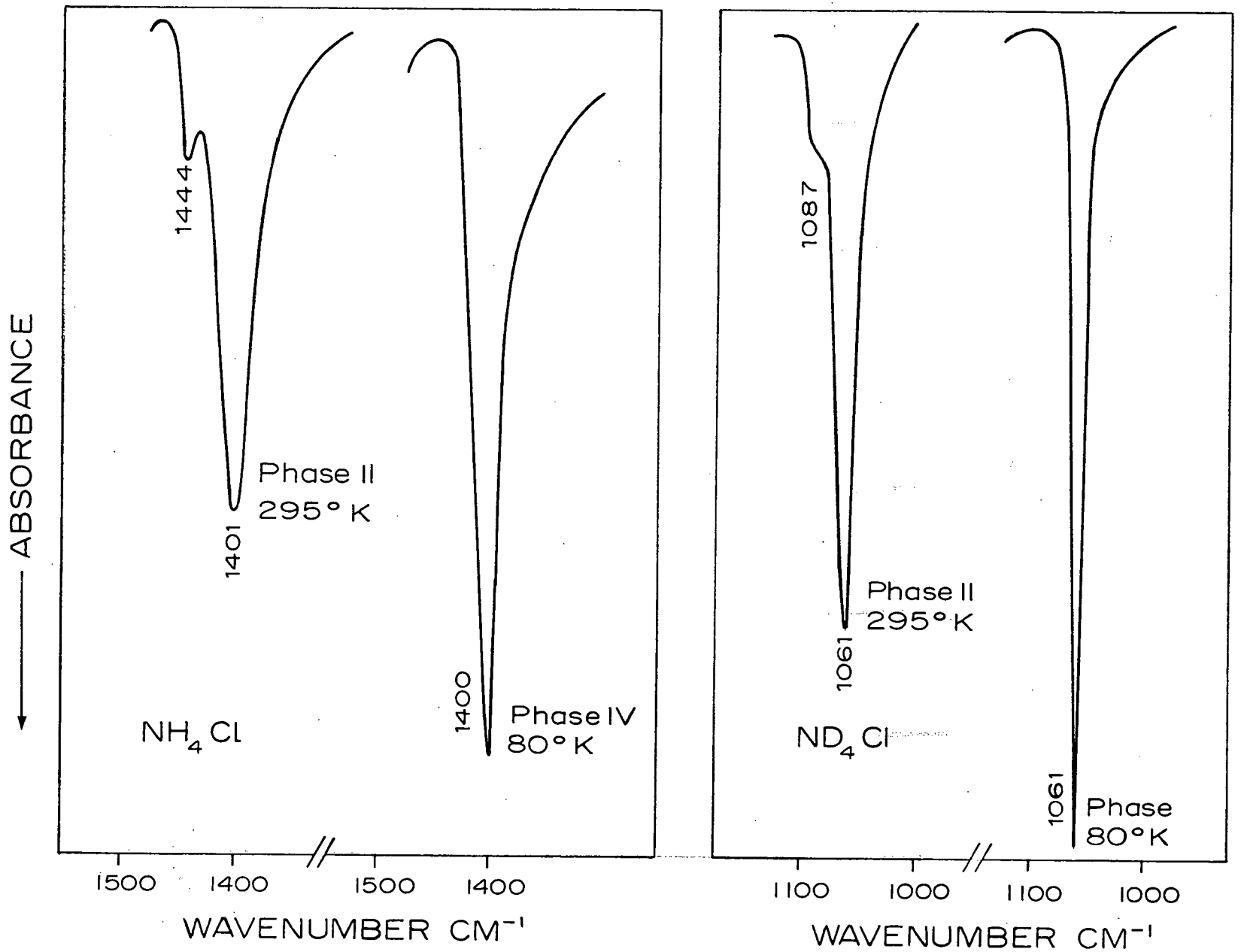

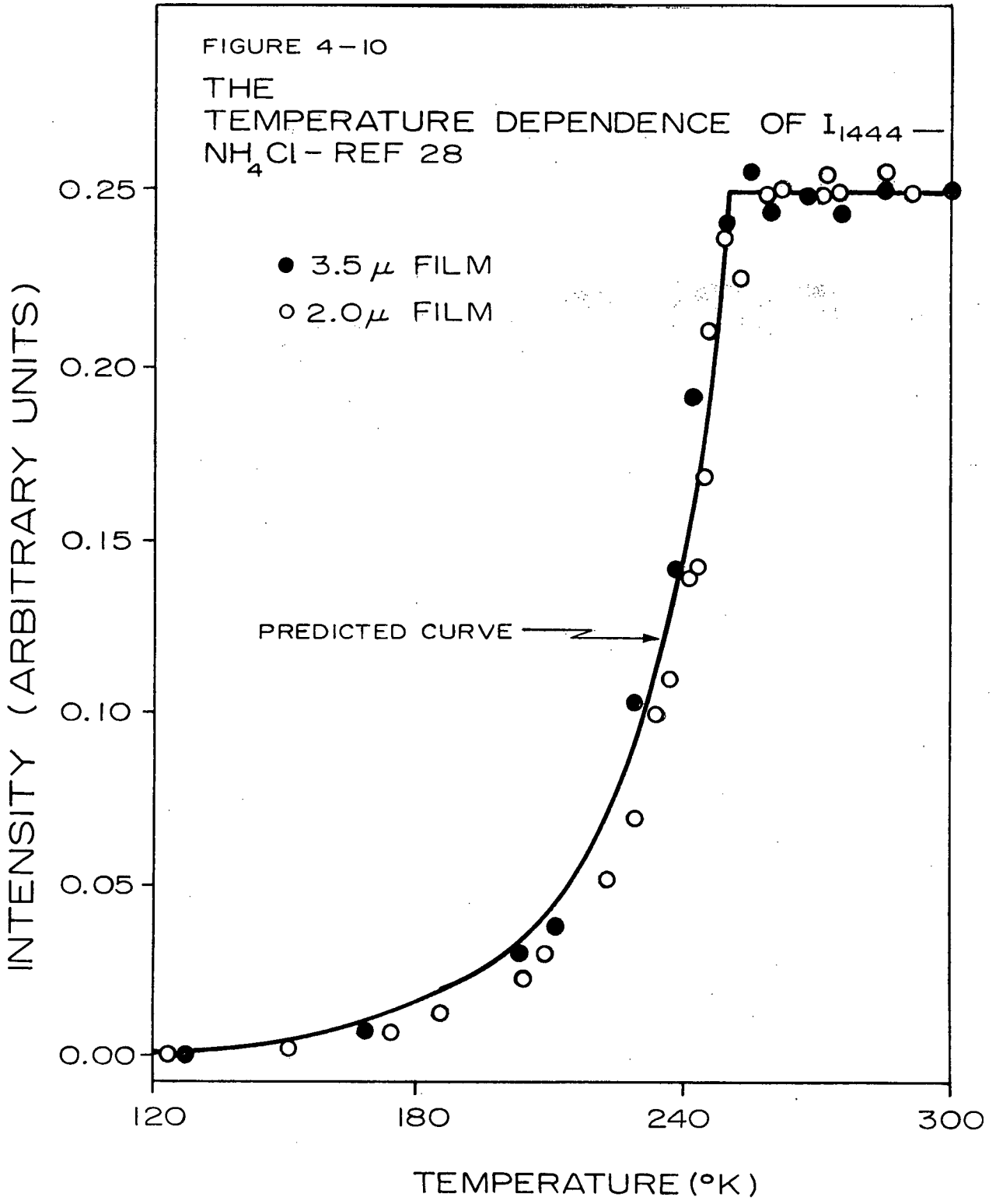
FIGURE 4-10
THE
TEMPERATURE DEPENDENCE OF I_{1444} —
NH_4Cl - REF 28
● 3.5 μ FILM
○ 2.0 μ FILM
PREDICTED CURVE
INTENSITY (ARBITRARY UNITS)
0.25
0.20
0.15
0.10
0.05
0.00
120
180
240
300
TEMPERATURE (°K)

data for ammonium chloride to the configurational energy of an Ising model and so calculate p(1-p) as a function of temperature. By referring to Figure 4-10 which reproduces Garland and Schumaker's results it is seen that the predicted and observed intensities of I_{1444} for the disorder-order process are in excellent agreement. At the transition temperature of 242.2°K there is seen to be a pronounced discontinuity in the intensity curve for I_{1444} and the progress of the ensuing ordering process is evidenced by a progressive loss in intensity for I_{1444}. When the ordering process is complete there is zero intensity. The behaviour of I_{1444} for the disorder-order process may be summarized as:

$$I_{1444}\ \{\nu_4(\underline{K} \neq 0)\} \rightarrow \text{zero intensity}$$

The fact that the intensity behaviour of I_{1444} so closely parallels that predicted by the Lifshitz theory suggests that similar considerations may apply to internal modes such as ν_4 as well as external modes of translatory origin.

Figure 4-12 shows the temperature dependence of ν_4 for ammonium bromide as observed in this work. The components appearing in phase II are $I_{1399}\ \{\nu_4(\underline{K} = 0)\}$ and $I_{1427}\ \{\nu_4(\underline{K} \neq 0)\}$. At the transition temperature of 234.57°K there is a discontinuity in the intensity curves for both I_{1399} and I_{1427}. As the ordering process progresses, I_{1399} over a temperature interval of about 25° gradually loses intensity and also gradually shifts to I_{1405}. This behaviour may be summarized as:

$$I_{1399}\{\nu_4(\underline{K}=0)\} \rightarrow I_{1405}\{\nu_4(E_u)\}.$$

For I_{1427} there is an apparent gradual increase in intensity and also a gradual shift to I_{1433} associated with the disorder-order process. This behaviour is summarized as follows:

$$I_{1427}\{\nu_4(K\neq 0)\} \rightarrow \text{zero intensity}$$

$$I_{1399}\{\nu_4(K=0)\} \rightarrow I_{1433}\{\nu_4(A_{2u})\}$$

Thus, the appearance of $I_{1433}\{\nu_4(A_{2u}\}$ obscures the temperature dependence of $I_{1427}\{\nu_4(K\neq 0)\}$. The intensity curves for ammonium bromide do not show experimental results for the order-order transition, III → IV. This is because this transition occurs at about 78°K on cooling (7) which is just below the low temperature limit of the liquid nitrogen cell used for these experiments. Reference to Figure 4-13, however, will show the results for the III → IV transition for the fully deuterated salt. It is seen that both $I_{1066}\{\nu_4(E_u)\}$ and $I_{1089}\{\nu_4(A_{2u})\}$ show marked discontinuities at the transition temperature of 166.7°K. At this temperature the intensity of I_{1089} begins to abruptly decrease to zero, while the intensity of I_{1066} shows an abrupt increase which is accompanied by an abrupt frequency shift to 1060 cm^{-1}. Thus we have:

$$I_{1089}\{\nu_4(A_{2u})\} \rightarrow \text{zero intensity}$$

$$I_{1066}\{\nu_4(E_u)\} \rightarrow I_{1060}\{\nu_4(F_2)\}$$

The discontinuous intensity changes and discontinuous frequency shifts associated with the III → IV order-order transition contrast sharply with the results for the II → III disorder-order transition which is

FIGURE 4 — 11

THE TEMPERATURE DEPENDENCE OF ν_4 — NH_4Br AND ND_4Br

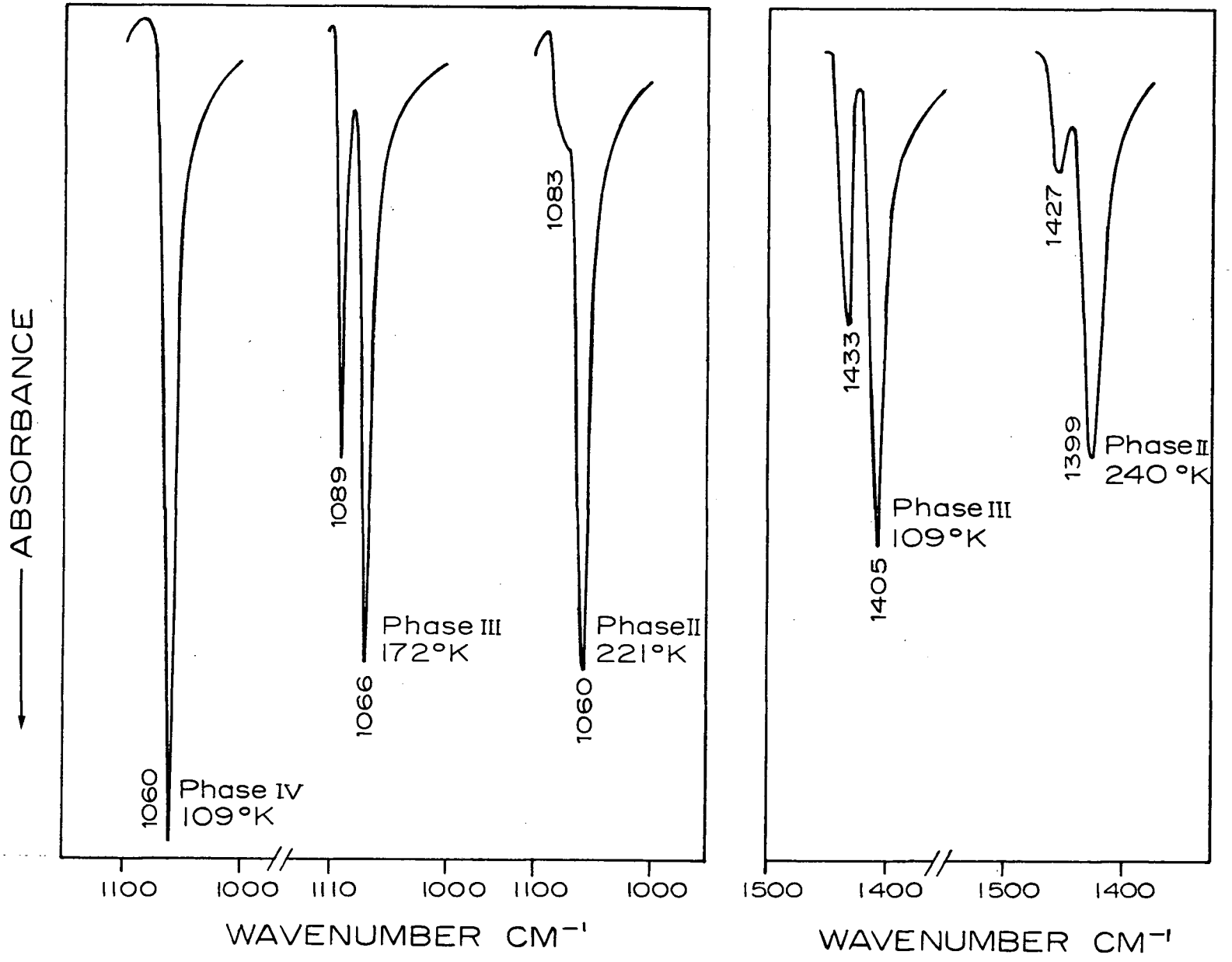

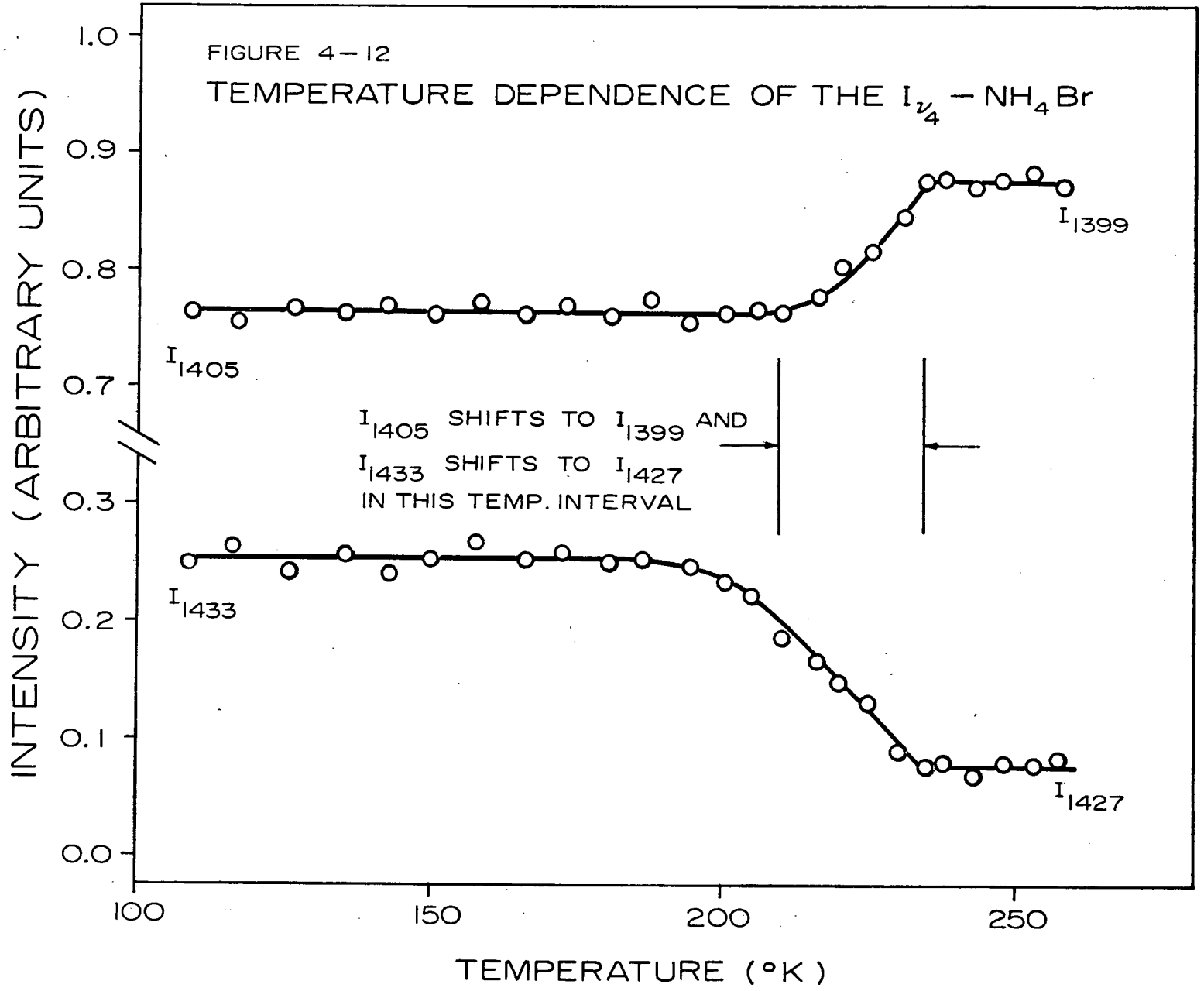
FIGURE 4-12
TEMPERATURE DEPENDENCE OF THE $I_{1/4}$ - NH_4Br
INTENSITY (ARBITRARY UNITS)
1.0
0.9
0.8
0.7
0.3
0.2
0.1
0.0
100
150
200
250
TEMPERATURE (°K)
I_{1399}
I_{1405}
I_{1405} SHIFTS TO I_{1399} AND
I_{1433} SHIFTS TO I_{1427}
IN THIS TEMP. INTERVAL
I_{1433}
I_{1427}

FIGURE 4—13

TEMPERATURE DEPENDENCE OF THE I_{ν_4}—ND_4 Br

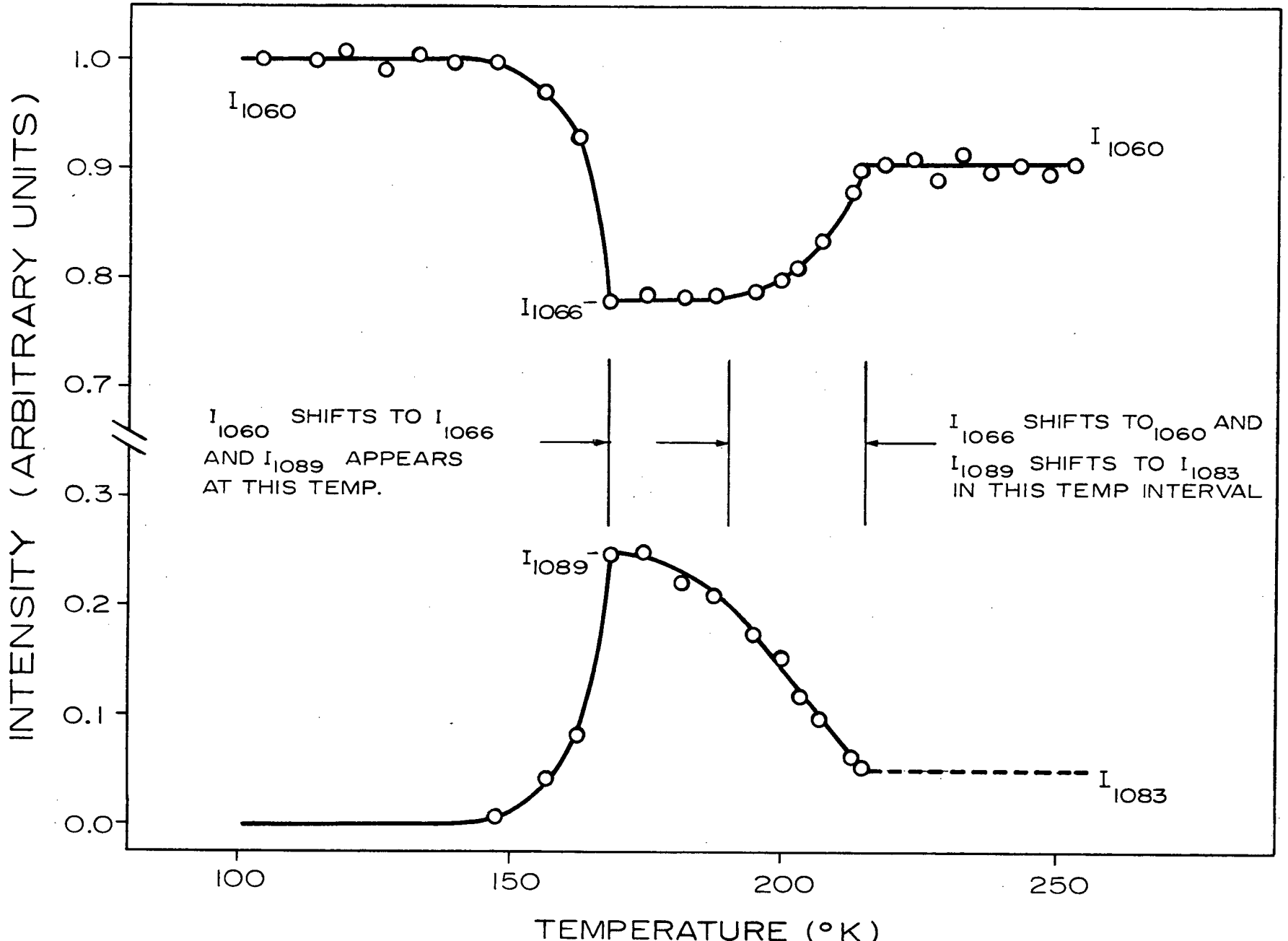

accompanied by gradual intensity changes and a gradual frequency shift. These results, then, provide striking spectroscopic evidence for the two different types of phase transitions which occur in ammonium bromide.

Figures 4-9 and 4-11 show the infrared spectra of ν_4 for the various phases of both ammonium chloride and ammonium bromide. It may be noted that the anomalous components of ν_4 did not appear with observable intensity in the Raman spectra.

The triply degenerate vibration, ν_3, as observed in phase II spectra shows no evidence of distinct components either in the infrared or Raman which may be assigned to states with $\underline{K} \neq 0$. However, ν_3 as observed in both the infrared and Raman is a very intense broad band. In the infrared the half-height band width is some 140 cm^{-1} for the protonated salts and some 120 cm^{-1} for the deuterated salts. These values compare with corresponding half-height band widths of some 60 and 75 cm^{-1} for the ordered phases of the protonated and deuterated salts respectively. It is found that there is pronounced ν_3 band sharpening as the disorder-order transition progresses and thus it is very likely that some of the intensity of ν_3 in phase II spectra is due to the presence of a density of states with $K \neq 0$. Also, ν_3 exhibits anomalous behaviour in that it shifts significantly to lower frequency as a result of the disorder-order transformation. For the ammonium chlorides and ammonium bromides this shift is 12 ± 2 cm^{-1}. Such behaviour is consistent with the presence of a density of states with $\underline{K} \neq 0$ on the high wave number side of a band due to an allowed $\underline{K} = 0$ transition. However, it is to be remembered

TABLE 4-6. Assignments for NH_4Cl(II) and ND_4Cl(II); cm^{-1}

Assignment	NH_4Cl(II) - THIS WORK See also refs. 29,31 R.	22 I.R.	ND_4Cl(II) - THIS WORK See also refs. R.	22 I.R.
ν_1	3050		2218	
ν_2	1709.5		1220	
ν_3	3138		2348	2346
ν_4	1403	1401	1064	1061
$\nu_4(K\neq 0)$		1444		1087(sh)
L_1		(359)*		(263)
T_1		177		170
$\nu_2+\nu_4$	—	3044	—	2248
$2\nu_4$	2818	2810	2140	2128
$2\nu_4$			2116	

* a neutron inelastic scattering result - Ref. 3.

TABLE 4-7. Assignments for NH_4Br(II) and ND_4Br(II); cm^{-1}

	NH_4Br(II) - THIS WORK See also refs.		ND_4Br(II) - THIS WORK See also refs.	
Assignment	29,31	23		23
	R.	I.R.	R.	I.R.
ν_1	3039		2215	
ν_2	1685.5		1205	
ν_3	3128	3128	2347	2345
ν_4	1401	1399	1063	1060
ν_4(K≠O)		1427		1083(sh)
L_1		(311)		(233)*
T_1		154		139
$\nu_2+\nu_4$		3028		2240
$2\nu_4$	2803	2797	2125	2119
$2\nu_4$			2104	

* a neutron inelastic scattering result - Ref. 3.

that such behaviour could also be related to an increase in hydrogen bonding as a result of the phase change.

A summary of the assignments for the fundamental modes associated with the phase II ammonium halides is given in Tables 4-6 and 4-7. It will be noted that included in these two tables are assignments for $2\nu_4$ and $\nu_2 + \nu_4$; the only lines which appear in the second order spectra of the phase II salts.

4-4 Ammonium Fluoride

Ammonium fluoride has a crystal structure compatible with the space group $C_{6v}^4(P6_3mc)$. The vibrational analysis is carried out under the C_{6v} factor group - results for the various types of vibrations are summarized below.

$$\Gamma(\text{internal}) = 3A_1 + 3B_1 + 3E_1 + 3E_2$$

$$\Gamma(OT) = A_1 + 2B_1 + E_1 + 2E_2$$

$$\Gamma(OL) = A_2 + B_2 + E_1\ E_2$$

$$\Gamma(AT) = A_1 + E_1$$

The four fundamental modes associated with the free ammonium ion become the precursors of the 12 internal crystal modes which arise from both static field (site group) and correlation field (factor group) splitting. This is illustrated by the correlation diagram which follows.

Fundamental Mode	Free Ion Symmetry-T_d		Site Group Symmetry-C_{3v}		Factor Group Symmetry-C_{6v}
ν_1	A_1	→	A_1	→	A_1, B_1
ν_2	E	→	E	→	E_1, E_2
ν_3	F_2	→	A_1, E	→	A_1, B_1, E_1, E_2
ν_4	F_2	→	A_1, E	→	A_1, B_1, E_1, E_2

The symmetry species A_1, E_1 and E_2 contain elements of the polarizability tensor and hence will be associated with Raman active vibrations. Only vibrations of A_1 and E_1 symmetry species are infrared active.

In section 1-1 the point was made that although the NH_4^+ ions in ammonium fluoride lie on sites of C_{3v} symmetry, the crystal geometry is such that it is compatible with a tetrahedral configuration for the NH_4^+ ions. It was further noted that a tetrahedral configuration is also supported by the fact that Plumb and Hornig (21) found no observable splitting for ν_4 in the infrared spectrum of crystalline ammonium fluoride. From the infrared spectra Plumb and Hornig were able to assign $\nu_3(A_1, E_1)$ and $\nu_4(A_1, E_1)$ for both NH_4F and ND_4F. The Raman spectra recorded in this work of both NH_4F and ND_4F show only three lines with observable intensity and these have been assigned to $\nu_1(A_1)$, $\nu_3(A_1, E_1, E_2)$ and $\nu_T(A_1, E_1, E_2)$. It was found that there was no significant frequency discrepancy between $\nu_3(A_1, E_1)$ as observed in the infrared and $\nu_3(A_1, E_1, E_2)$ as observed in the Raman. Unfortunately $\nu_2(E_1, E_2)$ was not observed in the Raman spectrum of either NH_4F or ND_4F. If the frequency of ν_2 is inferred from $\nu_2 + \nu_4$ as observed

in the infrared the frequencies of the internal fundamentals for NH_4F are 2874, 1728, 2815 and 1494 cm^{-1} for ν_1, ν_2, ν_3 and ν_4 respectively. For ND_4F the corresponding frequencies are 2117, 1240, 2148 and 1120 cm^{-1} (see also Table 4-8). As noted by Plumb and Hornig the most striking feature associated with these ammonium fluoride frequencies is the relatively low frequencies of the stretching modes as compared to the corresponding frequencies of, say, the phase IV ammonium chlorides. Comparing NH_4F and NH_4Cl(IV) it is found that ν_1 suffers a shift of 175 cm^{-1} and the corresponding shift for ν_3 is 311 cm^{-1}. For the deuterated analogs the corresponding ν_1 and ν_3 shifts are 98 and 184 cm^{-1} respectively. This behaviour is indicative of greatly enhanced hydrogen bonding in ammonium fluoride.

The obvious combinations and overtones appearing in the infrared spectra of the ammonium fluorides which were observed and assigned by Plumb and Hornig are $\nu_4 + \nu_R$, $\nu_2 + \nu_R$, $2\nu_4$ and $\nu_2 + \nu_4$. In addition to the above absorptions the infrared spectrum of both NH_4F and ND_4F possesses two absorptions of moderate to strong intensity which are not readily assigned. For NH_4F the absorptions in question appear at 3082 and 3010 cm^{-1}. Plumb and Hornig have assigned these two lines to $\nu_4 + 3\nu_R$ and a second component of $2\nu_4$ respectively. The corresponding anomalous lines for ND_4F appear at 2323 and 2251 cm^{-1}. They have been assigned respectively to $\nu_1 + \nu_T$ and $\nu_4 + 3\nu_R$. These assignments are not altogether satisfactory and, indeed, Plumb and Hornig (21) make the following comment on the assignments $\nu_4 + 3\nu_R$. "The biggest problem

(in making assignments) is the strong band at 3082 cm^{-1} in NH_4F and 2251 cm^{-1} in ND_4F. It has been assigned to $\nu_4 + 3\nu_6(\nu_4 + 3\nu_R)$, but it is startling that such a high combination should appear with such intensity. Furthermore, the observed frequency is some 40 cm^{-1} higher than predicted, and this can only be correct if the frequency is raised by Fermi resonance with some of the lower frequencies. At present the situation on this peak cannot be considered satisfactory." Also, the assignment of the 3010 line in the spectrum of NH_4F is not realistic for the following reasons: no such second component is observed for ND_4F and the frequency is some 20 cm^{-1} higher than that predicted by the frequency of ν_4 as observed in the infrared. It would appear that the assignment of the 2323 cm^{-1} line in the spectrum of ND_4F to $\nu_1 + \nu_T$ is correct. Such an assignment gives a frequency 31 cm^{-1} below that predicted providing ν_T is taken as the Raman observed frequency of 237 cm^{-1}. Now, if the original assignment of the 3082 cm^{-1} NH_4F absorption to $\nu_4 + 3\nu_R$ is changed to $\nu_1 + \nu_T$ the predicted-observed frequency discrepancy is -41 cm^{-1} providing ν_T has a frequency equal to the Raman frequency of 247 cm^{-1}. We are now left with the 3010 cm^{-1} NH_4F line and the 2251 cm^{-1} ND_4F line. A possible assignment is ν_1 in combination with acoustical modes. Such a situation would compare with that already inferred for the phase IV and phase III ammonium halides. Assuming the assignment $\nu_1 + \nu_A$ gives acoustical modes at 136 and 134 cm^{-1} respectively for NH_4F and ND_4F. Using the approximation of a linear lattice zone edge acoustical modes for NH_4F and ND_4F are calculated to lie at 179 and 176 cm^{-1}. Thus, the inferred modes are within the frequency limits predicted for the

TABLE 4-8. Assignments for NH_4F and ND_4F; cm^{-1}

	NH_4F		ND_4F	
Assignment	THIS WORK R.	Ref. 11 I.R.	THIS WORK R.	Ref. 11 I.R.
ν_1	2874		2117	
ν_2		(1728)*		(1240)
ν_3	2818	2815	2145	2148
ν_4		1494		1120
ν_R		(523)		(376)
ν_T	247		237	
$\nu_A(K\neq 0)$		(136)		(134)
$\nu_1+\nu_T$		3082		2323
$\nu_1+\nu_A$		3010		2251
$\nu_2+\nu_4$		3222		2360
$2\nu_4$		2974		2233
$\nu_2+\nu_R$		2277		1633
$\nu_4+\nu_R$		2017		1496

* the bracketed frequencies have been inferred from infrared active combinations; the ν_A frequencies are inferred assuming relatively flat ν_1 phonon dispersions.

acoustical modes.

4-5 The Barrier to Rotation

The barrier to rotation for NH_4^+ ions in a CsCl type lattice has been treated by Nagamiya (63). He assumed a particular charge distribution for the tetrahedral NH_4^+ ion by placing a charge of $+\delta e$ on each hydrogen atom. The potential energy of one of the hydrogen atoms at an arbitrary point, (X_i, Y_i, Z_i) in the unit cell with respect to all charges outside its own can then be written as:

$$\phi = \frac{1}{a}\left[C_o + C_4\left(\frac{r}{a}\right)^4\left(\frac{x_i^4 + y_i^4 + z_i^4}{r^4} - \frac{3}{5}\right) + \ldots\ldots\right] \qquad (1)$$

where a is the lattice parameter and N is the N-H distance in the NH_4^+ ion. The second term of this expression represents the angular dependence of the potential energy. Hence the potential appropriate for rotation of the ammonium ion in a CsCl type lattice is:

$$\phi = \frac{\phi_o}{2} \sum_{i=1}^{4}\left\{\frac{x_i^4 + y_i^4 + z_i^4}{r^4} - \frac{3}{5}\right\} \qquad (2)$$

In this expression ϕ_o is directly related to the barrier to rotation. For rotation about a four fold axis the barrier height is $(9/4)\phi_o$ (28).

Gutowsky, Pake and Bersohn (64) use equation 2 to consider the librational modes of the ammonium ion. Restricting their treatment to the simple case in which the ammonium ion executes only small vibrations about the cubic (x, y, z) axis of the unit cell, they developed an approximate potential which may be written:

$$V = \frac{V_o}{2}\left\{-\frac{12}{5} + 8(\xi^2 + \eta^2 + \zeta^2) - \frac{32}{5}(\xi^2 + \eta^2 + \zeta^2) - 8(\xi^2\eta^2 + \xi^2\zeta^2 + \eta^2\zeta^2) + \ldots\ldots\right\} \quad (3)$$

and where ξ, η and ζ are the angles of rotation about the cubic (X, Y, Z) axes. Clearly, the assumption of small oscillations implicit in the model yielding the above four-fold cosine type potential is appropriate for the ordered cubic phases of the ammonium halides.

With the use of first order perturbation theory Gutowsky, Pake and Bersohn were able to arrive at an expression for the energy levels of the anharmonic oscillator described by their model. The result they obtained is:

$$E_{n1,n2,n3} = -\frac{6}{5}V_o + \left\{n_1 + n_2 + n_3 + \frac{3}{2}\right\}\hbar\omega - \frac{1}{16}\left\{2n_1^2 + 2n_2^2 + 2n_3^2 + n_1n_2 + n_1n_3 + n_2n_3 + 3n_1 + 3n_2 + 3n_3 + \frac{5}{4}\right\}(\hbar\omega)^2/V_o \quad (4)$$

where $(\hbar\omega) = (16V_o\hbar^2/2I)^{\frac{1}{2}}$ and I is the moment of inertia of the NH_4^+ ion. Using equation 4 it is possible to calculate V_o when the value of $(E_{100} - E_{000})$ is known from the librational frequency; i.e.

$$V_o = \frac{1}{16}\frac{(\hbar\omega + 5\hbar^2/2I)^2}{\hbar^2/2I} \quad (5)$$

The expression for V_o defined by equation 5 although derived for the ordered cubic phase can reasonably be applied to the ordered tetragonal phase since the distortion from cubic symmetry is slight.

The computed values for Vo(G.P.B.) using equation 5 are included in Table 4-9. Also included are the barrier heights, Vo(N.M.R.), which

TABLE 4-9. Librational Frequencies and Barrier Heights; (cm^{-1})*

	NH_4Cl(IV)	NH_4Br(IV)	NH_4Br(III)	NH_4I(III)
ν_R(N.S.)	389	—	335	293
ν_R(R)			336	291
$\nu_R(\nu_4+\nu_R)$	390	349	337	290
V_o(G.P.B.)	1861	1515	1420	1080
V_o(N.M.R.)	1650	—	1400	1110

	ND_4Cl(IV)	ND_4Br(IV)	ND_4Br(III)	ND_4I(III)
ν_R(N.S.)	280	254	—	—
ν_R(R)			—	208
$\nu_R(\nu_4+\nu_R)$	280	251	241	208
V_o(G.P.B.)	1836	1492	1382	1049

* the frequencies ν_R(N.S.), ν_R(R) and $\nu_R(\nu_4+\nu_R)$ have been respectively obtained from neutron scattering (3), Raman and $\nu_4+\nu_R$ Raman results. The underlined frequencies have been used to calculate the V_o(G.P.B.). The V_o(N.M.R.) are found in references 65,66 and 67.

FIGURE 4-14

BARRIER HEIGHTS AS A FUNCTION OF THE LATTICE PARAMETER

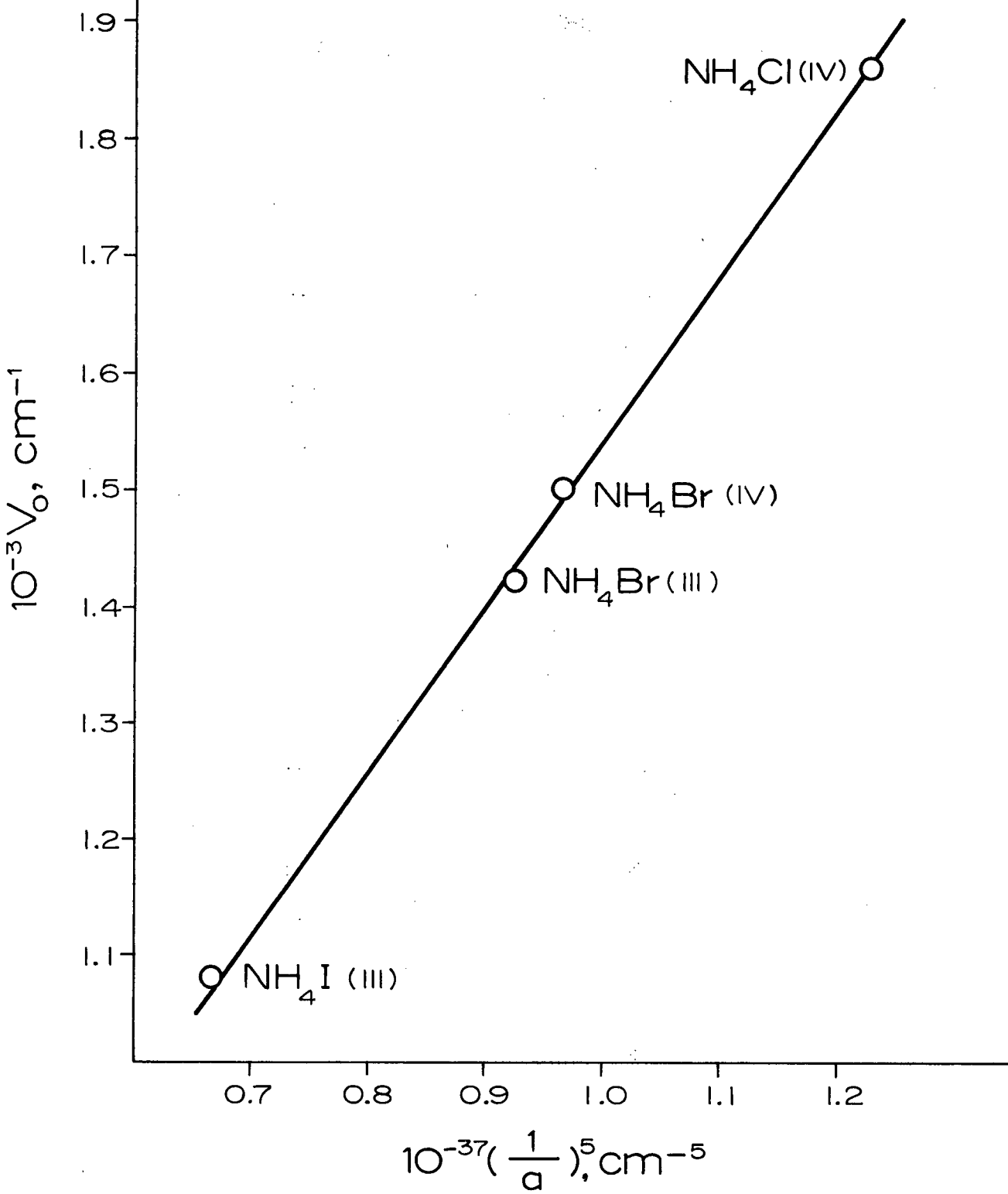

have been obtained from N.M.R. measurements (65,66,67). It is seen that the Vo(G.P.B.) and the Vo(N.M.R.) compare favorably.

Gutowsky, Pake and Bersohn (64) have shown that if the NH_4^+ ion is assumed electrically to be a system of point charges of + e/4 at the vertices of a rigid regular tetrahedron then the relation $Vo \alpha r^4/a^5$ holds. Figure 4-14 shows that a plot of Vo(G.P.B.) versus $a^{-5}(\{a/\sqrt{2}\}^{-5}$ for the tetragonal salts) gives a linear relation as predicted by the point charge model.

4-6 The Force Field of Crystalline NH_4^+

Since the frequencies of the fundamental modes of vibration of crystalline NH_4^+ are well known we may use these frequencies to compute the force field for the crystalline ammonium ion. The computations may be performed using the simple mixing program of Green and Harvey (47). The equation which is basic to this program is equation 29 of section 3-1; i.e.

$$\underline{\underline{F}} = \underline{\underline{U}}\ \underline{\underline{\Gamma}}^{-\frac{1}{2}}\underline{\underline{P}}\ \underline{\underline{\Lambda}}\ \underline{\underline{P}}^t\underline{\underline{\Gamma}}^{-\frac{1}{2}}\underline{\underline{U}}^t$$

In the case of tetrahedral NH_4^+ there is one redundant symmetry co-ordinate and so the dimension of all the matrices appearing in the above equation will be 10 x 10. Once the vibrational frequencies and the molecular geometry of the basis molecule are made available to the program, the $\underline{\underline{G}}$ matrix and also the orthogonal matrix $\underline{\underline{U}}$ diagonalizing $\underline{\underline{G}}$ are constructed. This yields the three matrices defined in equation 27 of section 3-1; i.e.

$$\underline{\underline{U}}^t\ \underline{\underline{G}}\ \underline{\underline{U}} = \underline{\underline{\Gamma}}$$

The vibrational frequencies directly yield the matrix $\underline{\underline{\Lambda}}$. The one remaining matrix required is the orthogonal matrix, $\underline{\underline{P}}$. It was noted in section 3-1 that this matrix has the important property that the elements P_{ij} of $\underline{\underline{P}}$ equal zero unless λ_i and λ_j belong to the same symmetry class.

For our calculations a suitable orthogonal matrix $\underline{\underline{P}}$ is:

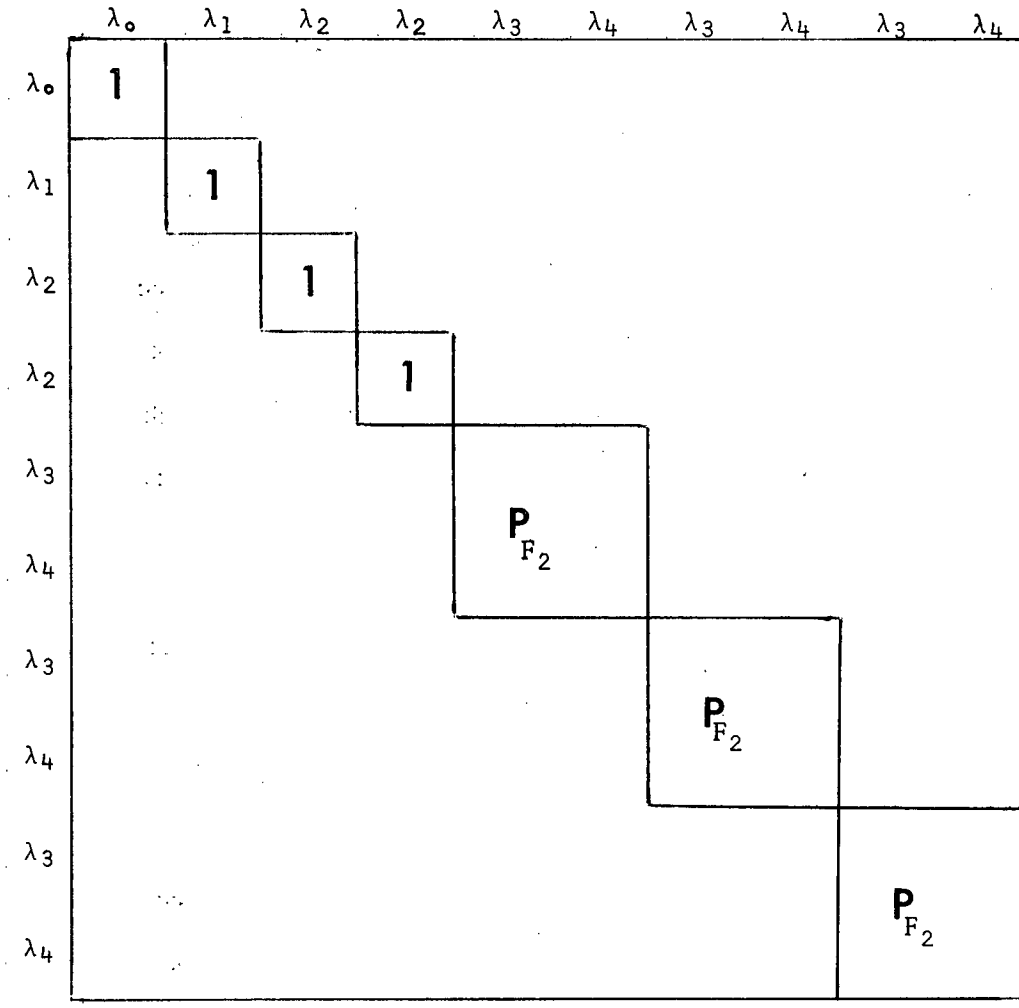

where:
$$P_{F_2} = \begin{bmatrix} 1/\sqrt{1+X^2} & -x/\sqrt{1+X^2} \\ x/\sqrt{1+X^2} & 1/\sqrt{1+X^2} \end{bmatrix}$$

Only the one parameter, X, appears and the force field problem is one dimensional. X has the effect of mixing the computed F_3 (stretching), F_4 (bending) and F_{34} (stretch-bend) symmetry force constants and may be referred to as the mixing parameter. There will be a family of acceptable force constants; each set in the family corresponding to a particular value of the mixing parameter. Inspection of the orthogonal matrix $\underline{\underline{P}}$ shows that the F_1 (stretching) and F_2 (bending) force constants do not depend on X.

Calculations have been carried out with the NH_4^+ ion of NH_4Br(IV) chosen as the basis molecule. Reference to Figures 4-15 and 4-16 shows the variation of F_3, F_4 and F_{34} with the mixing parameter on the interval $-1.2 \leq X \leq 1.2$. Calculated ND_4^+ ν_3 and ν_4 frequencies using the NH_4^+ force constants are shown in Figure 4-17. It is found that the two values of X which respectively reproduce the observed ND_4^+ ν_3 and ν_4 frequencies do not coincide; so it is convenient to choose their mean as the value of X which gives the "best" computed spectrum. In Table 4-10 which shows calculated and observed spectra this mean value of X is denoted as X_3. When NH_4^+ is chosen as the basis molecule the average absolute deviation of computed ND_4^+ frequencies from observed frequencies is 23 cm^{-1}. The NH_4^+ force constants used to compute the ND_4^+ spectrum are as follows:

Force Constant (10^5 Dynes/cm.)
F_1 = 5.51026
F_2 = 0.60485
F_3 = 5.28516
F_4 = 0.52378
F_{34} = 0.07670

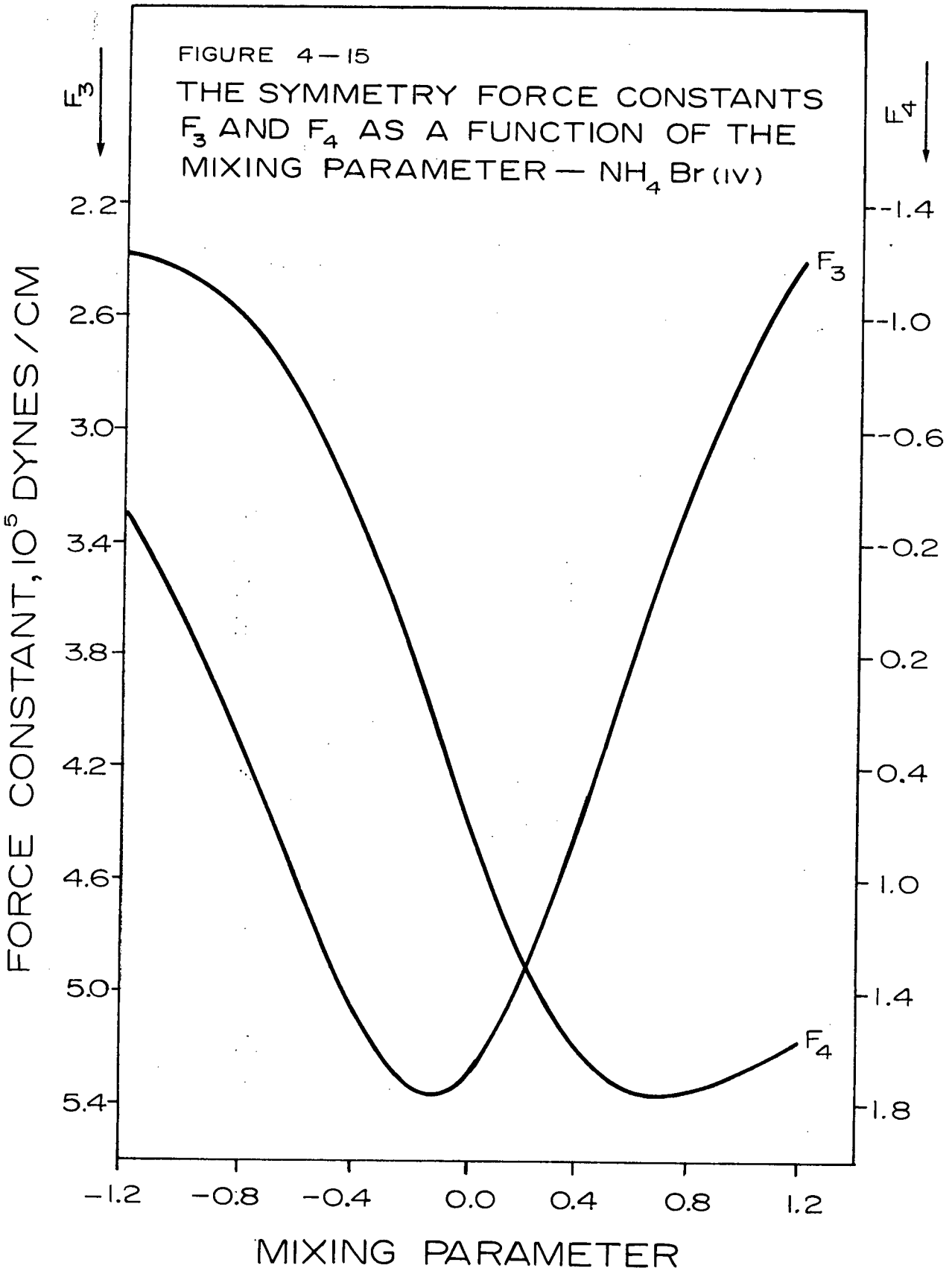

FIGURE 4—15

THE SYMMETRY FORCE CONSTANTS F_3 AND F_4 AS A FUNCTION OF THE MIXING PARAMETER — NH_4Br (IV)

FIGURE 4—16

THE SYMMETRY FORCE CONSTANT, F_{34} AS A FUNCTION OF THE MIXING PARAMETER — NH_4Br (IV)

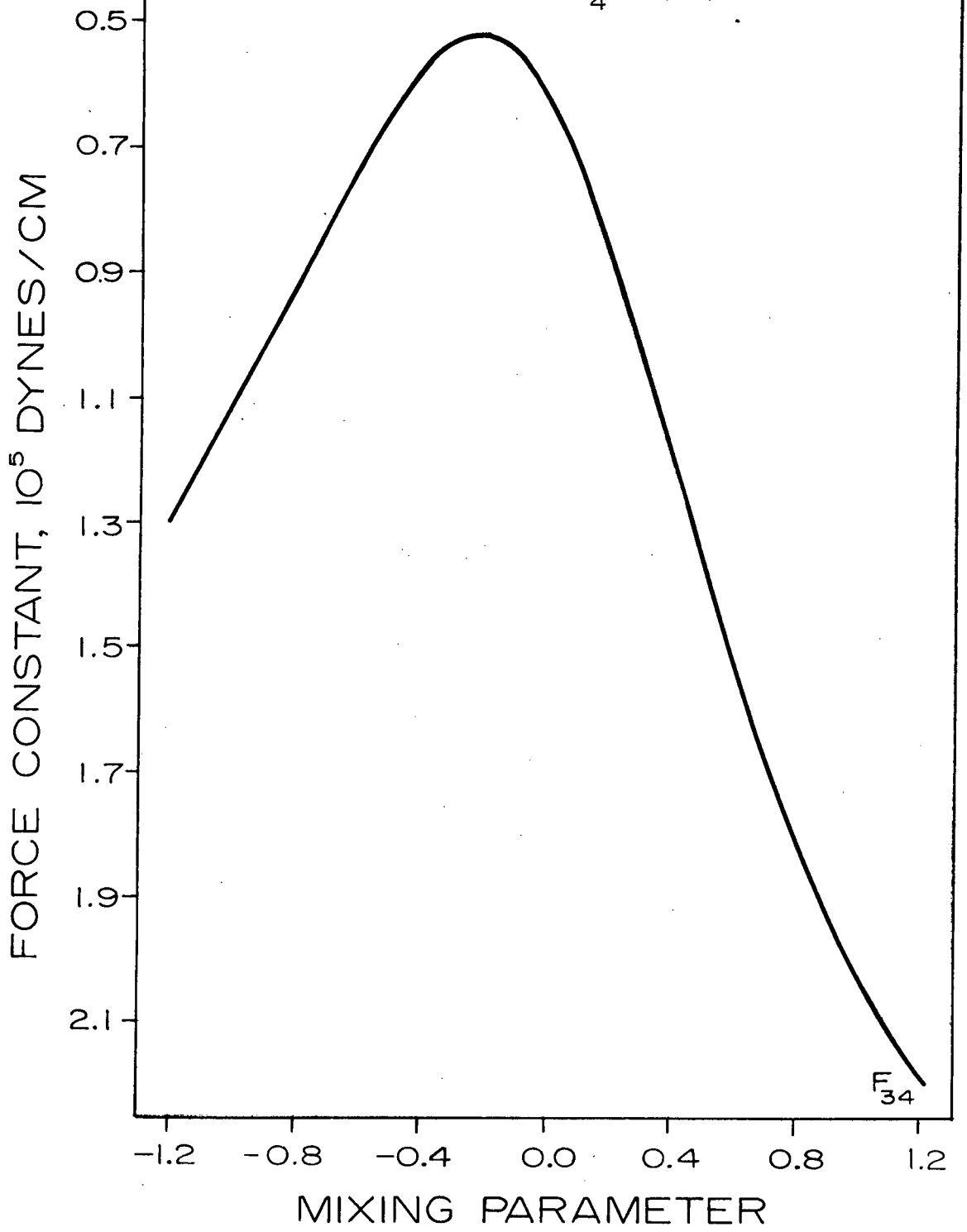

FIGURE 4–17

CALCULATED FREQUENCIES FOR ν_3 AND ν_4 AS A FUNCTION OF THE MIXING PARAMETER — NH_4Br (IV) ND_4Br (IV)

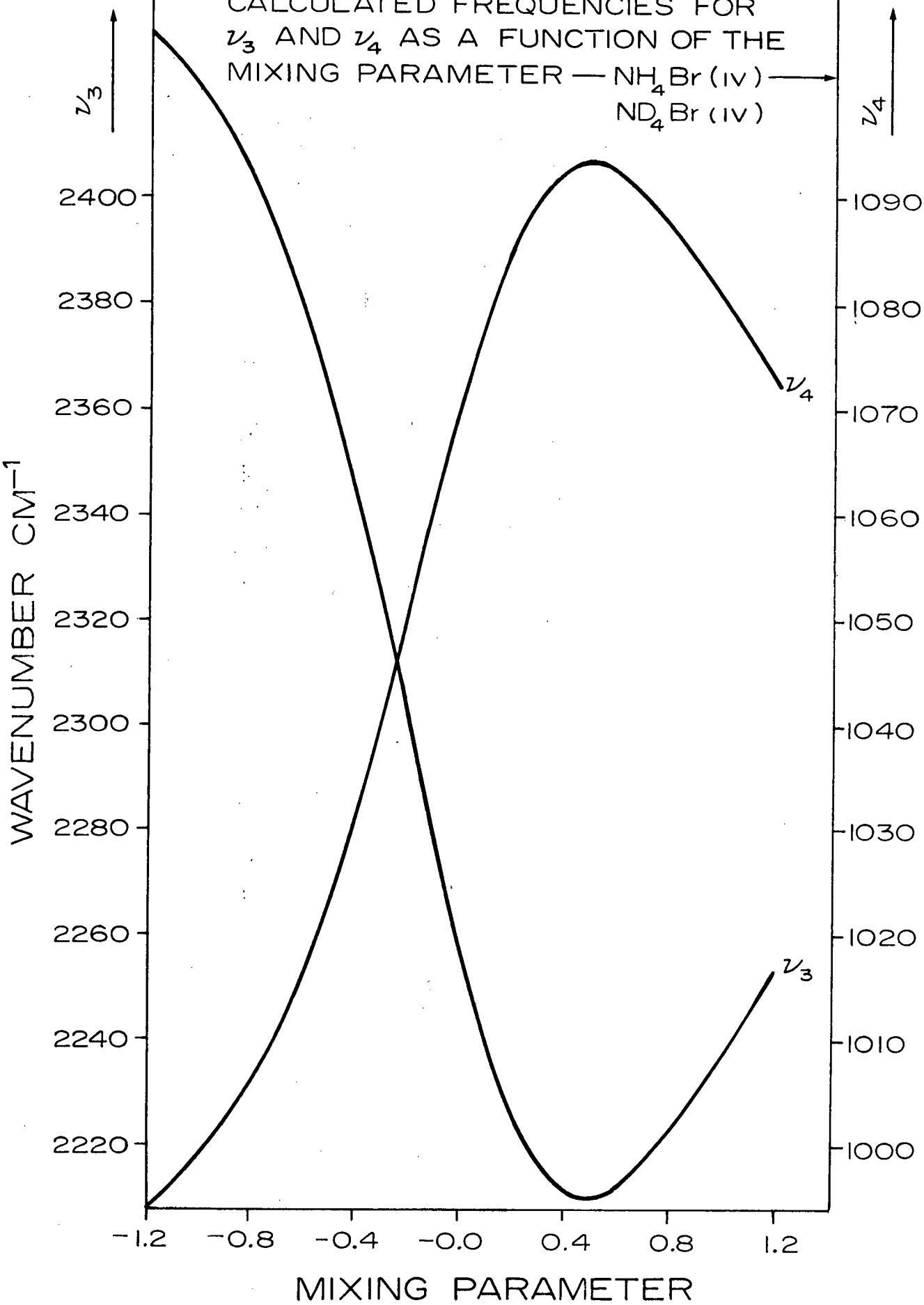

TABLE 4-10. Calculated and Observed Spectra - NH_4^+(Td).

(i) NH_4Br(IV) → ND_4Br(IV)

$X_1 = -0.36, \quad \nu_3 = 2330$

$X_2 = -0.11, \quad \nu_4 = 1060$

$X_3 = -0.235$

	ν_1	ν_2	ν_3	ν_4
Calculated Spectrum				
$X = X_3$	2155.4	1201.8	2305.7	1048.3
Observed Spectrum	2211	1211	2330	1060
Deviation	-45.6	-9.2	-24.3	-11.7

(ii) ND_4Br(IV) → NH_4Br(IV)

$X_1 = 0.54, \quad \nu_3 = 3124$

$X_2 = -0.28, \quad \nu_4 = 1398$

$X_3 = -0.36$

	ν_1	ν_2	ν_3	ν_4
Calculated Spectrum				
$X = X_3$	3125.6	1712.0	3169.9	1407.9
Observed Spectrum	3047	1699	3124	1398
Deviation	+78.6	+13.0	+25.9	+9.9

No other NH_4^+ force constants could be found for purposes of comparison.

4-7 The Effects of a D_{2d} Distortion

As an XY_4 molecule suffers a distortion from a T_d to a D_{2d} configuration both the kinetic and potential energies and thus $\underline{\underline{G}}$ and $\underline{\underline{F}}$ will change. The spectrum, $\{\lambda_i\}$, of the $XY_4(D_{2d})$ molecule may be computed providing both $\underline{\underline{G}}$ and $\underline{\underline{F}}$ are known. When the geometry of an $XY_4(D_{2d})$ molecule is known $\underline{\underline{G}}(D_{2d})$ is readily obtained. If we do not have a prior knowledge of the D_{2d} spectrum we cannot compute $\underline{\underline{F}}(D_{2d})$. A first approximation would be to use the $\underline{\underline{F}}(T_d)$ matrix of the $XY_4(T_d)$ molecule which undergoes a slight angular distortion to give the $XY_4(D_{2d})$ molecule.

The computed D_{2d} spectrum, $\{\lambda_i\}$, is then the solution of:

$$\left|\underline{\underline{G}}(D_{2d}) \cdot \underline{\underline{F}}(T_d) - \lambda_i \underline{\underline{I}}\right| = 0 \qquad (1)$$

where $\underline{\underline{F}}(T_d)$ may be calculated according to:

$$\underline{\underline{F}}(T_d) = \underline{\underline{U}}\underline{\underline{\Gamma}}^{-\frac{1}{2}}\underline{\underline{P}}\ \underline{\underline{\Lambda}}\ \underline{\underline{P}}^t\underline{\underline{\Gamma}}^{-\frac{1}{2}}\underline{\underline{U}} \qquad (2)$$

Here $\underline{\underline{U}}$ is the orthogonal matrix diagonalizing $\underline{\underline{G}}(T_d)$ to give $\underline{\underline{\Gamma}}$. $\underline{\underline{P}}$ is the orthogonal matrix of the previous section. The matrix $\underline{\underline{G}}(D_{2d})$ appearing in the secular equations is computed from the D_{2d} molecular geometry.

When we use the above approximation to predict the kinetic energy contribution to the spectrum of the crystalline $NH_4^+(D_{2d})$ ion, the $NH_4^+(T_d)$ ion is a hypothetical ion and there is necessarily an element of arbitrariness introduced when selecting its unperturbed frequencies. We may choose the $\nu_1(D_{2d})$, $\nu_2(D_{2d})$, $\nu_3(E_u)$ and $\nu_4(E_u)$ frequencies (recall that only the one

component of ν_2 is observed). When performing the actual calculations it was found that frequency shifts of up to about 50 cm^{-1} for the unperturbed frequencies, whether singly or in combination, had little quantitative effect on the predicted splitting pattern. The computed ν_3/ν_4 splitting will be a function of the mixing parameter, X, which appears in $\underline{\underline{P}}$ (see Figures 4-18 and 4-19). At X = 0 the ammonium bromide splitting pattern predicted for small angular distortions involving two angles greater than 109.47° and four angles less than 109.47° is the following:

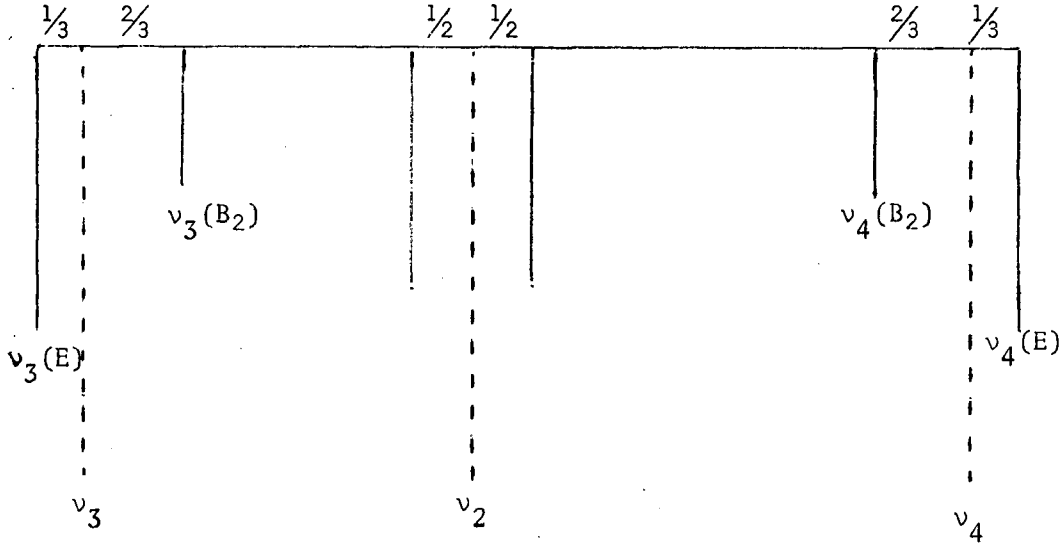

This result agrees with the observed spectral results and thus supports a structure for NH_4Br(III) where the NH_4^+ ions have two angles greater than 109.47° and four angles less than 109.47°. We may note that when the situation for the distortions is reversed the order of the predicted B_2, E splittings at X = 0 reverses (see Figure 4-20).

Table 4-11 reports the maximum ν_3/ν_4 splittings predicted on the interval $-1.2 \leq X \leq 1.2$ when the angular distortion is +3.09° and -1.52°. In the case of NH_4Br X =-0.35 maximizes the predicted splittings. They are 15.8 and 7.2 cm^{-1} for ν_3 and ν_4 respectively. These values compare with the observed splittings of 38 and 28 cm^{-1} which arise from the probable angular distortion of +3.09° and -1.52°. Figures 4-18 and 4-19 show that at X = +0.47 which corresponds to the unperturbed ν_3/ν_4 frequencies zero splitting is predicted. The splitting pattern reverses as we go from $X < 0.47$ to $X > 0.47$. We have favoured a predicted splitting pattern with $X < 0.47$ since the results of numerous force constant calculations for many small molecules have shown that when the force constant solutions are of the form $F = U\Gamma^{-\frac{1}{2}}P\Lambda P^{t}\Gamma^{-\frac{1}{2}}U$ the most acceptable values of the mixing parameters are invariably less than zero (68), e.g. for $NH_4Br(T_d) \rightarrow ND_4Br(T_d)$ the value of X giving optimum force constant transferability is -0.235 (see Table 4-10)

If we fix the mixing parameter at say X = -0.235 and vary the $NH_4^+(D_{2d})$ geometry we may use:

$$|\underline{\underline{G}}(D_{2d})\underline{\underline{F}}(T_d) - \lambda_i\underline{\underline{I}}| = 0$$

to compute the D_{2d} spectrum as a function of angular distortion (see Figures 4-20 and 4-21). We see that the observed ν_3 splitting requires an angular distortion of -3.7° and +7.8°. For ν_4 the required angular distortion is -6.0° and +12.8°. These values compare with the probable distortion of -1.5° and +3.1°.

FIGURE 4—18

PREDICTED SPLITTING OF ν_3 AS A FUNCTION OF THE MIXING PARAMETER— NH_4Br (T_d) ⟶ NH_4Br (D_{2d})

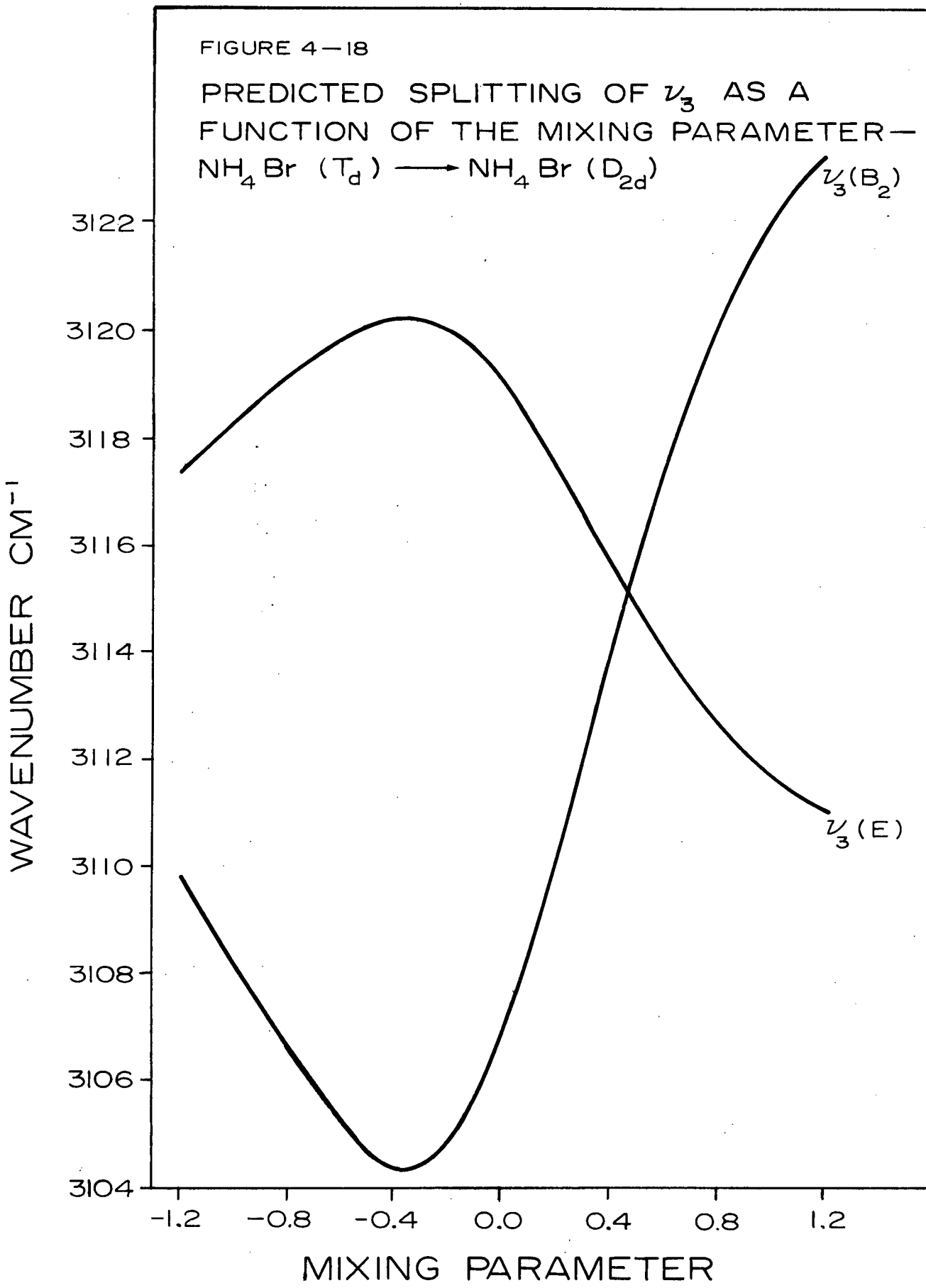

FIGURE 4—19

PREDICTED SPLITTING OF ν_4 AS A FUNCTION OF THE MIXING PARAMETER—

$NH_4Br\ (T_d) \longrightarrow NH_4Br\ (D_{2d})$

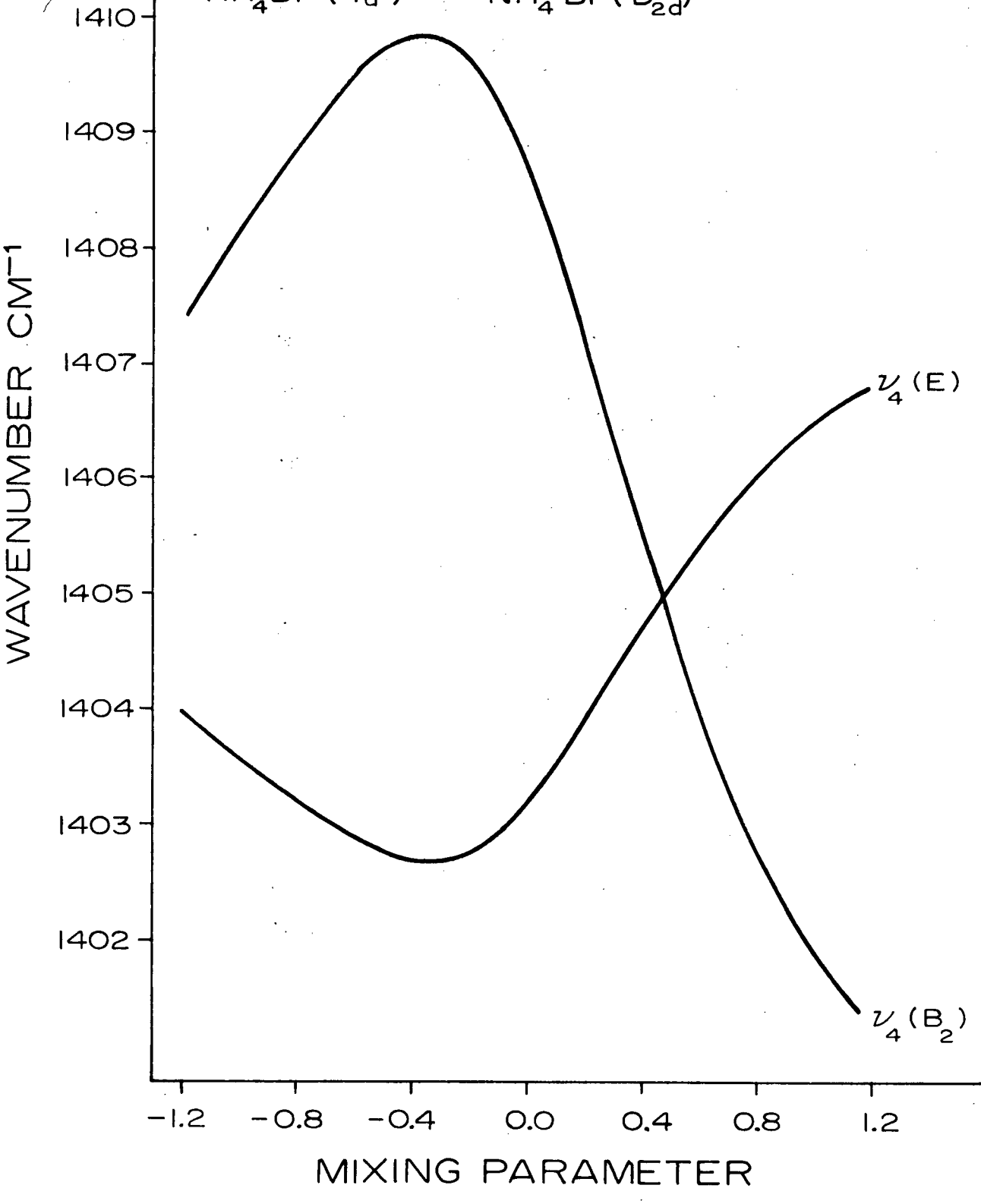

TABLE 4-11. Calculated and Observed Spectra - $NH_4^+(D_{2d})$

(i) $NH_4Br(T_d) \rightarrow NH_4Br(D_{2d})$; $X_4 = -0.35$

	$\nu_1(A_1)$	$\nu_2(A_1)$	$\nu_2(B_1)$	$\nu_3(B_2)$	$\nu_3(E)$	$\nu_4(B_2)$	$\nu_4(E)$
OBS.	3037.5	1694		3079	3117	1433	1405
Δ				38		28	
CALC.	3037.5	1710.2	1677.5	3104.2	3120.2	1409.8	1402.6
Δ		32.7		15.8		7.2	

(ii) $ND_4Br(T_d) \rightarrow ND_4Br(D_{2d})$; $X_4 = -0.45$

	$\nu_1(A_1)$	$\nu_2(A_1)$	$\nu_2(B_1)$	$\nu_3(B_2)$	$\nu_3(E)$	$\nu_4(B_2)$	$\nu_4(E)$
OBS.	2209	1209.5		—	2339	1089	1066
Δ				—		23	
CALC.	2209	1221.1	1197.7	2321.6	2343.1	1072.6	1062.7
Δ		23.4		21.5		9.9	

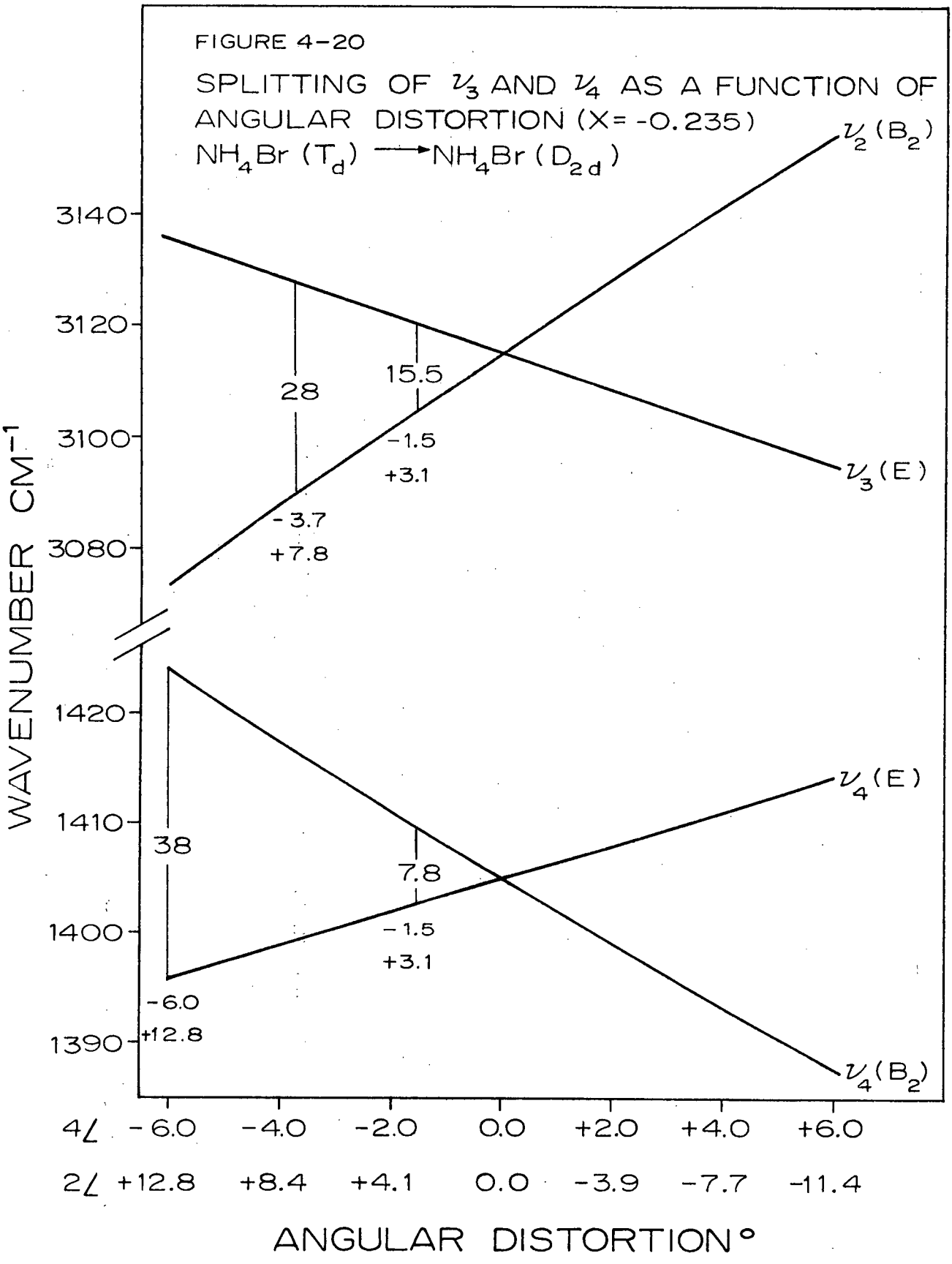
FIGURE 4-20
SPLITTING OF ν_3 AND ν_4 AS A FUNCTION OF ANGULAR DISTORTION (X= -0.235)
NH_4Br (T_d) ⟶ NH_4Br (D_{2d})
ν_2 (B_2)
ν_3 (E)
ν_4 (E)
ν_4 (B_2)
28
15.5
-1.5
+3.1
-3.7
+7.8
38
7.8
-1.5
+3.1
-6.0
+12.8
3140
3120
3100
3080
1420
1410
1400
1390
WAVENUMBER CM^{-1}
4ζ -6.0 -4.0 -2.0 0.0 +2.0 +4.0 +6.0
2ζ +12.8 +8.4 +4.1 0.0 -3.9 -7.7 -11.4
ANGULAR DISTORTION°

FIGURE 4-21

SPLITTING OF ν_2 AS A FUNCTION OF ANGULAR DISTORTION

$NH_4Br\ (T_d) \longrightarrow NH_4Br\ (D_{2d})$

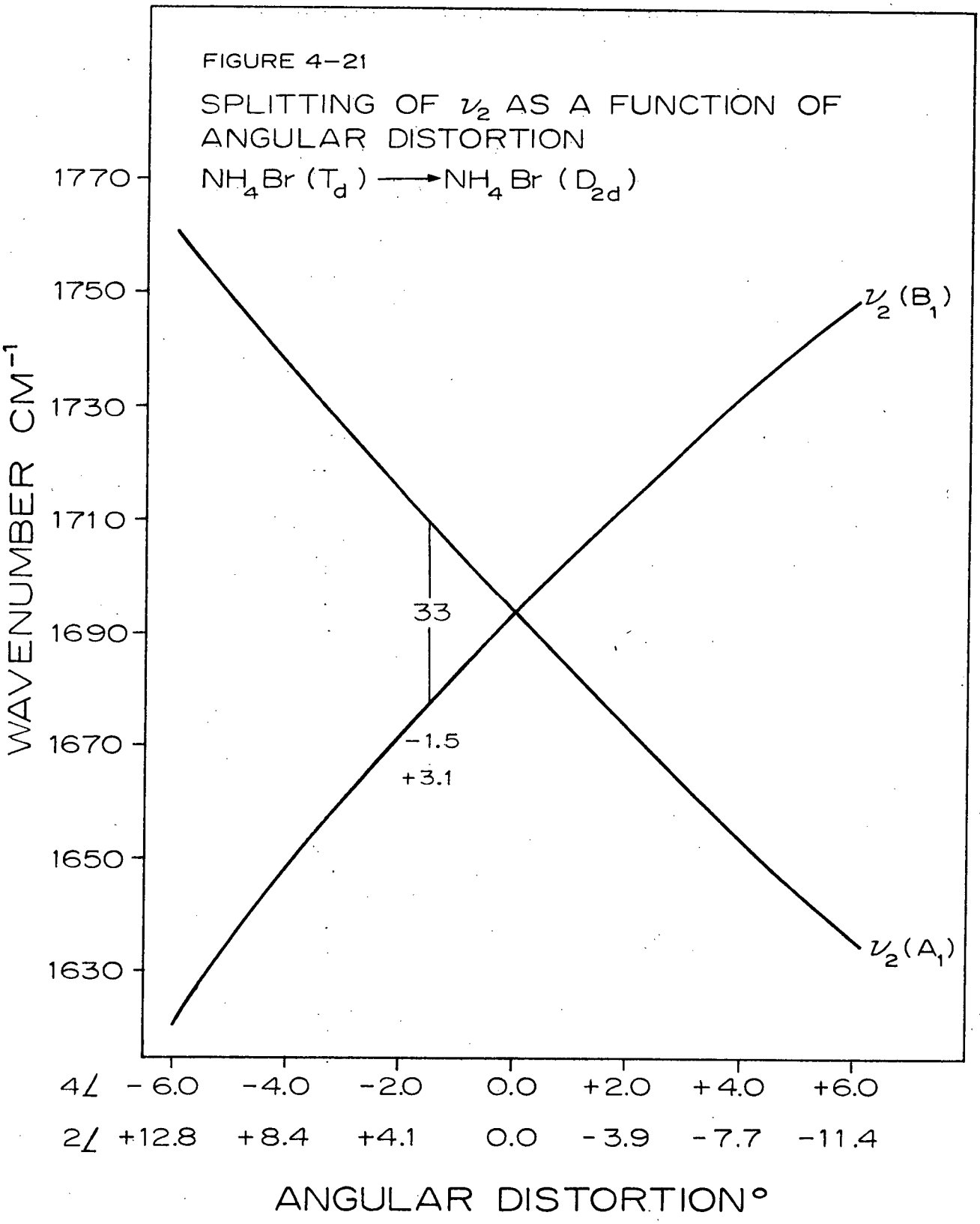

CHAPTER V

THE VIBRATIONS OF THE ALKALI METAL BOROHYDRIDES

5-1 The Phase III Alkali Metal Borohydrides

The crystal structure of the phase III alkali metal borohydrides is compatible with the space group $T_d^2(F\bar{4}3m)$. When the factor group analysis is carried out the following vibrations are obtained:

$$\Gamma(\text{internal}) = A_1 + E + 2F_2$$

$$\Gamma(OT) = F_2$$

$$\Gamma(OL) = F_1$$

$$\Gamma(AT) = F_2$$

In the Raman spectrum the modes of F_2 symmetry can be expected to split into transverse and longitudinal components.

From the infrared spectra recorded at 10°K (see Figure 5-1) $\nu_3(F_2)$ and $\nu_4(F_2)$ are readily assigned for both KBH_4(III) and KBD_4(III). The Raman spectra were recorded at 80°K (see Figure 5-2) and since the phase transformation II → III is thought to undergo completion at 77.2°K the Raman spectra do not show the true ν_1 and ν_2 phase III frequencies. However, for ν_3 and ν_4 there is a negligible frequency shift in the observed frequencies as the temperature is lowered from 80°K to 10°K. Therefore in Table 5-1 we have included the $\nu_1(A_1)$ and $\nu_2(E)$ frequencies as observed at 80°K in the phase III results. On this basis the observed frequencies for the internal fundamental modes for KBH_4(III) become 2314.5, 1251.5, 2281 and 1121 cm^{-1} respectively for $\nu_1(A_1)$, $\nu_2(E)$, $\nu_3(F_2)$ and $\nu_4(F_2)$. The corresponding frequencies for KBD_4(III) are 1599.2, 892, 1724 and 855 cm^{-1}.

As expected, lines for ν_3 and ν_4 are observed in the Raman as well as the infrared spectra. This, however, is not the case for $T_1(F_2)$ which is observed only in the infrared. The $T_1(F_2)$ frequencies are 178 cm^{-1} for KBH_4(III) and 172 cm^{-1} for KBD_4(III). The Raman spectra gave no evidence for the appearance of the longitudinal components of ν_3 and ν_4.

Since the ^{10}B - ^{11}B isotopes occur with a natural abundance of about 1:4 we may expect to see; (i) the effects of ^{10}B - ^{11}B (and ^{39}K - ^{40}K) disorder after the treatment of Lifshitz (62) and (ii) a ^{10}B - ^{11}B isotopic splitting for ν_3, ν_4 and T_1. Evidently any frequency shifts due to disorder are too small to be observed. The isotopic shifts for ν_3 and ν_4 are, however, observed. The infrared spectrum of KBD_4(III), where the line widths at half-height are about 5 cm^{-1}, gives a striking example of isotopic ^{10}B - ^{11}B splitting which is fully resolved (see Figure 5-5). In the spectrum of KBD_4(III), $^{10}\nu_3(F_2)$ and $^{10}\nu_4(F_2)$ are observed at 1739 and 864 cm^{-1}. These frequencies give respective isotopic shifts of 15 and 9 cm^{-1}. The corresponding shifts for KBH_4(III) are 16 and 10 cm^{-1}.

In the second order spectrum of the phase III potassium borohydrides only three principal lines are observed; these are $2\nu_4(A_1 + E + F_2)$, $\nu_2 + \nu_4(F_1 + F_2)$ and $2\nu_2(A_1 + E)$. The overtone $2\nu_2$ is observed only in the Raman effect but $2\nu_4$ and $\nu_2 + \nu_4$ are common to both the infrared and Raman spectra. $2\nu_4(F_2)$ is strongly affected by Fermi resonance with $\nu_3(F_2)$; i.e. in the infrared $2\nu_4(F_2)$ has considerably enhanced intensity and the observed KBH_4(III) and KBD_4(III) frequencies are 25 and 28 cm^{-1} lower than those predicted. In the Raman spectrum of KBH_4(III) $2\nu_4$ appears as a doublet with

frequencies of 2185.5 and 2224 cm^{-1}. Since both $\nu_1(A_1)$ and $\nu_3(F_2)$ lie nearby at 2314.5 and 2291 cm^{-1} it is likely that $2\nu_4(A_1 + E + F_2)$ undergoes Fermi resonance with both these fundamentals. On this basis the low wave number component of $2\nu_4$ can be assigned as $2\nu_4(A_1)$ and the high wave number component to $2\nu_4(F_2)$. Both of these components are observed as sharp lines and it is unlikely that either component could contain any appreciable intensity contribution from $2\nu_4(E)$. The Raman line appearing at 2238 cm^{-1} can be assigned as $2\,^{10}\nu_4(F)$. This compares with an infrared frequency of 2235 cm^{-1} which gives an observed-predicted frequency discrepancy of 27 cm^{-1}. In the spectrum of KBD_4(III) $2\,^{10}\nu_4(F)$ appears in the infrared at 1697 cm^{-1}; the resulting frequency discrepancy is 30 cm^{-1}.

The predicted $\nu_2 + \nu_4(F_2)$ frequencies are 2374 cm^{-1} for KBH_4(III) and 1747 cm^{-1} for KBD_4(III). The corresponding infrared frequencies are 2386 and 1757 cm^{-1}. Since these observed frequencies are about 10 cm^{-1} higher than those predicted $\nu_2 + \nu_4(F_2)$ must undergo Fermi resonance with $\nu_3(F_2)$. In the infrared spectrum of KBD_4(III) $^{10}\nu_2 + {}^{10}\nu_4(F_2)$ is also observed. It appears at 1767 cm^{-1}.

Finally we come to $2\nu_2(A_1 + E)$. This line appears with frequencies of 2497 and 1782 respectively in the spectra of KBH_4(III) and KBD_4(III). The respective anharmonicities are 7 and 2 cm^{-1}.

The assignments for the phase III salts are found in Tables 5-1 and 5-2. The corresponding spectra are included in Figures 5-1, 5-2, 5-3, 5-4, 5-6 and 5-8. The Raman results obtained for rubidium and cesium borohydride at 80°K are included in the phase III results. Since the

TABLE 5-1. Assignments for KBH_4(III) and KBD_4(III); cm^{-1}

ASSIGNMENT	KBH_4(III) - THIS WORK		KBD_4(III) - THIS WORK	
	R.	I.R.	R.	I.R.
ν_1	2314.5		1599.5	
ν_2	1251.5		892	
$^{10}\nu_3$		2297(sh)	1737	1739
ν_3	2291	2281	1723.5	1724
$^{10}\nu_4$		1131		864
ν_4	1122	1121	856	855
T_1		178		172
$2\nu_2$	2497		1782	
$\nu_2+^{10}\nu_4(F_2)$			1770	1767
$\nu_2+\nu_4(F_2)$	2386	2384	1757	1757
$2^{10}\nu_4(F_2)$	2238	2235	1698	1697
$2\nu_4(F_2)$	2224	2217	1682	1682
$2^{10}\nu_4(A_1)$				
$2\nu_4(A_1)$	2185.5			

TABLE 5-2. Assignments for $RbBH_4$(III) and $CsBH_4$(III); cm^{-1}

ASSIGNMENT	$RbBH_4$(III) - THIS WORK		$CsBH_4$(III) - THIS WORK	
	R.	I.R.	R.	I.R.
ν_1	2301		2281.5	
ν_2	1239		1222	
$^{10}\nu_3$				2268(sh)
ν_3	2278	2277	2255	2252
$^{10}\nu_4$				1113
ν_4	1119	1116	1104.5	1103
$2\nu_2$	2477		2443	
$\nu_2+^{10}\nu_4(F_2)$				2345
$\nu_2+\nu_4(F_2)$	2365	2361	2338	2336
$2^{10}\nu_4(F_2)$	2224	2218(sh)	2202	2201
$2\nu_4(F_2)$	2209	2207	2187.5	2185
$2^{10}\nu_4(A_1)$	2183		2156	
$2^{10}\nu_4(A_1)$	2174(sh)		2166	

Figure 5-1 The I.R. spectra of $NaBH_4$(I), KBH_4(I) $NaBH_4$(II) and KBH_4(III)

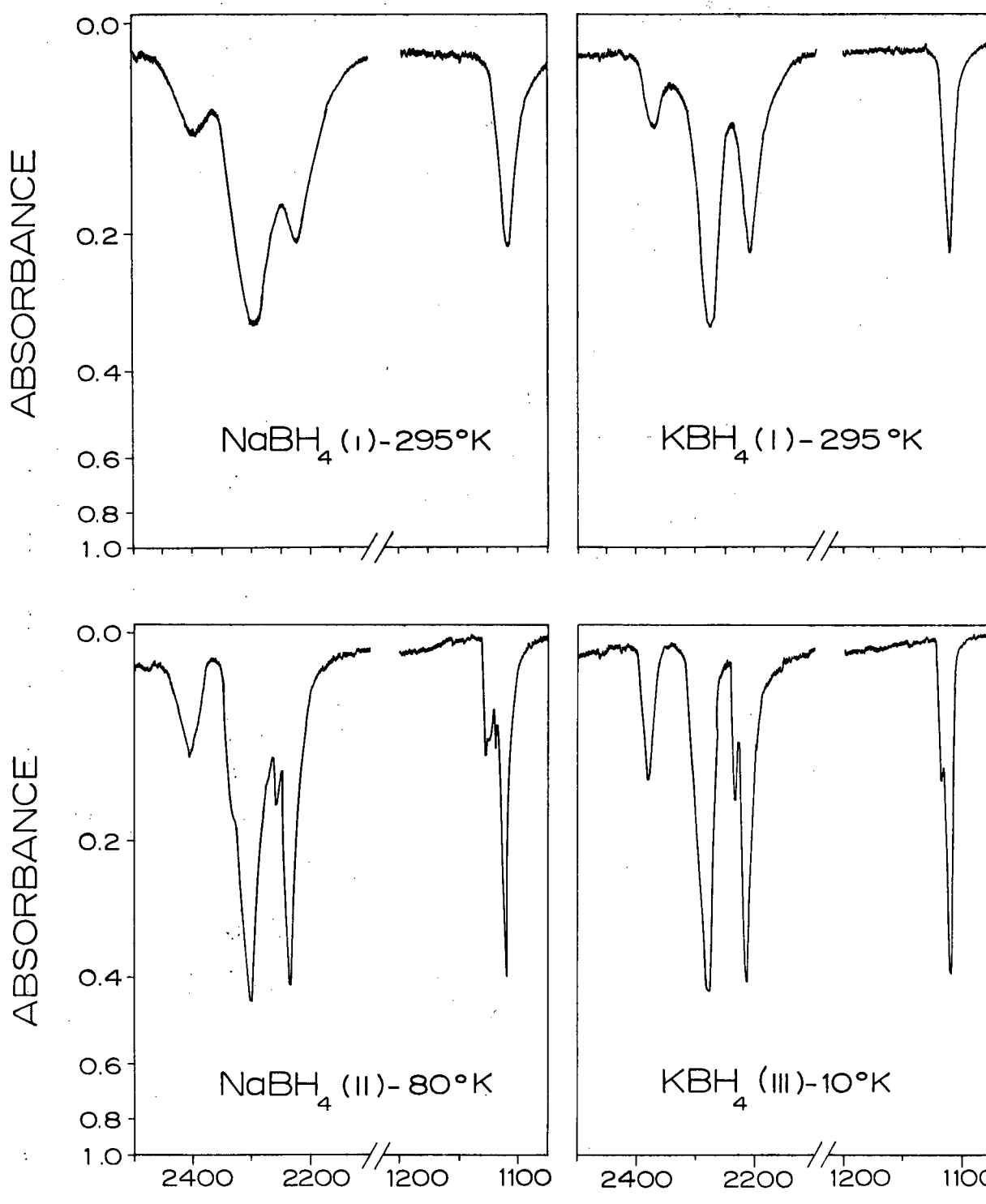

Figure 5-2 The Raman Spectra of $NaBH_4$(I), KBH_4(I) $NaBH_4$(II) and KBH_4(80°K)

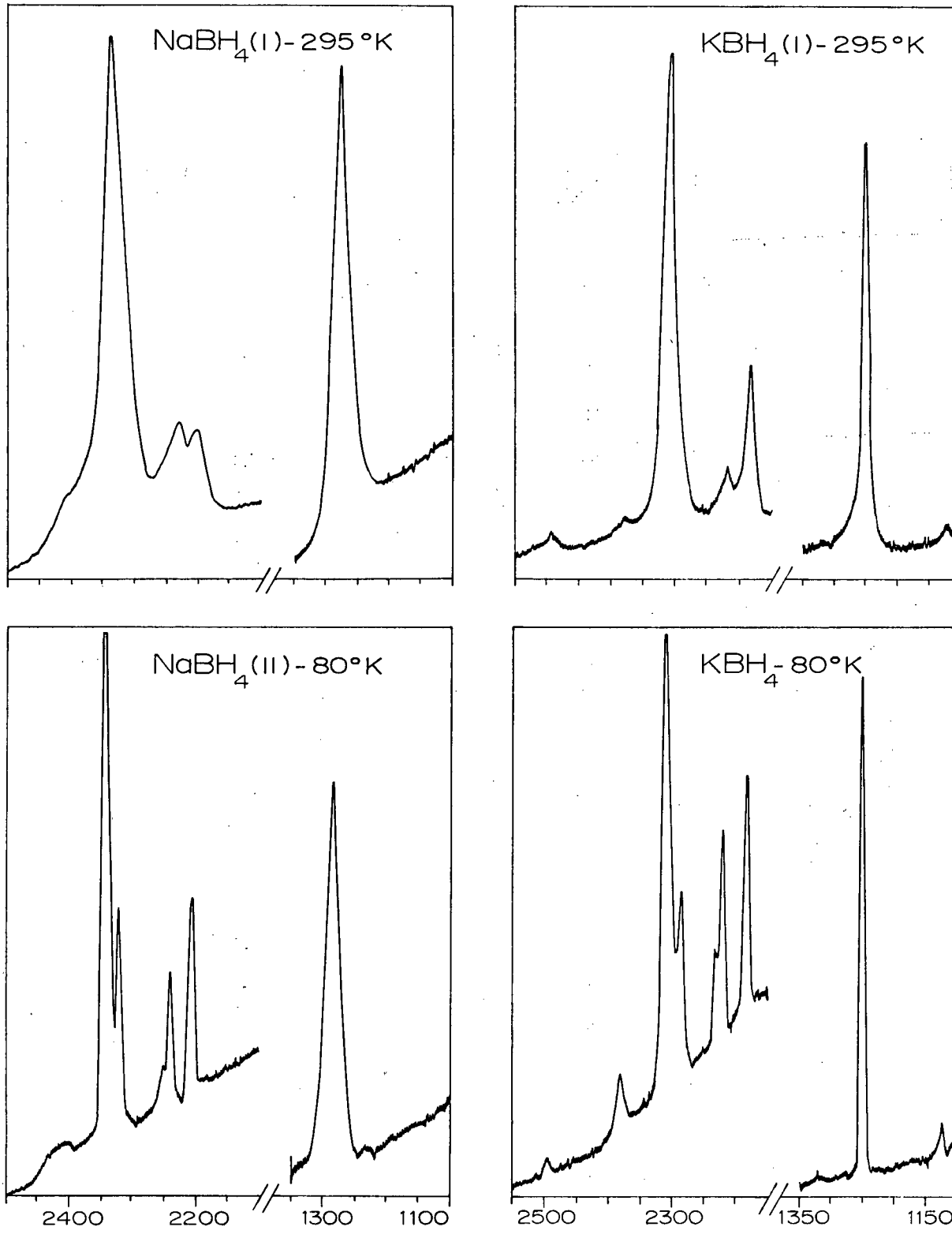

Figure 5-3 The I.R. spectra of $NaBD_4$(I), KBD_4(I) $NaBD_4$(II) and KBD_4(III)

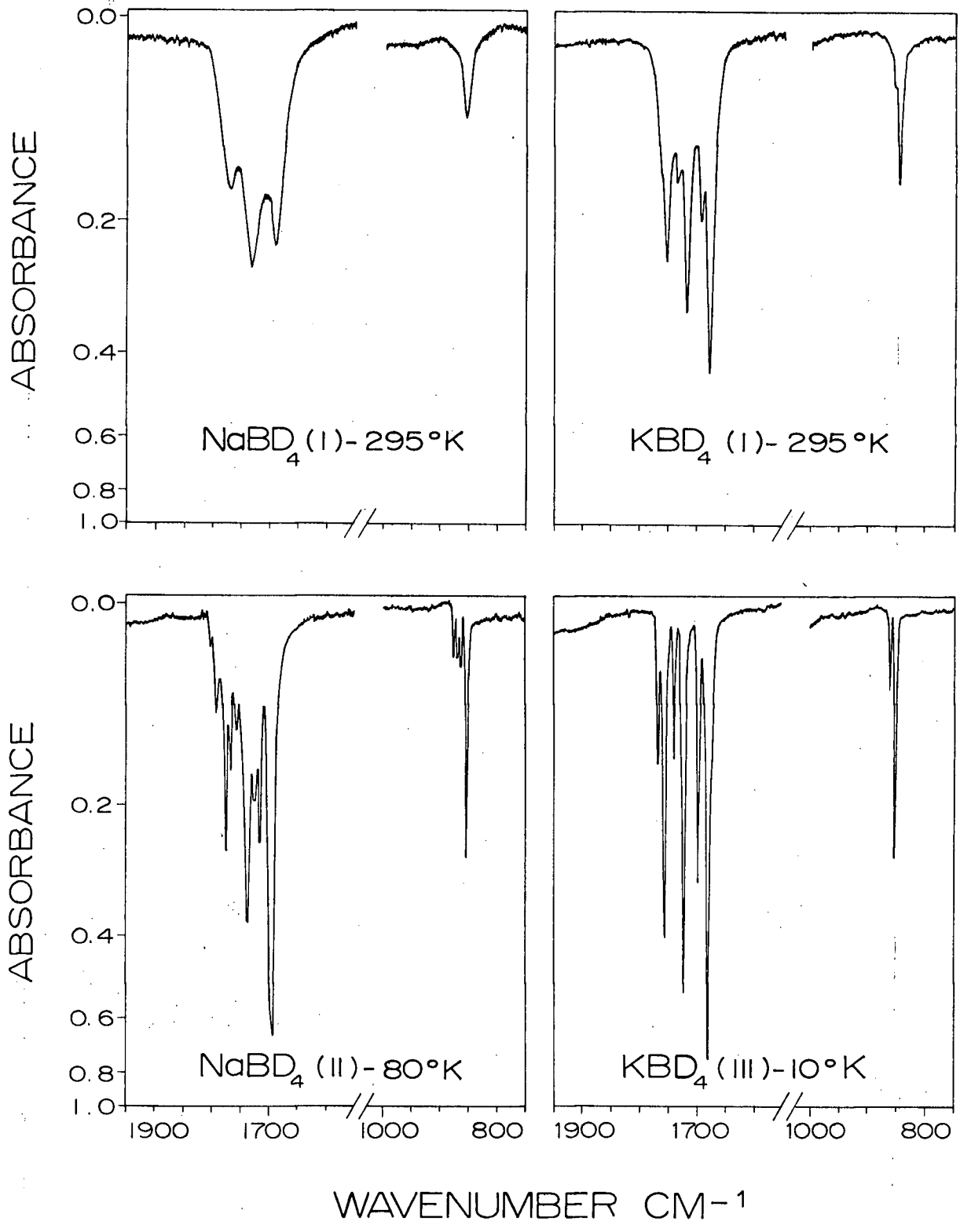

Figure 5-4 The Raman Spectra of $NaBD_4$(I), KBD_4(I) $NaBD_4$(II) and KBD_4(80°K)

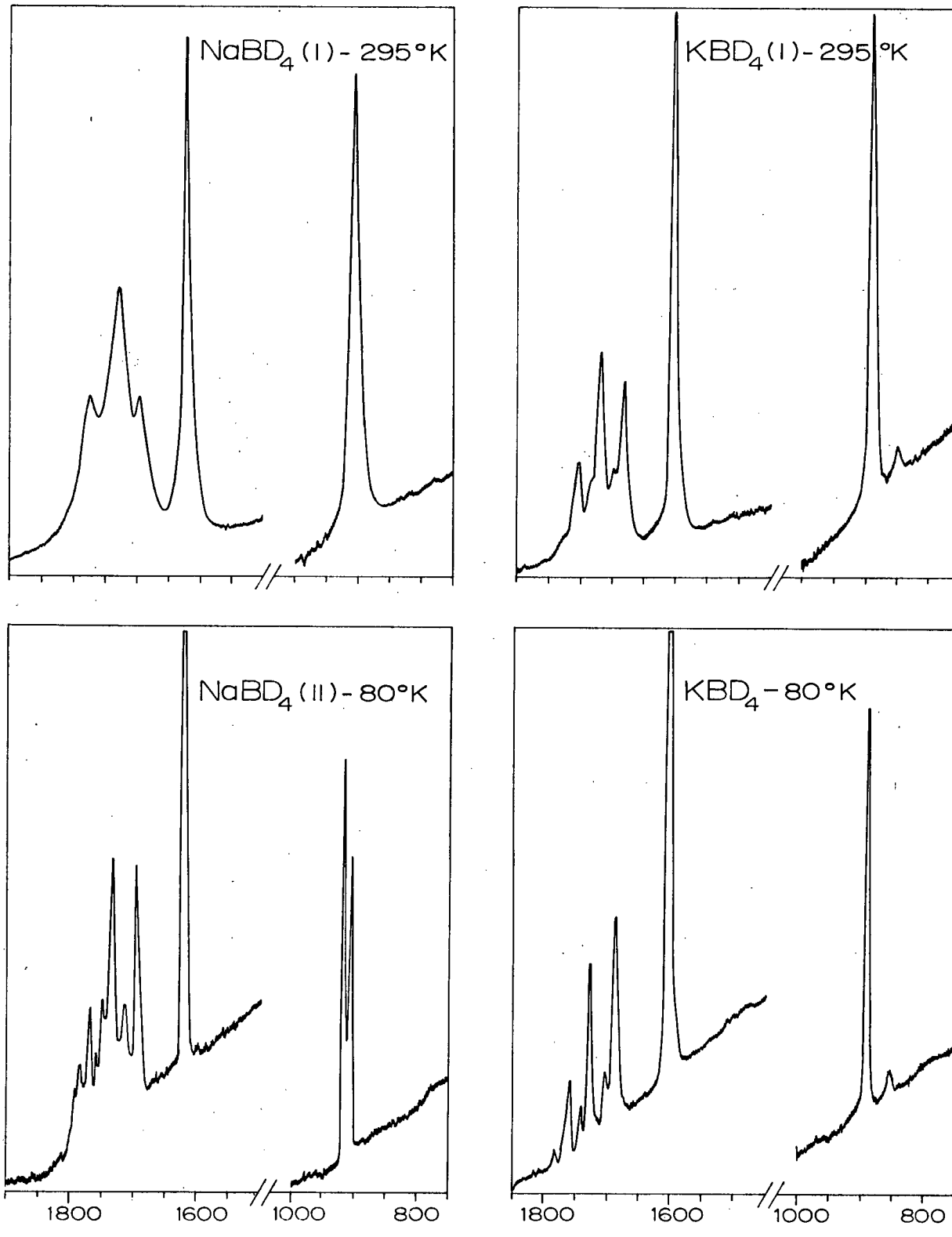

Figure 5-5 The I.R. spectra of $NaBD_4$ (II), $NaBH_4$ (II) KBD_4 (III) and KBH_4 (III)

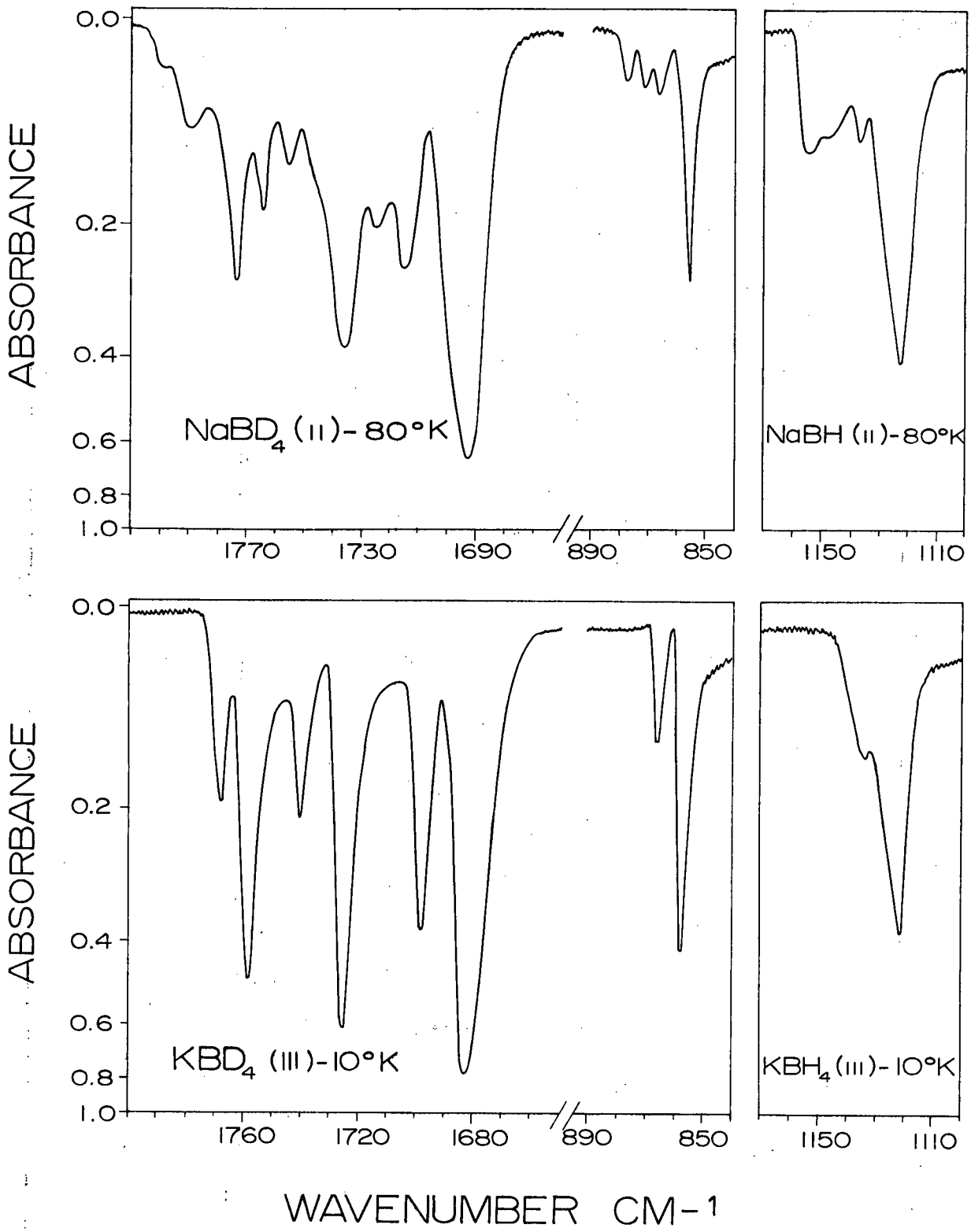

Figure 5-6 The I.R. spectra of $RbBH_4$(I), $CsBH_4$(I), $RbBH_4$(III) and $CsBH_4$(III)

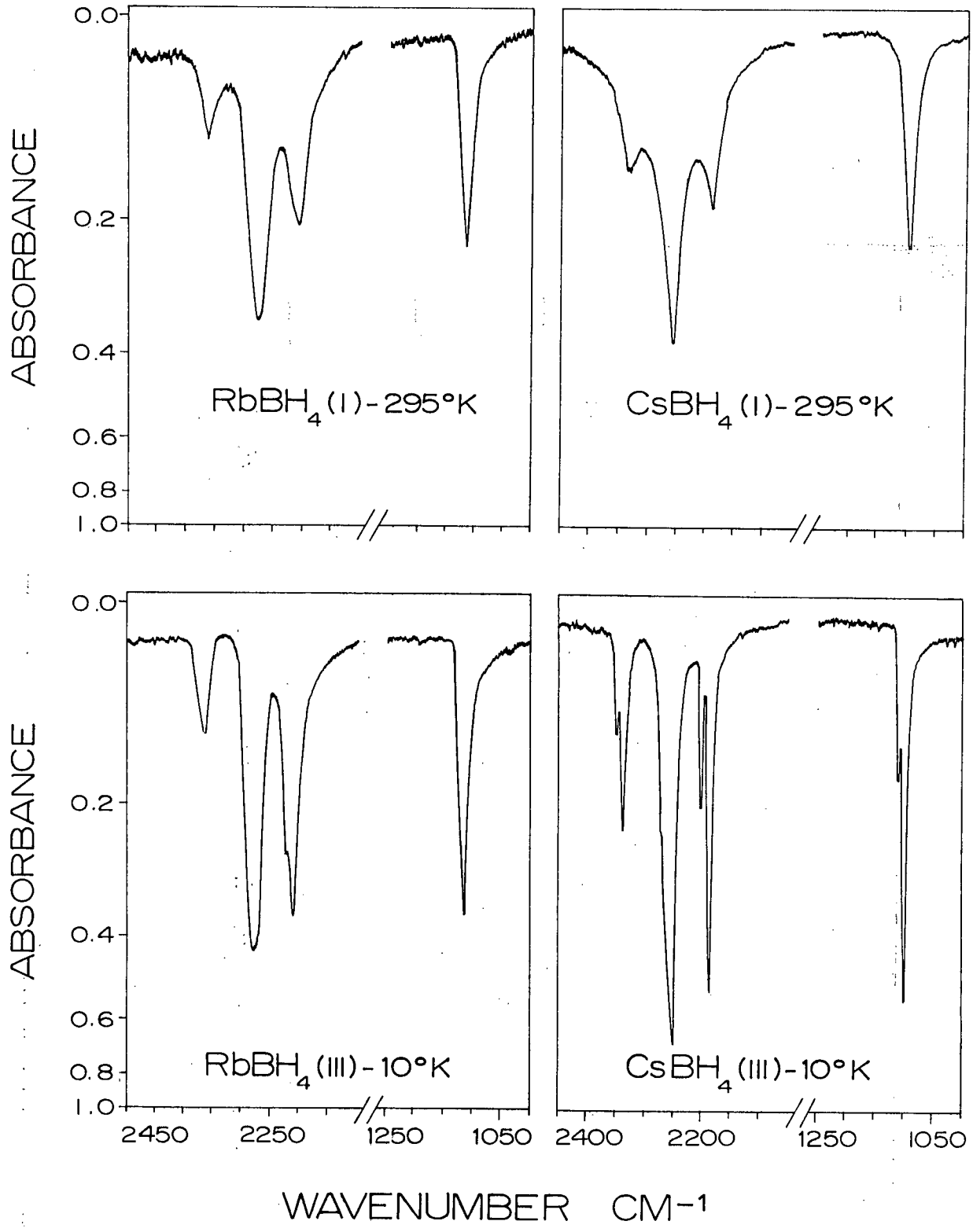

Figure 5-7 The Raman Spectra of $RbBH_4$(l), $CsBH_4$(l), $RbBH_4$(80°K) and $CsBH_4$(80°K)

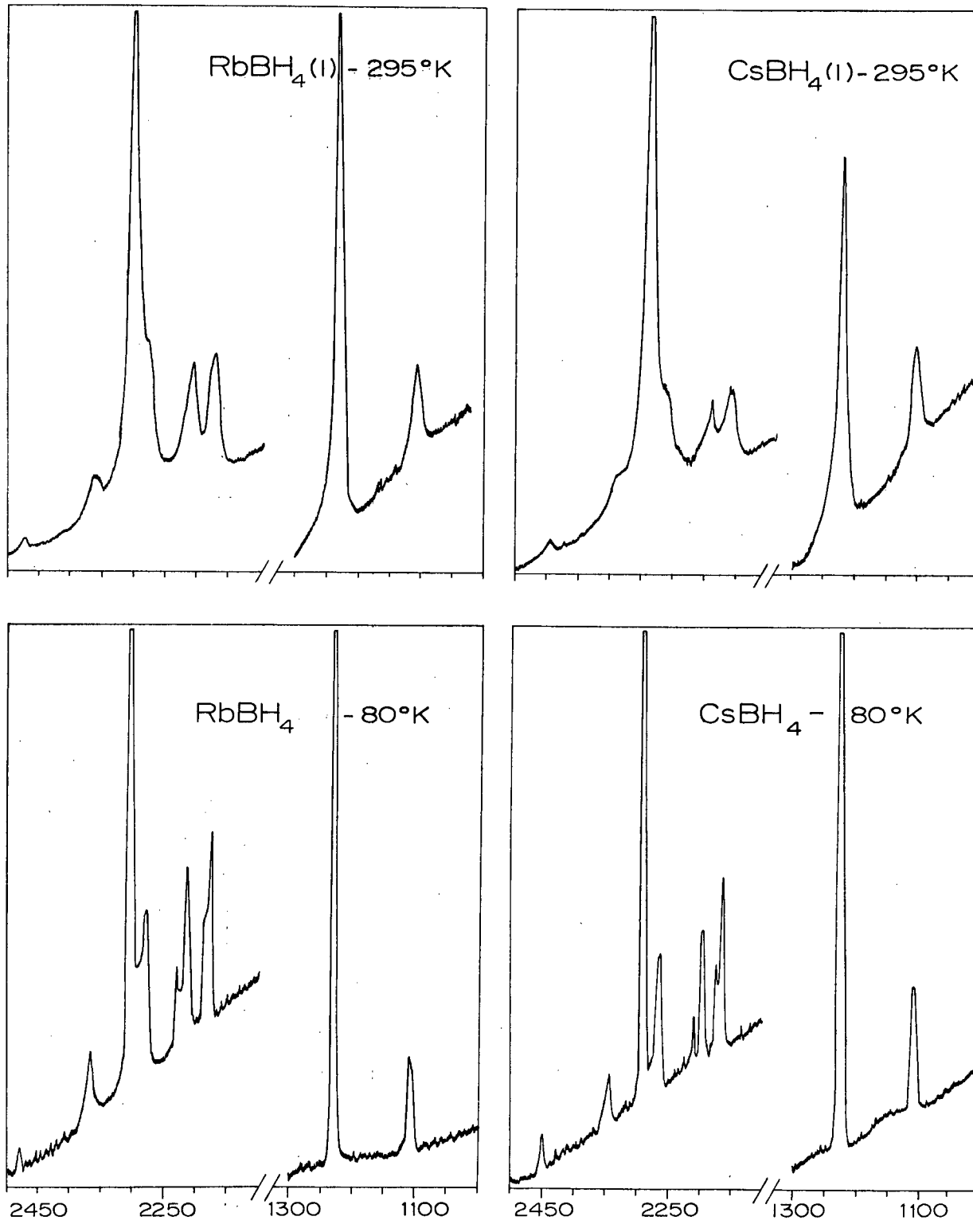

frequencies in the infrared spectra of these salts showed a negligible shift as the temperature was lowered from 80° to 10°K, it can be assumed that the Raman spectra as observed at 80°K will closely approximate the true phase III spectra.

5-2 The Phase II Alkali Metal Borohydrides

Phase II sodium borohydride has a tetragonal structure under the space group $D_{2d}^{9}(I\bar{4}m2)$. The results of the factor group analysis under the D_{2d} factor group can be summarized as follows:

$$\Gamma(\text{internal}) = 2A_1 + B_1 + 2B_2 + 2E$$

$$\Gamma(\text{OT}) = B_2 + E$$

$$\Gamma(\text{OL}) = A_2 + E$$

$$\Gamma(\text{AT}) = B_2 + E$$

For the internal vibrations associated with the BH_4^- ion the site group and factor group coincide; hence, there are no correlation field effects and the four vibrations associated with the free BH_4^- ion become the precursors of 7 crystal modes which arise from a splitting of the degenerate modes by the static field as shown by the following correlation diagram.

Vibrational Mode	Free Ion Symmetry-T_d		Site/Factor Group Symmetry-D_{2d}
ν_1	A_1	→	A_1
ν_2	E	→	A_1, B_1
ν_3	F_2	→	B_2, E
ν_4	F_2	→	B_2, E

For the phase III alkali metal borohydrides it is relatively easy to sort out the modes arising from ^{10}B - ^{11}B isotopic splitting. However, for the phase II sodium salts where the site group splitting is of the same order of magnitude as the ^{10}B - ^{11}B isotopic splitting the situation is much more complicated. Nevertheless it has been possible to make a complete set of vibrational assignments for both $NaBH_4$(II) and $NaBD_4$(II). Since the vibrational spectrum of $NaBD_4$(II) is characterized by sharp well resolved lines assignments for this salt will be made first.

The Raman spectrum of $NaBD_4$(II)(see Figure 5-4) allows us to place $\nu_1(A_1)$ at 1622 cm^{-1}. The two expected components of ν_2 also appear; the line appearing at 916 cm^{-1} is arbitrarily assigned to $\nu_2(A_1)$ and the line appearing at 904 cm^{-1} is then assigned to $\nu_2(B_1)$. (It will be seen shortly that these assignments can be confirmed when the possible combinations for $\nu_2 + \nu_4$ are considered). Of the four D_{2d} lines associated with ν_3 and ν_4 only one, $\nu_3(E)$ appears in the Raman spectrum of $NaBD_4$(II), (the same situation occurs for $NaBH_4$(II)) therefore it is convenient to consider the infrared spectrum (see Figures 5-3 and 5-5). The infrared bending region shows four lines. These appear at 854.5, 865, 870 and 877 cm^{-1}. Clearly, the most intense line appearing at 854.5 cm^{-1} can be assigned to $\nu_4(E)$. Now, for KBD_4(III) the ν_4 isotopic splitting is 9 cm^{-1}; therefore it is reasonable to assign the 865 cm^{-1} line as $\nu_4(E)$. This leaves two lines either one of which could be assigned as $\nu_4(B_2)$. The most reasonable choice is the 870 cm^{-1} line since as will be seen shortly, it predicts $2\nu_4$ and $\nu_2 + \nu_4$ overtones and combinations which are compatible with the experi-

mental results. The anomalous line at 877 cm^{-1} has been assigned to the second overtone of a mode of rotatory origin. A further comment on this assignment is made later.

The stretching region of the infrared spectrum is very rich in spectral information. A convenient line to start with is the 1735.5 cm^{-1} line; because of its intensity it is readily assigned as $\nu_3(E)$. A second line possessing striking intensity is found at 1692 cm^{-1} and it must be assigned to a component of $2\nu_4$. Since it is observed with such enhanced intensity it can be assumed to be undergoing Fermi resonance with $\nu_3(E)$. This immediately selects E type symmetry for this line and hence it must originate from the combination $\nu_4(E) + \nu_4(B_2) = 2\nu_4(E)$ which has a predicted frequency of 1725 cm^{-1}. The discrepancy of 33 cm^{-1} between the predicted and observed frequencies is further evidence of Fermi resonance. The line appearing at 1715 cm^{-1} on the high frequency side of $2\nu_4(E)$ can be assigned to $2^{10}\nu_4(E)$; $^{10}\nu_4(B_2)$ has a predicted frequency of 880 cm^{-1} and therefore the predicted frequency of $2^{10}\nu_4(E)$ is 1745 cm^{-1} which gives a predicted-observed frequency discrepancy of 30 cm^{-1}. Besides $2\nu_4(E)$ there are two other possible $2\nu_4$ components. These are $\nu_4(B_2) + \nu_4(B_2) = 2\nu_4(A_1)$ and $\nu_4(E) + \nu_4(E) = 2\nu_4(A_1 + B_1 + B_2)$. This latter component is infrared active and therefore expected to appear in the infrared with a predicted frequency of 1709 cm^{-1}. However, no evidence was found for the appearance of this line. Having assigned the lines at 1692 and 1715 cm^{-1} respectively to $2\nu_4(E)$ and $2^{10}\nu_4(E)$ the remaining line on the low frequency side of $\nu_3(E)$ at 1724 cm^{-1} can be assigned to $\nu_3(B_2)$. On the high wave number side of $\nu_3(E)$ a line appears at

1755 cm^{-1} which must be assigned to $^{10}\nu_3(E)$. The resulting $^{10}B - ^{11}B$ isotopic splitting of 20 cm^{-1} compares with the ν_3 isotopic splitting of 15 cm^{-1} observed for KBD_4(III). The remaining lines appearing at 1764, 1773, 1789 and 1798 cm^{-1} must be assigned to the combinations $\nu_2 + \nu_4$. There are 8 possible predicted combinations. These are:

$$\nu_2(B_1) + \nu_4(E) = 1759(E)$$
$$^{10}\nu_2(B_1) + {}^{10}\nu_4(E) = 1769(E)$$

$$\nu_2(A_1) + \nu_4(E) = 1771(E)$$
$$^{10}\nu_2(A_1) + {}^{10}\nu_4(E) = 1781(E)$$

$$\nu_2(B_1) + \nu_4(B_2) = 1774(A_2)$$
$$^{10}\nu_2(B_1) + {}^{10}\nu_4(B_2) = 1784(A_2)$$

$$\nu_2(A_1) + \nu_4(B_2) = 1786(B_2)$$
$$^{10}\nu_2(A_1) + {}^{10}\nu_4(B_2) = 1796(B_2)$$

The combinations of E and B_2 symmetry types will be both infrared and Raman active, while the combinations of A_2 symmetry type will be inactive. Since combinations of E type symmetry can undergo Fermi resonance with $\nu_3(E)$ and those of B_2 symmetry can interact with $\nu_3(B_2)$, it can be expected that the observed combinations may have enhanced intensities and may also lie at frequencies slightly higher than those predicted. On this basis the observed lines at 1764, 1773, 1789 and 1798 cm^{-1} may respectively be assigned to: $\nu_2(B_1) + \nu_4(E)$, $\nu_2(A_1) + \nu_4(E)$, $\nu_2(A_1) + \nu_4(B_2)$ and $^{10}\nu_2(A_1) + {}^{10}\nu_4(B_2)$. This choice of assignments is the only reasonable one and allows us to remove the arbitrariness associated with the assignments $\nu_2(A_1)$, $\nu_2(B_1)$ and $\nu_4(B_2)$.

For the Raman observed lines $2\nu_4$ and $\nu_2 + \nu_4$ the second order spectrum closely parallels the infrared spectrum. The Raman spectrum shows a band for $2\nu_2$ which is absent in the infrared. It is observed at 1821 cm^{-1} and very likely the three predicted components for $2\nu_2$ all contribute to its intensity. The foregoing assignments for $NaBD_4$(II) are summarized in Table 5-3.

We turn next to the spectrum of $NaBH_4$(II). The Raman spectrum (see Figure 5-2) allows us to place $\nu_1(A_1)$ at 2341 cm^{-1} and ν_2 appears as a relatively broad band at 1280 cm^{-1} which undoubtedly contains the two expected ν_2 components. Therefore the only assignment which can be made is $\nu_2(A_1, B_1)$ = 1280 cm^{-1}.

Just as for $NaBD_4$(II) four lines appear in the infrared bending region of the spectrum (see Figures 5-1 and 5-5). These lines appear at 1122, 1134, 1148 and 1153 cm^{-1}. The most intense line is the 1122 cm^{-1} line and hence can be assigned as $\nu_4(E)$. For KBH_4(III) the ν_4 ^{10}B - ^{11}B isotopic splitting is 10 cm^{-1}. This indicates the assignment $^{10}\nu_4(E)$ for the 1134 cm^{-1} line. Either of the the lines appearing at 1148 and 1153 cm^{-1} could reasonably be assigned to $\nu_4(B_2)$ and, while a choice of either one will involve some degree of arbitrariness, it is found that on the basis of expected predicted-observed frequency discrepancies for the overtones and combinations the 1148 cm^{-1} line appears to be the best choice. The 1153 cm^{-1} line has been assigned to the second overtone of a mode of rotatory origin. This assignment is commented on later.

The infrared stretching region of the $NaBH_4$(II) spectrum is not nearly

as well resolved as the corresponding $NaBD_4$(II) spectral region. However, much valuable information is present. The intense line appearing at 2303 cm^{-1} can be assigned to $\nu_3(E)$ and the intense line appearing at 2236 cm^{-1} which may be assigned to a component of $2\nu_4$ must certainly undergo Fermi resonance with $\nu_3(E)$. This fixes E type symmetry for the 2236 cm^{-1} line and in analogy with the situation for $NaBD_4$(II) we have the assignment $\nu_4(B_2) + \nu_4(E) = 2\nu_4(E)$. The predicted-observed frequency discrepancy is 34 cm^{-1} which compares with a corresponding value of 33 cm^{-1} for $NaBD_4$(II). Just as for $NaBD_4$(II) the expected absorption, $\nu_4(E) + \nu_4(E) = 2\nu_4(A_1 + B_1 + B_2)$ does not appear in the infrared spectrum. The line appearing at 2256 cm^{-1} can be assigned to $2\,{}^{10}\nu_4(E)$, and the shoulder which appears at 2272 cm^{-1} on the low frequency side of $\nu_3(E)$ must be assigned as $\nu_3(B_2)$. The shoulder appearing on the high frequency side of $\nu_3(E)$ at 2334 cm^{-1} can be assigned to ${}^{10}\nu_3(E)$. This gives a ${}^{10}B - {}^{11}B$ isotopic splitting of 31 cm^{-1} and compares with a corresponding ν_3 isotopic splitting of 30 cm^{-1} for KBH_4(III). The remaining line appearing in the infrared stretching region appears at 2404 cm^{-1} and can be assigned as $\nu_2(A_1, B_1) + \nu_4(E)$ which has a predicted frequency of 2402 cm^{-1}.

The lines appearing in the second order Raman spectrum of $NaBH_4$(II) may be assigned to $2\nu_4$, $\nu_2 + \nu_4$ and $2\nu_2$. For $\nu_2 + \nu_4$ and $2\nu_4$ weak bands, which most likely contain more than one component, are observed at 2408 and 2560 cm^{-1} respectively. A doublet is observed for $2\nu_4$; the components appear at 2210 and 2244 cm^{-1}. The low wave number component likely originates from the overtone $\nu_4(E) + \nu_4(E) = 2\nu_4(A_1 + B_1 + B_2)$ and since it very

likely undergoes Fermi resonance with $\nu_1(A_1)$ the correct assignment is probably $2\nu_4(A_1)$. For the highest wave number component the most likely assignment is $\nu_4(B_2) + \nu_4(E) = 2\nu_4(E)$. A complete summary of the assignments for $NaBH_4$(II) and $NaBD_4$(II) are found in Table 5-3.

Unfortunately the Raman spectra of the phase II sodium borohydrides give a dearth of information for the modes of translatory and rotatory origin and in the infrared only one absorption appears which may be associated with the external fundamentals. In the spectrum of $NaBH_4$(II) it appears at 172 cm^{-1} and in the spectrum of $NaBD_4$(II) at 167 cm^{-1}. The assignment is $\nu_T(B_2, E)$. As has previously been indicated, an anomalous line appears in the spectra of the phase II sodium borohydrides which has tentatively been assigned to $3\nu_R$. In the spectrum of $NaBH_4$(II) it appears at 1153 cm^{-1} and in the spectrum of $NaBD_4$(II) it appears at 877 cm^{-1}. Assuming the $3\nu_R$ assignment, modes of rotatory origin, without correction for anharmonicity, are placed at 384 cm^{-1} for $NaBH_4$(II) and at 292 cm^{-1} for $NaBD_4$(II). The frequency ratio is 0.76 which compares with an expected ratio of 0.71. There is only one piece of experimental information with which to check the $3\nu_R$ assignment. Stockmayer and Stephenson (35) using heat capacity data have estimated that ν_R for $NaBH_4$(II) should lie at about 350 cm^{-1}. While this result does not exclude the $3\nu_R$ assignment, it does not give exceptionally strong support for it either and hence the $3\nu_R$ assignment must be regarded as only tentative.

Finally it is appropriate to compare the earlier infrared results of Schutte (32) for $NaBH_4$ with those obtained in this work. The two sets of

TABLE 5-3. Assignments for $NaBH_4$(II) and $NaBD_4$(II); cm^{-1}

ASSIGNMENT	$NaBH_4$(II) - THIS WORK		$NaBD_4$(II) - THIS WORK	
	R.	I.R.	R.	I.R.
$\nu_1(A_1)$	2341		1622	
$\nu_2(A_1)$	1280		916	
$\nu_2(B_1)$			904	
$\nu_3(B_2)$		2272(sh)	1740.5	1724.5
$\nu_3(E)$	2322	2303		1735.5
$^{10}\nu_3(E)$		2334(sh)	1757	1755
$\nu_4(B_2)$		1148(sh)		870
$\nu_4(E)$		1122		854.5
$^{10}\nu_4(E)$		1134		865
$\nu_T(B_2,E)$		172		167
$\nu_R(A_2,E)$		(384)*		(292)
$2\nu_2$	2560		1821	
$\nu_2+^{10}\nu_4(B_2)$			1800	1798
$\nu_2+\nu_4(B_2)$			1791	1789
$\nu_2+\nu_4(E)$	2408	2404	1775	1773
$\nu_2+\nu_4(E)$			1766	1764
$2^{10}\nu_4(E)$	2257	2256	1720	1715
$2\nu_4(E)$	2244	2236	1701	1692
$2\nu_4(A_1)$	2210			
$3\nu_R$		1153		877

* bracketed frequencies for ν_R are inferred from $3\nu_R$

results are summarized below.

Assignment.	This Work	Schutte - REF. 32
$\nu_4(E)$	1122	1123
$^{10}\nu_4(E)$	1134	1135 v.w.
$3\nu_R$	1148(sh)	
$\nu_4(B_2)$	1153	1152 w.
		2197(sh) w.
		2223 s.
$2\nu_4(E)$	2236	2238 s.
$^{10}2\nu_4(E)$	2256	2256 m.
$\nu_3(B_2)$	2272	
		2287 v.s.
$\nu_3(E)$	2303	2305 v.s.
$^{10}\nu_3(E)$	2334(sh)	
$\nu_2+\nu_4$	2404	2404 w.

From the above comparison it is seen that Schutte reports two lines for $2\nu_4$ which are not compatible with the results of this work. It is possible that the 2223 cm^{-1} absorption could be assigned to $\nu_4(E) + \nu_4(E) = 2\nu_4(B_2)$ which has a predicted frequency of 2244 cm^{-1}. However, if this is the case such a line should certainly also be observed in the spectrum of $NaBD_4$(II) where the lines are exceptionally well resolved. The shoulder at 2197 cm^{-1} appears to be completely spurious. Also, the 2287 cm^{-1} line reported by

Schutte does not appear in the spectrum recorded in this work and since it is reported as a strong distinct absorption it is difficult to associate it with the shoulder we observed at 2272 cm^{-1}. The remaining discrepancies involve the absorptions we observe as shoulders at 1148 and 2334 cm^{-1}. These may have been missed in the earlier work because of their low intensity. There is a possible explanation for the discrepancies between the results. Schutte's samples may have been prepared while exposed to the atmosphere. Earlier work (39) done in this laboratory has shown that such exposure to the atmosphere can allow for the occurrence of slight decomposition and perhaps more important the formation of $NaBH_4 \cdot H_2O$ (69). Such introduction of impurities into the sample could easily explain the discrepancies. The point to be emphasized though is that Schutte's results, like those of this work, show an unambiguous splitting of ν_4 which may be associated with the disorder-order phase transformation.

5-3 The Phase I Alkali Metal Borohydrides

The interpretation of the phase I spectra of the alkali metal borohydrides must take into account the disorder introduced into the lattice via the randomness associated with the hydrogen atoms. However, since the heat capacity data (36, 37) give evidence of different situations for the ordering processes, $NaBH_4(I) \rightarrow NaBH_4(II)$ and $KBH_4(I) \rightarrow KBH_4(III)$, it is appropriate to review this data before attempting to interpret the experimental results.

It will be recalled from Chapter I that the heat capacity data (36) for sodium borohydride indicate a well defined disorder-order phase trans-

formation, with the anomaly at 189.9°K in the heat capacity curve accounting for the excess entropy of transition expected for a disorder-order process. For potassium borohydride the situation is somewhat different (37). In this case the heat capacity anomaly at 77.2°K accounts for only 0.70 of the expected 1.36 e.u. with the heat capacity measurements giving evidence for the original onset of the disorder-order transformation at a much higher temperature. It is possible that a simple steric argument can be used to explain the difference between the situations for sodium borohydride and potassium borohydride. The effective ionic radius of the BH_4^- ion has been given (38) as 2.03 Å and the ionic radii of the Na^+ and K^+ ions may be taken as 0.98 and 1.33 Å respectively (55). Using these radii the predicted B-Na and B-K distances are 3.01 and 3.36 Å respectively. These predicted distances compare with the respective crystal distances of 3.08 and 3.36 Å at 298°K. If these predicted and observed inter-ionic distances are at all reliable for purposes of comparison it is immediately evident that at 298°K relatively tighter crystal packing occurs in KBH_4 than in $NaBH_4$. Pursuing this idea further we can extend the comparison of predicted and observed inter-ionic distances to include the remaining alkali metal borohydrides as well as the phase II ammonium halides. Using an effective NH_4^+ ionic radius of 1.48 Å (55) and alkali metal ion and halide ion radii found in Kittel (55) the results may be summarized as follows:

	r(B-X) Predicted	r(B-X) Observed	Difference		r(N-X) Predicted	r(N-X) Observed	Difference
$NaBH_4$	3.01	3.08	0.07	NH_4Cl	3.29	3.36	0.07
KBH_4	3.36	3.36	0.00	NH_4Br	3.44	3.52	0.08
$RbBH_4$	3.51	3.51	0.00	NH_4I	3.67	3.75	0.08
$CsBH_4$	3.70	3.71	0.01				

It is clearly seen that two groups of salts emerge; those with a difference of about 0.07 Å between the predicted and observed inter-ionic distances and those with predicted and observed inter-ionic distances which essentially coincide. The first group of salts are known to undergo well defined disorder-order phase transformations and with respect to the second group it is known that the disorder-order transformation for KBH_4 is poorly defined. It is possible that these two different situations are indeed related to differences in the relative looseness of the crystal packing. It is to be noted also that over the temperature interval 293-90°K (40) $NaBH_4$ suffers an axial contraction of 4.02% whereas KBH_4 suffers an axial contraction of only 1.32%.

Turning now to the spectra of the alkali metal borohydrides we can see that they too are indicative of the two different situations being considered. For the series of salts, $NaBH_4$, KBH_4, $RbBH_4$ and $CsBH_4$ the frequencies of the translatory modes at 295°K are respectively 160, 173, 164 and 155 cm^{-1} (see also Tables 5-4, 5-5 and 5-6). The anomalously low translatory frequency observed for $NaBH_4$ may be attributed to a relatively looser crystal packing for this salt. Furthermore, a comparison of the

half-height band width ratios, $\nu_3(10°K)/\nu_3(295°K)$ for the same series of salts shows that the ratio for $NaBH_4$ is anomalously low. The results which show this to be so are presented below. The half-height band widths shown are for band heights of 9.5 ± 0.5 cm.

	Half-height band widths		Ratios
	$\nu_3(295°K)$ (cm^{-1})	$\nu_3(10°K)$ (cm^{-1})	$\nu_3(10°K)/\nu_3(295°K)$
$NaBH_4$	80	38	0.47
KBH_4	45	28	0.62
$RbBH_4$	45	36	0.80
$CsBH_4$	45	25	0.56
$NaBD_4$	47.5	14	0.26
KBD_4	15	6	0.47

If we assume that the contribution to band width at 295°K due to the population of vibrational levels lying above the ground state is constant for the series of salts, then the discrepancies in the ratios are largely due to contributions to the high temperature intensities from densities of states with $\underline{K} \neq 0$. Therefore, if we assume complete disorder for $NaBH_4$ at 295°K the observed half-height band width ratios indicate that at 295°K complete disorder is perhaps not associated with KBH_4, $RbBH_4$ and $CsBH_4$ and that if this is so the relative disorder for these three salts as indicated by the observed ratios is $CsBH_4 > KBH_4 > RbBH_4$. Although the neutron diffraction results obtained by Peterson (34) were interpreted as being compatible with a completely disordered KBH_4 structure at 298°K, the heat capacity data

TABLE 5-4. Assignments for $NaBH_4(l)$ and $NaBD_4(l)$; cm^{-1}

ASSIGNMENT	$NaBH_4(l)$ - THIS WORK		$NaBD_4(l)$ - THIS WORK	
	R.	I.R.	R.	I.R.
ν_1	2335		1618	
ν_2	1278		907.5	
ν_3		2297	1728	1729
ν_4		1119		853
ν_T		160		155
$2\nu_2$				
$\nu_2+\nu_4$	2403(sh)	2393	1772.5	1767
$2\nu_4$	2229	2222	1695	1690
$2\nu_4$	2197.5			

TABLE 5-5. Assignments for KBH_4(I) and KBD_4(I)*; cm^{-1}

ASSIGNMENT	KBH_4(I) - THIS WORK		KBD_4(I) - THIS WORK	
	R.	I.R.	R.	I.R.
ν_1	2310		1599	
ν_2	1248.5		890.5	
$^{10}\nu_3$			1733(sh)	1732
ν_3		2279	1717	1717
$^{10}\nu_4$				858(sh)
ν_4	1118	1117	851	850
T_1		173		168
$2\nu_2$	2495		1782	
$\nu_2+^{10}\nu_4$				1762(sh)
$\nu_2+\nu_4$	2380	2377	1752.5	1752
$2^{10}\nu_4$			1694	1693
$2\nu_4$	2217	2213	1679	1677
$2\nu_4$	2181			

* The assignments are probably for a pseudo Phase I structure. This point is amplified in the text.

TABLE 5-6. Assignments for $RbBH_4(I)$ and $CsBH_4(I)$*; cm^{-1}

ASSIGNMENT	$RbBH_4(I)$ - THIS WORK		$CsBH_4(I)$ - THIS WORK	
	R.	I.R.	R.	I.R.
ν_1	2297		2281	
ν_2	1237.5		1222	
ν_3	2276(sh)	2273	2256(sh)	2251
ν_4	1113	1112	1102.5	1100
ν_T		164		155
$2\nu_2$	2472		2440	
$\nu_2+\nu_4$	2360	2361	2335(sh)	2330
$2\nu_4$	2202	2202	2182	2181
$2\nu_4$	2167		2151	

*The assignments are probably for a pseudo Phase I structure. This point is amplified in the text.

(37) which show a broad transition from about 200 to 450°K were interpreted as giving evidence that the original onset of the disorder-order transformation was at about 450°K. This latter situation is clearly compatible with the spectroscopic results and also with steric considerations. Therefore, it is very likely that the structures of KBH_4, $RbBH_4$ and $CsBH_4$, at 295°K possess considerable disorder but not complete disorder.

The infrared and Raman spectra together of $NaBH_4$, KBH_4, $RbBH_4$ and $CsBH_4$ at 295°K (see Figures 5-1 - 5-8) possess bands which may be assigned as ν_1, ν_2, ν_3, ν_4, T_1, $2\nu_4$, $\nu_2 + \nu_4$ and $2\nu_2$. A complete summary of assignments is contained in Tables 5-4, 5-5 and 5-6.

5-4 Lithium Borohydride

The crystal structure of lithium borohydride is compatible with the space group D_{2h}^{16}(Pcmn) and hence the factor group analysis is carried out under the D_{2h} factor group. The results for the various types of vibrations may be summarized as follows:

$$\Gamma(\text{internal}) = 6A_g + 3B_{1g} + 6B_{2g} + 3B_{3g} + 3A_u + 6B_{1u} + 3B_{2u} + 6B_{3u}$$

$$\Gamma(\text{OT}) = 4A_g + 2B_{1g} + 4B_{2g} + 2B_{3g} + 2A_u + 3B_{1u} + B_{2u} + 3B_{3u}$$

$$\Gamma(\text{OL}) = A_g + 2B_{1g} + B_{2g} + 2B_{3g} + 2A_u + B_{1u} + 2B_{2u} + B_{3u}$$

$$\Gamma(\text{AT}) = B_{1u} + B_{2u} + B_{3u}$$

It is found that the four fundamental vibrations associated with the free BH_4^- ion become the precursors of 36 crystal modes. The correlation diagram for site group splitting follows.

Vibrational Mode	Free Ion Symmetry - T_d		Site Group Symmetry - C_s
ν_1	A_1	→	A'
ν_2	E	→	A', A''
ν_3	F_2	→	A', A', A''
ν_4	F_2	→	A', A', A''

Under the D_{2h} factor group each A' mode will give four crystal modes of symmetries A_g, B_{2g}, B_{1u} and B_{3u} and each A'' mode will give four crystal modes of symmetries B_{1g}, B_{3g}, A_u and B_{2u}. Modes of gerade symmetry all possess elements of the polarizability tensor and therefore will be Raman active. Only modes of B_{1u}, B_{2u} and B_{3u} symmetries are infrared active.

Since it is found that splitting for the internal fundamentals arising from correlation field effects is not experimentally observable, it is convenient to make the infrared assignments for the internal fundamentals according to the following scheme:

$$\nu_1(B_{1u} + B_{3u})$$
$$\nu_2(B_{1u} + B_{3u}),\ \nu_2'(B_{2u})$$
$$\nu_3(B_{1u} + B_{3u}),\ \nu_3'(B_{1u} + B_{3u}),\ \nu_3''(B_{2u})$$
$$\nu_4(B_{1u} + B_{3u}),\ \nu_4'(B_{1u} + B_{3u}),\ \nu_4''(B_{2u})$$

For the Raman assignments the corresponding scheme is:

$$\nu_1(A_g + B_{2g})$$
$$\nu_2(A_g + B_{2g}),\ \nu_2'(B_{1g} + B_{3g})$$
$$\nu_3(A_g + B_{2g}),\ \nu_3'(A_g + B_{2g}),\ \nu_3''(B_{2g} + B_{3g})$$
$$\nu_4(A_g + B_{2g}),\ \nu_4'(A_g + B_{2g}),\ \nu_4''(B_{1g} + B_{3g})$$

TABLE 5-7. Assignments for $LiBH_4$ and $LiBD_4$; cm^{-1}

ASSIGNMENT	$LiBH_4$ - THIS WORK		$LiBD_4$ - THIS WORK	
	R.	I.R.	I.R.	R.
ν_1	2300		1605.5	1606
ν_2	1287	1284	923	919
ν_2'	1325	1323	937	933
ν_3	2274	2277	1721	1722
ν_3'	2309(sh)	2307	1739	1736
ν_3''		2350		1757
ν_4		1089		828
$^{10}\nu_4$		1099(sh)		837
ν_R		(418)		(319)
T_1		391		340
T_2		324		276
T_3		274		248
T_4		232		215
T_5		175.5		
T_6		162.5		149.5
$\nu_2'+\nu_4$		2423		1785(sh)
$\nu_2+\nu_4$		2387(sh)		
$2^{10}\nu_4$		2197		1679
$2\nu_4$		2176		1654
$3\nu_R$	1253	1254	959	957

* bracketed frequencies for ν_R have been inferred from $3\nu_R$

Figure 5–8 The I.R. spectra of $LiBH_4$ and $LiBD_4$

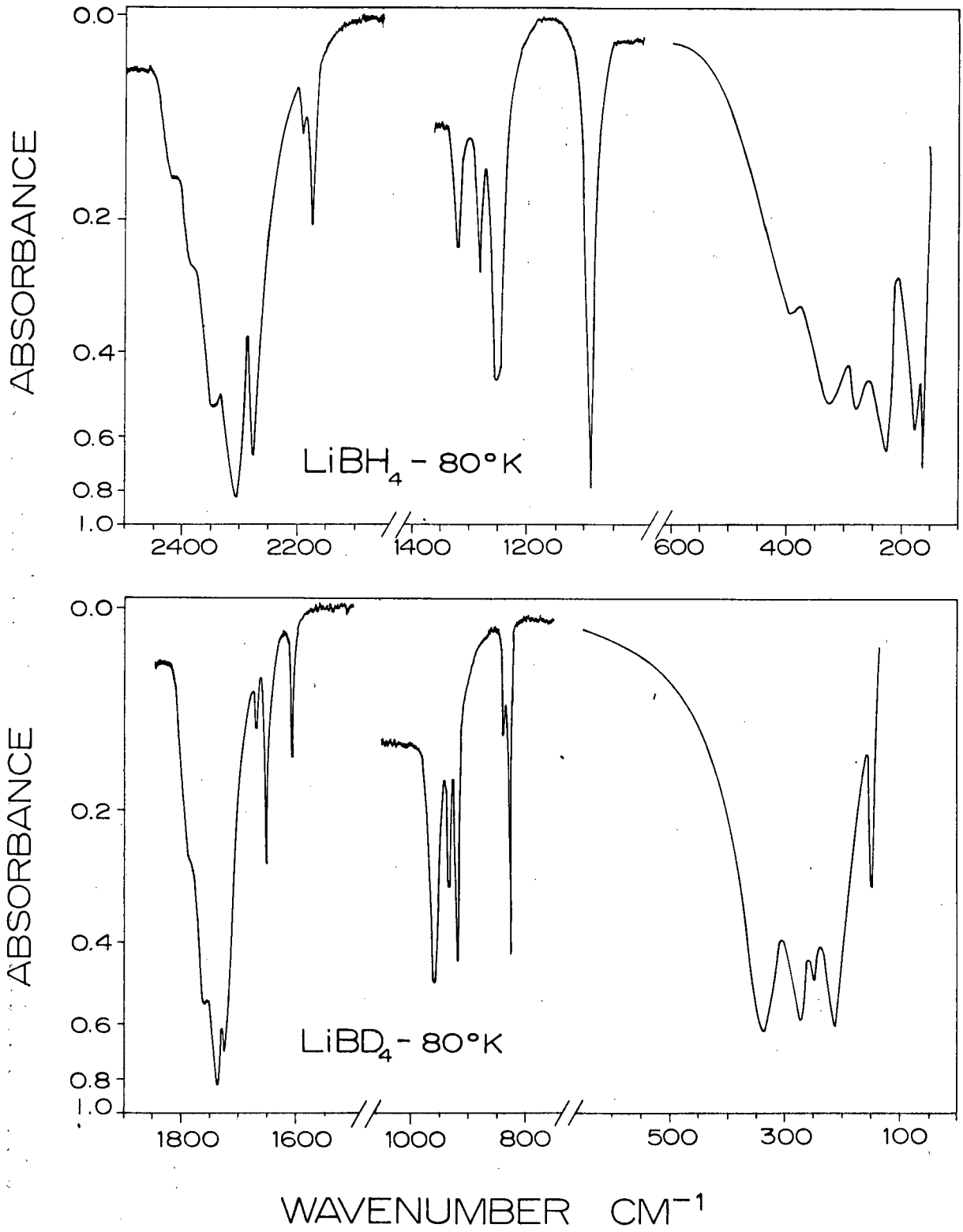

Figure 5-9 The Raman Spectra of $LiBH_4$ and $LiBD_4$

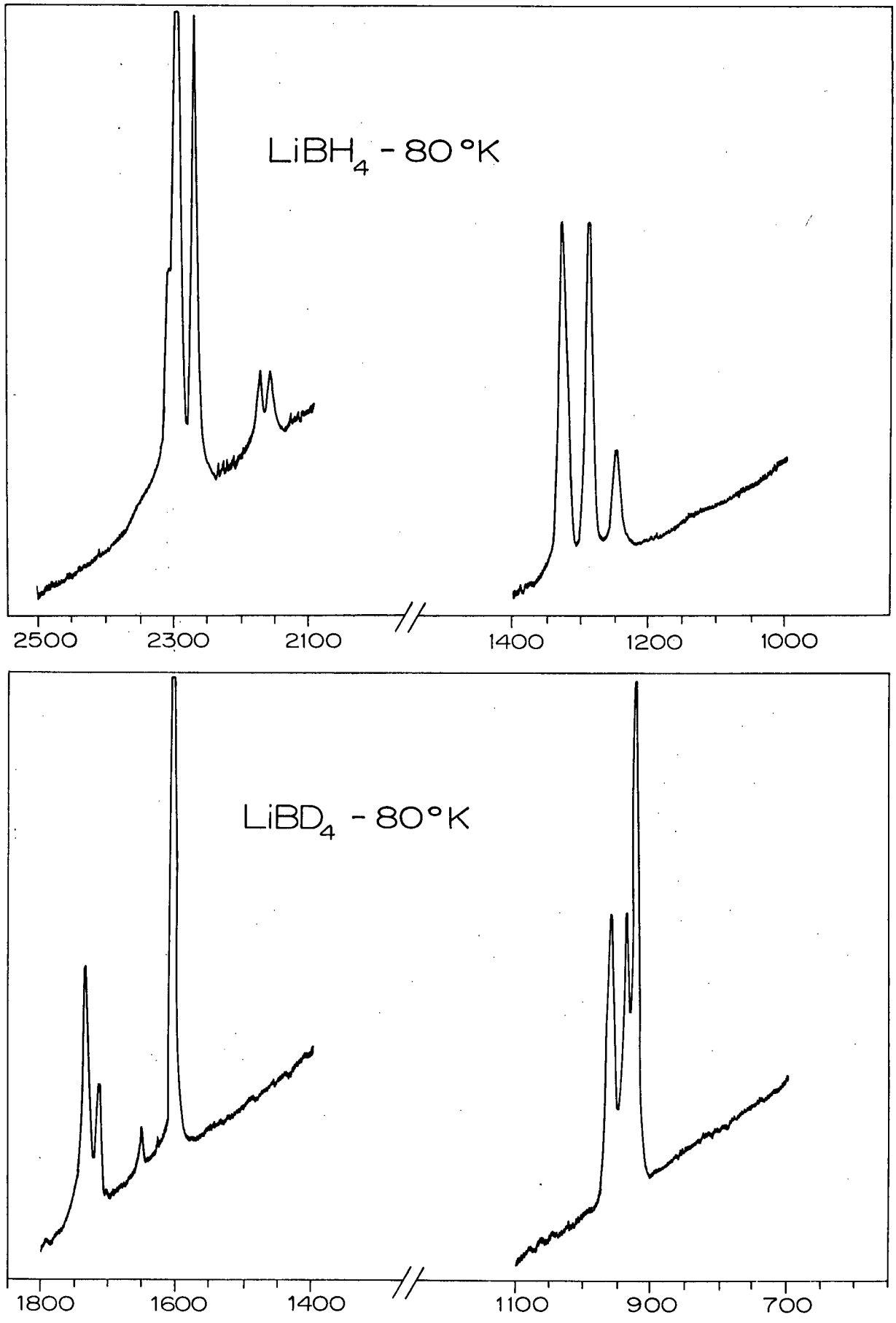

It should be noted that for negligible factor group splittings that the frequencies of corresponding assignments for the two schemes will essentially coincide.

The Raman spectra (see Figure 5-9) of the lithium borohydrides allow us to place $\nu_1(A_{1g} + B_{2g})$ for $LiBH_4$ at 2300 cm^{-1} and ν_1 for $LiBD_4$ at 1605.5 cm^{-1}. Turning now to the infrared spectra (see Figure 5-8) we find that for both $LiBH_4$ and $LiBD_4$ four lines appear in the bending region of the spectra. In both cases the absorption lying at lowest wave number must be assigned to a component of ν_4; very unexpectedly no other nearby lines are found which may be assigned to the two remaining predicted components. In the spectrum of $LiBD_4$ the absorption associated with ν_4 appears at 828 cm^{-1}. It is very sharp and has a half-height band width of 6 cm^{-1}. Therefore, it is unlikely that more than one component of ν_4 contributes to its intensity and thus it is likely that the remaining components just do not appear. Since none of the components of ν_4 appear in the Raman spectrum only the one ν_4 line can be assigned. In the spectrum of $LiBH_4$ it appears at 1089 cm^{-1}.

Of the three remaining lines appearing in the bending region of the spectrum of each of the lithium borohydrides, two must be assigned to the two predicted ν_2 components. In the spectrum of $LiBH_4$ we may associate the two sharpest lines of the triplet with ν_2 and if we further choose the most intense line of the ν_2 doublet as $\nu_2(B_{1u} + B_{3u})$ then the following assignments can be made: $\nu_2(B_{1u} + B_{3u}) = 1284$ cm^{-1} and $\nu_2'(B_{2u}) = 1323$ cm^{-1}. The corresponding assignments for $LiBD_4$ are $\nu_2(B_{1u} + B_{3u}) = 919$ cm^{-1} and $\nu_2'(B_{2u}) = 933$ cm^{-1}. The mean ν_2 frequencies for $LiBH_4$ and $LiBD_4$ are 1304 and 926 cm^{-1} and the

frequency ratio is 0.711 which compares with a predicted frequency ratio of 0.707 for the free ion.

After assigning the components of ν_2 there remains an anomalous line at 1254 cm^{-1} in the spectrum of $LiBH_4$ and an anomalous line at 957 cm^{-1} in the spectrum of $LiBD_4$. It is very likely that these lines have the same origin as the anomalous lines observed in the bending regions of the spectra of the phase II sodium borohydrides. It will be recalled that for the sodium borohydrides these lines were tentatively assigned as $3\nu_R$. If the same assignment is made for the lithium borohydrides, modes of rotatory origin, without correction for anharmonicity, are placed at 418 and 319 cm^{-1} for $LiBH_4$ and $LiBD_4$ respectively. The frequency ratio is 0.76 which compares with an identical frequency ratio for the corresponding lines as observed in the sodium borohydrides. The predicted frequency ratio is 0.71.

Turning now to the stretching region of the infrared spectrum of $LiBH_4$ we find that the most prominent feature is a triplet of intense lines which appear at 2277, 2307 and 2350 cm^{-1}. These lines may be associated with ν_3. The two most intense lowest lying lines may be assigned as $\nu_3(B_{1u} + B_{3u}) = 2277\ cm^{-1}$ and $\nu_3'(B_{1u} + B_{3u}) = 2307\ cm^{-1}$. The highest wave number absorption is then assigned as $\nu_3''(B_{2u}) = 2350\ cm^{-1}$. It is found that the two low wave number components also appear in the Raman spectrum where the respective frequencies are 2274 and 2309 cm^{-1}. The two absorptions appearing on the high frequency side of ν_3'' at 2387(sh) and 2423 cm^{-1} can be assigned as $\nu_2 + \nu_4$ and $\nu_2' + \nu_4$. If ν_4 is taken as 1089 cm^{-1} then the predicted frequencies for $\nu_2 + \nu_4$ and $\nu_2' + \nu_4$ are respectively 14 and 11 cm^{-1} lower than those observed. This situation can be attributed to Fermi

resonance with a component of ν_3. The two remaining lines appearing in the stretching region of the spectrum of $LiBH_4$ can be assigned as $2\nu_4$ and $2\,{}^{10}\nu_4$. They appear at 2176 and 2188 cm^{-1} respectively and if ν_4 and ${}^{10}\nu_4$ are taken to be the observed infrared frequencies then the respective anharmonicities are two wave numbers and one wave number. The only lines appearing in the second order Raman spectrum of $LiBH_4$ are associated with $2\nu_4$. A doublet appears with frequencies of 2169 and 2173 cm^{-1}. The high wave number component can be associated with the 2176 cm^{-1} absorption observed in the infrared. The low wave number component, no doubt, involves different components of ν_4 and may have an intensity which is enhanced by Fermi resonance with $\nu_1(A_g + B_{2g})$ which appears at 2300 cm^{-1}.

The infrared stretching region of the spectrum of $LiBD_4$ has features which closely parallel those observed for $LiBH_4$. One important difference is that in the infrared spectrum of $LiBD_4$ $\nu_1(B_{1u} + B_{3u})$ is observed. In the infrared spectrum of $LiBH_4$ its appearance is obscured by the lines associated with ν_3. The $\nu_1(B_{1u} + B_{3u})$ frequency for $LiBD_4$ is 1606 cm^{-1}. This compares with the corresponding Raman line at 1605.5 cm^{-1}. The lines associated with ν_3 in the $LiBD_4$ infrared spectrum may be assigned as $\nu_3(B_{1u} + B_{3u}) = 1722$ cm^{-1}, $\nu_3'(B_{1u} + B_{3u}) = 1736$ cm^{-1} and $\nu_3''(B_{2u}) = 1757$ cm^{-1}. The two low wave number absorptions compare with lines observed in the Raman spectrum at 1721 and 1739 cm^{-1}. On the high wave number side of ν_3'' an absorption appears at 1785(sh) cm^{-1}. It can be assigned as $\nu_2' + \nu_4$. If ν_4 is taken as 828 cm^{-1} the predicted frequency is 24 cm^{-1} lower than that observed. This situation can be attributed to Fermi resonance with a

component of ν_3. The two remaining lines appearing in the infrared stretching region of the $LiBD_4$ spectrum have frequencies of 1654 and 1672 cm^{-1}. These lines can be assigned as $2\nu_4$ and $2\,^{10}\nu_4$ respectively.

In the vibrational Raman spectra of the lithium borohydrides none of the predicted modes of either rotatory or translatory origin appear. However, the long wave length infrared spectra are very rich in spectral information. No modes were observed which could be assigned to rotatory oscillations but 6 $LiBH_4$ modes and 5 $LiBD_4$ modes of translatory origin were observed. We may note that the ^{6}Li- ^{7}Li and ^{10}B- ^{11}B natural abundances of about 1:12 and 1:4 will introduce disorder into the lattice which will destroy true translational periodicity. Therefore some of the observed modes may originate from states with $\underline{K} \neq 0$. In the zero wavevector limit 7 infrared active translatory modes are predicted.

Meaningful assignments for the translatory modes with respect to symmetry type are impossible without undertaking a study involving single crystals and polarized radiation and therefore no attempt at making such assignments will be made. The assignments for the lithium borohydrides are summarized in Table 5-7.

5-5 The Barrier to Rotation

In Chapter IV it was seen that barrier height, Vo(N.M.R.) as obtained from N.M.R. experiments provided good estimates of the barrier to rotation for the ordered phases of the ammonium halides. It is very likely that a similar situation holds for the ordered phases of the alkali metal borohydrides. However, the four fold cosine potential used to calculate the

barrier heights, Vo(G.P.B.), for the ammonium halides will not be reliable for the alkali metal borohydrides. For the phase III and IV ammonium halides rotation of the NH_4^+ ion about the $\bar{4}$ axis gives four essentially equivalent positions of minimum potential energy. A similar situation holds for the phase II and III alkali metal borohydrides but with the important difference that intermediate between the four equivalent positions of minimum potential energy there are four additional equivalent positions which will probably lie close in energy to the positions of minimum potential energy. This will have the effect of lowering the barrier height from that predicted by the four fold cosine potential. That this is so is indicated by considering the N.M.R. results (70) for the barrier heights of the alkali metal borohydrides. For $NaBH_4$(II) Vo(N.M.R.) is 1230 ± 70 cm^{-1}. The results for the torsional frequency of $NaBH_4$(II) as inferred from heat capacity data (35) and the second overtone, $3\nu_R$, are 350 and 384 cm^{-1} respectively. For these torsional frequencies the four-fold cosine potential predicts respective barrier heights, Vo(G.P.B.), of 2160 and 2850 cm^{-1}. These results for the barrier height are not within the limits predicted by Vo(N.M.R.) and indicate that a four fold cosine potential cannot be meaningfully related to the oscillations of the BH_4^- ions in the ordered phases of the alkali metal borohydrides. The barrier height Vo(N.M.R.) for potassium borohydride as determined by Tsang and Farrar (70) is 1240 ± 40 cm^{-1}. These same authors interpret their N.M.R. results for lithium borohydride as giving evidence for two crystallographically non-equivalent BH_4^- ions in the unit cell which have barriers to rotation of 1650 ± 100 and 1330 ± 100 cm^{-1}. This interpretation is probably subject to review since both the

previous X-ray results (42) and the infrared results of this work unambiguously indicate that each of the four BH_4^- ions in the unit cell has identical C_s site symmetry; i.e. once a single BH_4^- ion of specific C_s symmetry is appropriately placed in the unit cell the symmetry operations of the space group generate three more BH_4^- ions of identical symmetry at positions in the unit cell which satisfy the symmetry requirements of the space group.

5-6 The Force Field for Crystalline BH_4^-

The fundamental frequencies of the tetrahedral borohydride ion as observed in the vibrational spectrum of KBH_4(III) have been used to compute the force field of the crystalline BH_4^- ion. The force constants calculated at $X_3 = -0.48$ are as follows

	Force Constant (10^5 Dynes/cm)
F_1	3.17937
F_2	0.49194
F_3	2.76021
F_4	0.48640
F_{34}	0.06611

When these force constants are used to compute the spectrum of the crystalline BD_4^- ion in KBD_4(III) the average absolute deviation is 18 cm^{-1} (see Table 5-8). Figures 5-10 and 5-11 show the dependence of F_3, F_4 and F_{34} on the mixing parameter in the interval $-1.2 \leq X \leq 1.2$. The dependence of ν_3 and ν_4 on the mixing parameter in this same interval is shown in Figure 5-12.

FIGURE 5—10

THE SYMMETRY FORCE CONSTANTS F_3 AND F_4 AS A FUNCTION OF THE MIXING PARAMETER — KBH_4 (III)

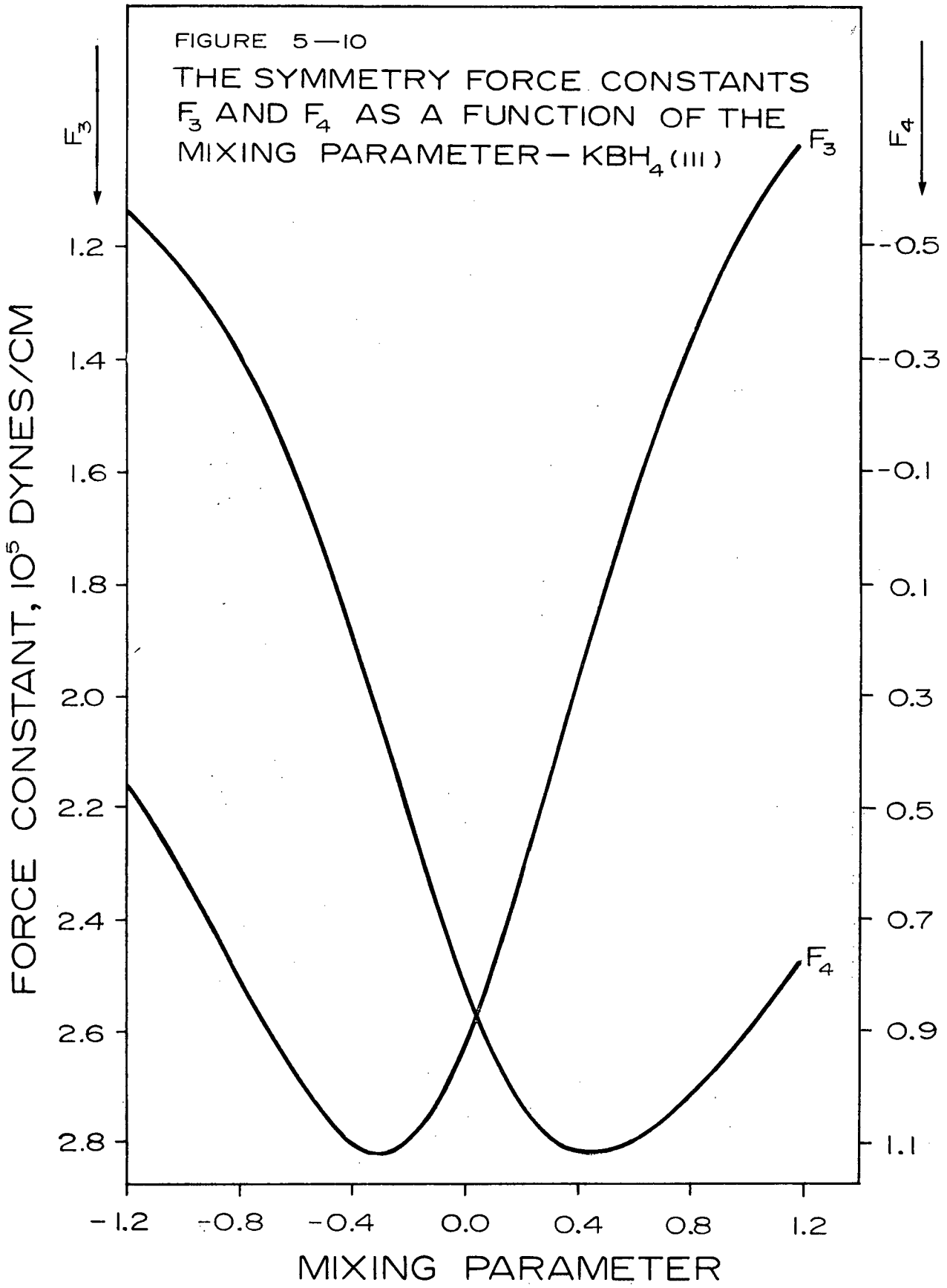

FIGURE 5—11

THE SYMMETRY FORCE CONSTANT F_{34} AS A FUNCTION OF THE MIXING PARAMETER — KBH_4 (III)

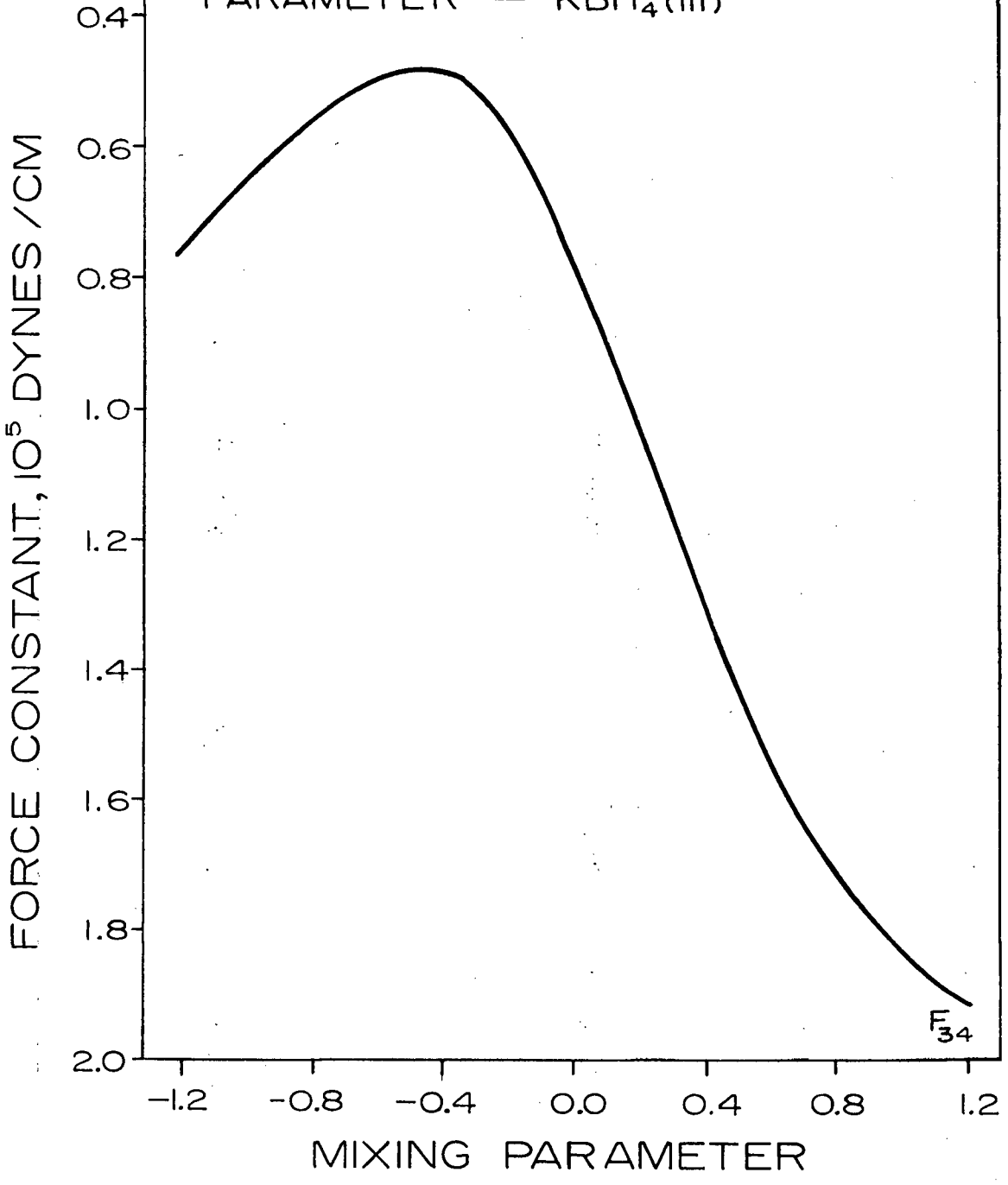

FIGURE 5-12

CALCULATED FREQUENCIES FOR ν_3 AND ν_4 AS A FUNCTION OF THE MIXING PARAMETER – KBH_4 (III) ⟶ KBD_4 (III)

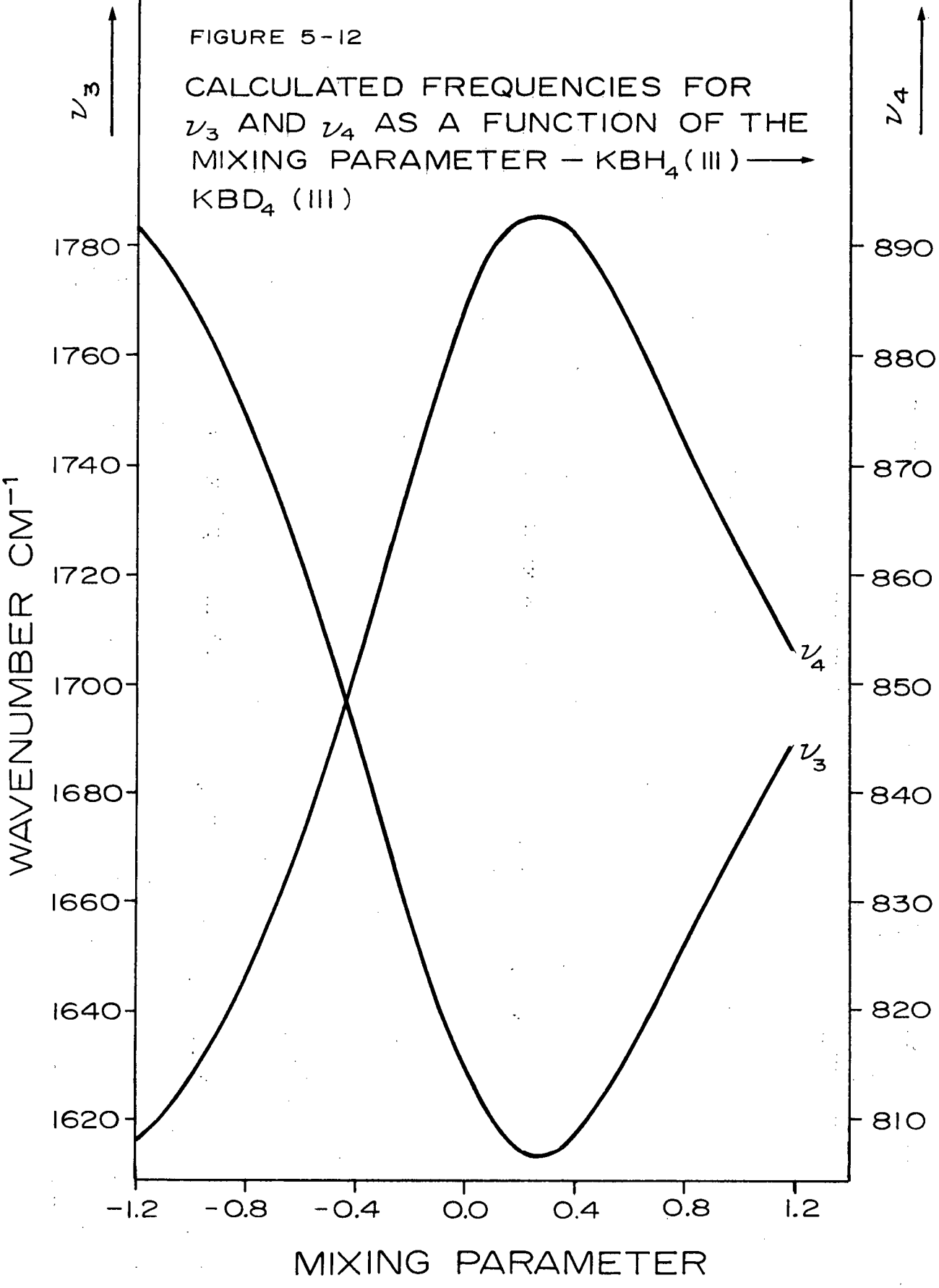

TABLE 5-8. Calculated and Observed Spectra - $BH_4^-(T_d)$

(i) $KBH_4(III) \rightarrow KBD_4(III)$

$X_1 = -0.60 \quad \nu_3 = 1724$

$X_2 = -0.36 \quad \nu_4 = 855$

$X_3 = -0.48$

	ν_1	ν_2	ν_3	ν_4
Calculated Spectrum				
$X = X_3$	1637.2	885.3	1704.6	845.1
Observed Spectrum	1599.5	892	1724	855
Deviation	+37.7	-6.7	-19.4	-9.9

(ii) $KBD_4(III) \rightarrow KBH_4(III)$

$X_1 = -0.89 \quad \nu_3 = 2281$

$X_2 = -0.59 \quad \nu_4 = 1121$

$X_3 = -0.74$

	ν_1	ν_2	ν_3	ν_4
Calculated Spectrum				
$X = X_3$	2261.2	1261.0	2306.0	1134.6
Observed Spectrum	2314.5	1251.5	2281	1121
Deviation	-53.3	+9.5	+25.0	+13.6

5-7 The Effects of a D_{2d} Distortion on BH_4^-

The "unperturbed" vibrational frequencies of the hypothetical $BH_4^-(T_d)$ ion used to calculate the contribution of the kinetic energy to the spectrum of the $BH_4^-(D_{2d})$ ion were chosen according to the following scheme:

$$\nu_1 = \nu_1(A_1)$$
$$\nu_2 = [\nu_2(A_1) + \nu_2(B_1)]/2$$
$$\nu_3 = \nu_3(E) - 1/3\Delta$$
$$\nu_4 = \nu_4(E) + 1/3\Delta$$

Here Δ is the magnitude of the splitting associated with the appropriate triply degenerate T_d vibration. It is easily seen that the above scheme is based on the splitting pattern predicted in section 4-7. We recall that this splitting pattern was for small D_{2d} angular distortions involving two angles greater than the tetrahedral angle and four angles less than the tetrahedral angle. This situation is compatible with the geometry of the phase II BH_4^- ion given in Table 1-8; i.e. there are two angles with a distortion of +2.22° and four angles with a distortion of -1.10°.

Figures 5-13 and 5-14 show the $NaBH_4$(II) ν_3/ν_4 splittings as a function of the mixing parameter for an angular distortion of +2.22° and -1.10°. When the mixing parameter is chosen so as to maximize the ν_3/ν_4 splitting on the interval $-1.2 \leq X \leq 1.2$ the predicted splittings are those of Table 5-9. In the case of $NaBD_4$ there is a complete set of experimentally observed splittings which can be compared with the predicted splittings. For ν_2, ν_3 and ν_4 the observed splittings are 12.0, 11.0 and 15.5 cm^{-1}. These compare with respective predicted splittings of 12.6, 13.9 and 8.9 cm^{-1}.

Figures 5-15 and 5-16 show the results when $\underline{\underline{F}}(T_d)$ (X =-0.48) is fixed and $\underline{\underline{G}}(D_{2d})$ is varied (X = -0.48 gives optimum transferability of force constants for $KBH_4(T_d) \rightarrow KBD_4(T_d)$ - see Table 5-8). We see that the observed ν_3 splitting of 31 cm^{-1} requires an angular distortion of -3.3° and +6.9°. The 26 cm^{-1} ν_4 splitting requires a distortion of -5.6° and+11.90°. These values compare with the probable distortion of -1.1°and+2.20°.

FIGURE 5–13

PREDICTED SPLITTING OF ν_3 AS A FUNCTION OF THE MIXING PARAMETER

$NaBH_4$ (Td) ⟶ $NaBH_4$ (D_{2d})

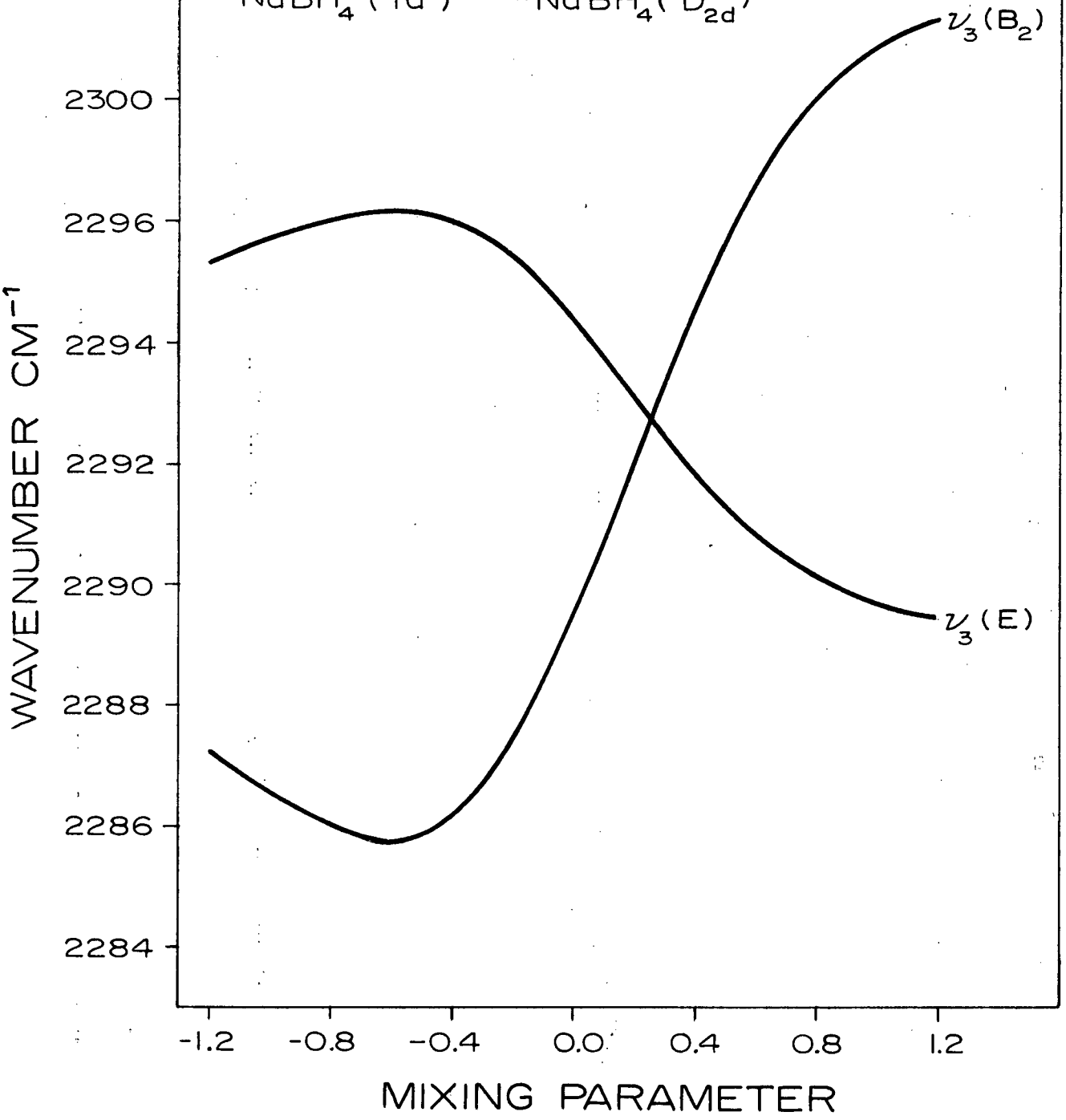

FIGURE 5-14

PREDICTED SPLITTING OF ν_4 AS A FUNCTION OF THE MIXING PARAMETER — $NaBH_4$ (T_d) ⟶ NaBH (D_{2d})

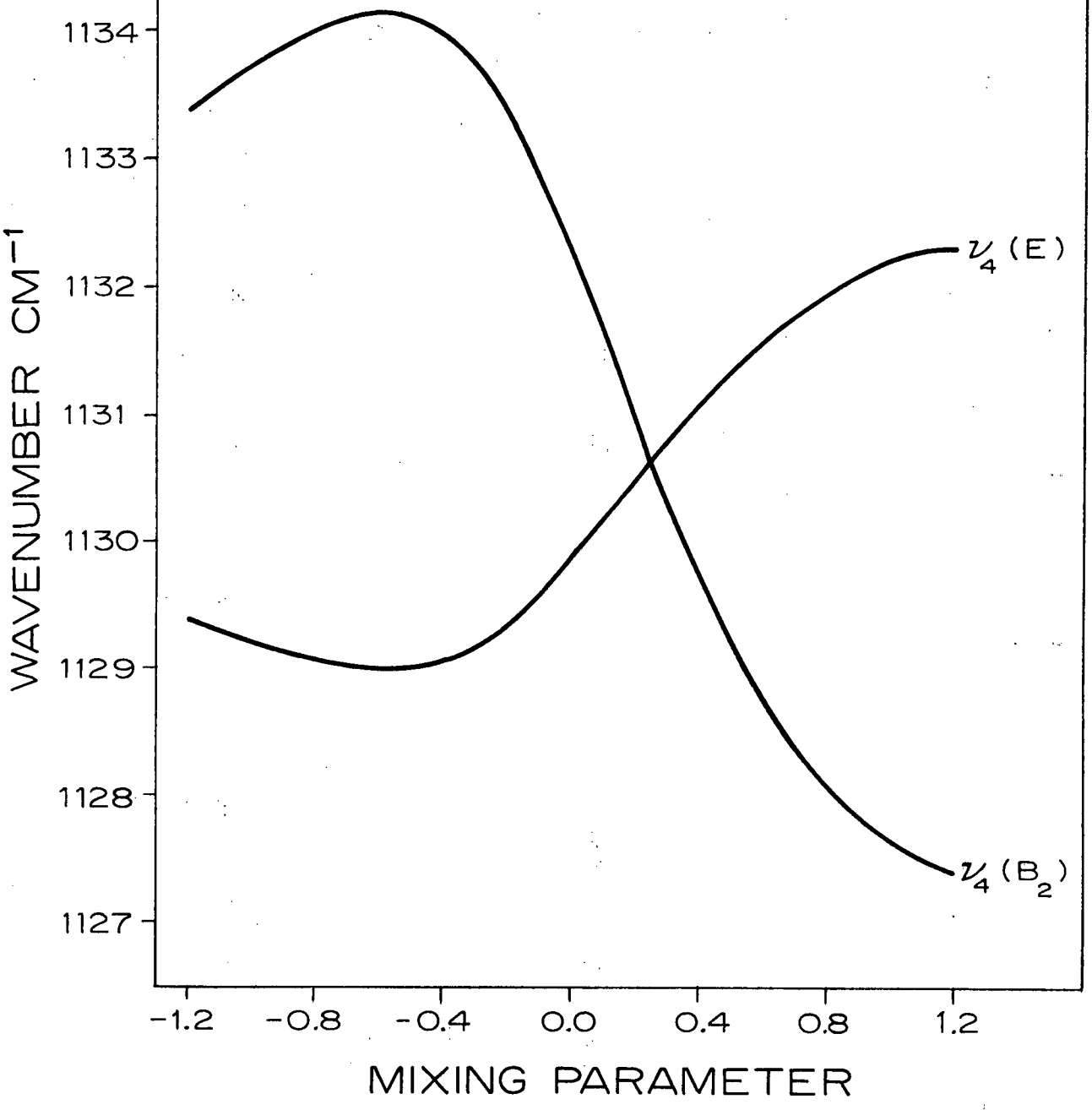

TABLE 5-9. Calculated and Observed Spectra - $BH_4^-(D_{2d})$

(i) $NaBH_4(T_d) \rightarrow NaBH_4(D_{2d})$; $X_4 = -0.60$

	$\nu_1(A_1)$	$\nu_2(A_1)$	$\nu_2(B_1)$	$\nu_3(B_2)$	$\nu_3(E)$	$\nu_4(B_2)$	$\nu_4(E)$
OBS.	2341	1280		2272	2303	1148	1122
Δ				31.0		26.0	
CALC.	2341	1288.8	1271.1	2285.7	2296.2	1134.1	1129.0
Δ		17.7		10.5		5.1	

(ii) $NaBD_4(T_d) \rightarrow NaBD_4(D_{2d})$; $X_4 = -0.70$

	$\nu_1(A_1)$	$\nu_2(A_1)$	$\nu_2(B_1)$	$\nu_3(B_2)$	$\nu_3(E)$	$\nu_4(B_2)$	$\nu_4(E)$
OBS.	1622	916	904	1724.5	1735.5	870	854.5
Δ		12.0		11.0		15.5	
CALC.	1622	916.3	903.7	1722.5	1736.4	864.3	857.4
Δ		12.6		13.9		8.9	

FIGURE 5–15

SPLITTING OF ν_3 AND ν_4 AS A FUNCTION OF ANGULAR DISTORTION (X=-0.48)

$NaBH_4(T_d) \longrightarrow NaBH_4(D_{2d})$

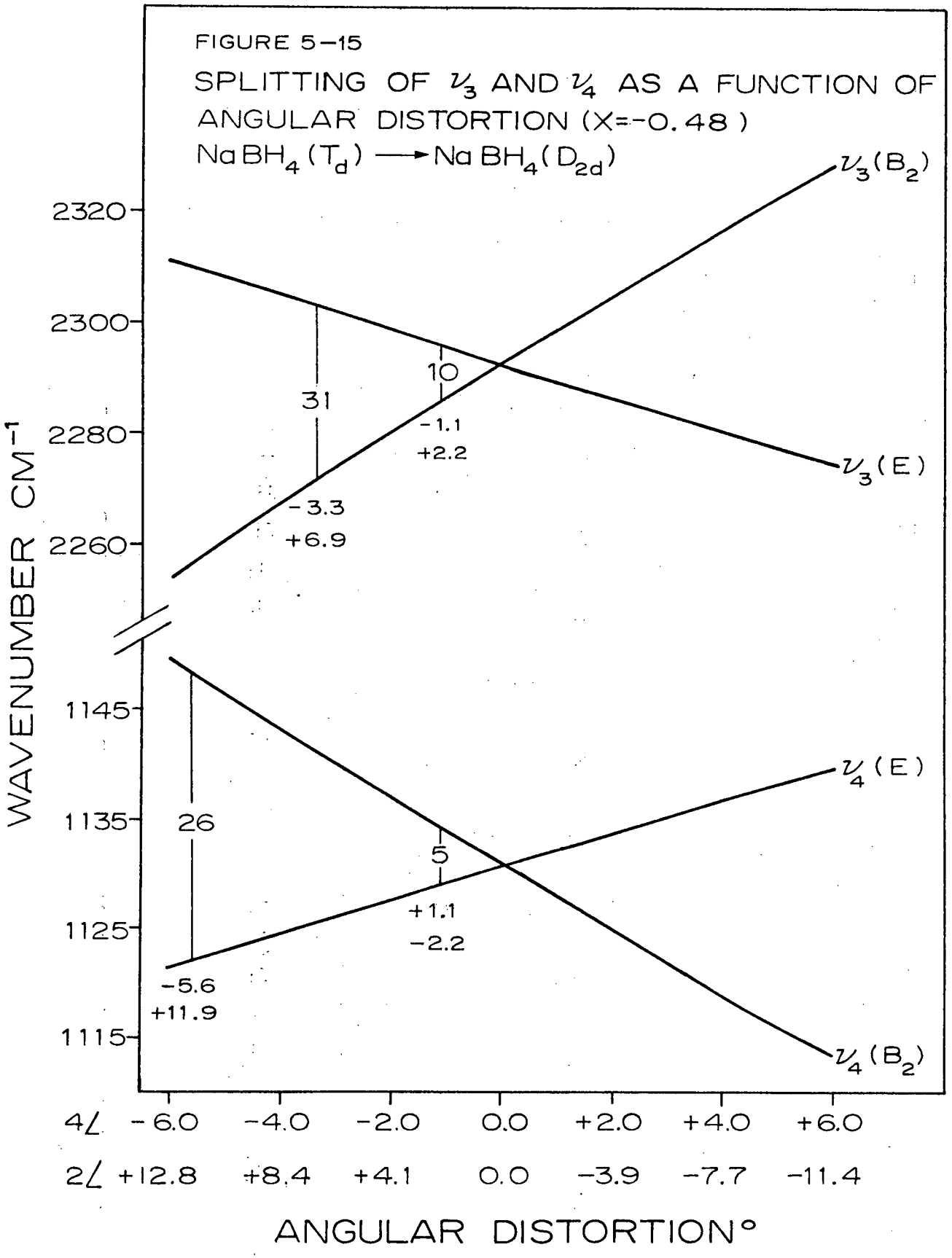

FIGURE 5-16

SPLITTING OF ν_2 AS A FUNCTION OF ANGULAR DISTORTION
$NaBH_4 (T_d) \longrightarrow NaBH_4 (D_{2d})$

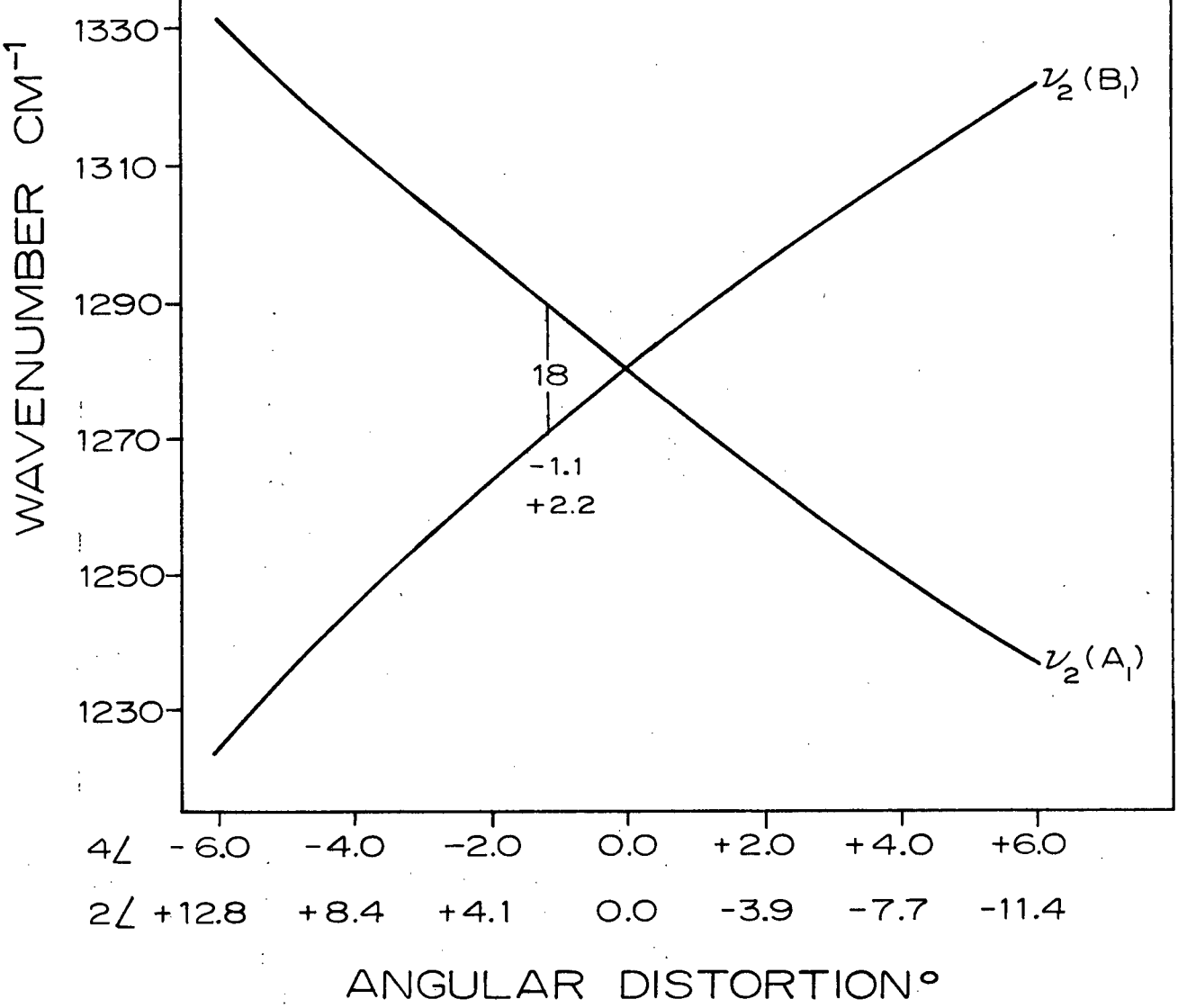

CHAPTER VI

CONCLUSION

It is apparent from the results of this work that for crystalline tetrahedral ions an average angular distortion of about two degrees from a tetrahedral configuration can result in splittings of the degenerate bending and stretching vibrations of up to some 30 cm^{-1}. This sensitivity of the spectrum to angular distortions associated with the absorbing or scattering molecule has important implications. For example, both N.M.R. (71) and X-ray (42) results for lithium borohydride have been reported as being compatible with a BH_4^- ion in the lattice which has an effective tetrahedral symmetry but the site group splitting observed in this work is clearly indicative of a distorted BH_4^- ion; i.e. the ν_2 splitting of 14 cm^{-1} observed in the spectrum of $LiBD_4$ compares with a ν_2 splitting of 12 cm^{-1} for $NaBD_4$(II) and thus indicates an average angular distortion of at least one or two degrees for the crystalline borohydride ion in the lithium borohydride lattice. Attempts to calculate the spectrum of the $XY_4(D_{2d})$ ($XY_4 = NH_4^+$, BH_4^-) ion using the F matrix associated with an $XY_4(T_d)$ ion and the G matrix associated with the same ion which has undergone a slight angular distortion to give the $XY_4(D_{2d})$ ion were successful in that the order of appearance in the spectrum of the B_2 and E components associated with the two F_2 vibrations of the $XY_4(T_d)$ ion were correctly predicted. This result indicates that similar calculations could be used in analysing the vibrational spectra of other systems providing the spectrum of an appropriate basis molecule is known.

Further interesting features of this work are the assignments associated with the second order spectrum of the ammounium halides which involve phonons with $\underline{K} \neq 0$. Of particular interest are the assignments involving ν_1 in combination with acoustical modes. These combinations indicate a valuable source of information about the phonon dispersions and also the densities of states associated with the acoustical phonons.

A most important area of interest with respect to this work is the effect of the phase transitions on the vibrational spectra of the various crystals studied. For the vibrational spectra of the ammonium halides it is found that the intensity versus temperature curves for the absorptions associated with the triply degenerate free NH_4^+ ion bending vibration give evidence of the two types of transitions which occur; i.e. the disorder-order transitions are characterized by gradual intensity changes and the order-order transitions are characterized by abrupt intensity changes. It is further found that the first order spectra of the ordered phases can be satisfactorily interpreted on the basis of fundamental modes predicted in the zero wavevector limit, but that for the lowest temperature disordered cubic phase this is no longer the case, since there is distinct evidence of densities of states with $\underline{K} \neq 0$ appearing in the first order spectrum. This situation is most pronounced for the triply degenerate bending mode. In this case the intensity dependence of the density of states with $\underline{K} \neq 0$ on the ordering process has satisfactorily been explained by Garland and Schumaker (28). Since Garland and Schumaker's work shows that the disorder associated with the phase II ammonium halide

lattice can appreciably contribute to the intensity of the fundamental vibrations via densities of states with $\underline{K} \neq 0$, it is very likely that this same situation also occurs in other disordered systems. An example would be the ices I_h and I_c which possess disorder (72) involving half-hydrogens. Whalley and Bertie (73) and Whalley and Labbé (74) have interpreted the spectrum of the ice I_h and I_c translatory modes by allowing for the presence of $\underline{K} \neq 0$ absorptions. The results for the ammonium halides which indicate the presence of $\underline{K} \neq 0$ absorptions in the spectrum of the internal fundamentals suggest that the band shape of the very broad ν_1/ν_3 ice absorptions may also be influenced by the presence of $\underline{K} \neq 0$ absorptions.

Turning now to the alkali metal borohydrides it is found that the spectroscopic results for sodium borohydride at 295°K and 10°K are compatible with a disorder-order phase transformation which involves a transition from a disordered cubic phase to an ordered tetragonal phase. In the case of potassium borohydride the low temperature spectrum is interpreted as indicating a low temperature ordered cubic phase which has a structure compatible with the space group T_d^2 and the spectrum recorded at 295°K is interpreted as indicating a cubic strucutre intermediate between the ordered T_d^2 structure and the disordered O_h^5 cubic structure of sodium borohydride. A neutron diffraction study of potassium borohydride should be able to determine if the T_d^2 structure is, indeed, correct. An X-ray determination of the lattice parameters of KBH_4 over the temperature interval 0-500°K would also be useful, since any phase transitions are very likely to be characterized by a discontinuous percent volume

change for the unit cell just as in the case of the ammonium halides. Such a study would be an important adjunct to the heat capacity data (37) and perhaps could more accurately fix the temperature at which the onset of the disorder-order transition begins.

There is one final item that will be commented on and this is the assignment $3\nu_R$ associated with the spectra of both sodium and lithium borohydride. In the spectrum of sodium borohydride this absorption appears with observable intensity only in the ordered tetragonal phase. This situation is comparable with that observed for the ammonium halides where lines associated with ν_R appearing in the second order spectra suffer a striking loss in intensity as a result of a transition from an ordered phase to a disordered phase. Also, with respect to the members of the series KBH_4(III), $NaBH_4$(II) and $LiBH_4$, where the BH_4^- ion suffers a progressive distortion from T_d to D_{2d} to C_s site symmetry, it is found that the intensity of $3\nu_R$ starting with zero observable intensity for KBH_4(II), is progressively enhanced. This is evidently a result of the fact that for the members of the series KBH_4(III), $NaBH_4$(II) and $LiBH_4$ there is a progressively greater number of possible components which can contribute to the intensity of $3\nu_R$. A recent communication (75) from T.C. Farrar indicates that neutron inelastic studies of the alkali metal borohydrides will be undertaken at the National Bureau of Standards Laboratories in the near future. These studies will, no doubt, place the modes of rotatory origin and in so doing will indicate if the assignments $3\nu_R$ are indeed correct.

REFERENCES

1. R. Ewald, Ann. Physik. 44, 1213 (1914)
2. H.A. Levy and S.W. Peterson, J. Am. Chem. Soc. 75, 1536 (1952)
3. G. Venkataraman, K. Usha Deniz, P.K. Iyengar, A.P. Roy and P.R. Vijayaraghavan, J. Phys. Chem. Solids 27, 1103 (1966)
4. R.C. Plumb and D.F. Hornig, J. Chem. Phys. 21, 366 (1952)
5. H.A. Levy and S.W. Peterson, Phys. Rev. 83, 1270 (1952)
6. H.A. Levy and S.W. Peterson, Phys. Rev. 86, 766 (1952)
7. A.G. Cole, Ph.D. Thesis, Massachusetts Institute of Technology, 1950
8. C.C. Stephenson, R.W. Blue and J.W. Stout, J. Chem. Phys. 21, 1046 (1952)
9. C.C. Stephenson and A.M. Karo, J. Chem. Phys. 48, 104 (1968)
10. J.A.A. Ketelaar, Nature 134, 250 (1934)
11. R.W.G. Wyckoff, Crystal Structures, Vol. 7, Interscience Publishers, Inc., New York, N.Y., 1963
12. V. Hovi, K. Paavola and O. Urvas, Ann. Acad. Sci. Fenn. VIA, No. 291 (1968)
13. V. Hovi and J. Lainio, Ann. Acad. Sci. Fenn. VIA, No. 215 (1966)
14. K. Mansikka and J. Pöyhönen, Ann. Acad. Sci. Fenn. VIA, No. 118 (1962)
15. J. Pöyhönen, K. Mansikka and K. Heiskánen, Ann. Acad. Sci. Fenn. VIA, No. 168 (1964
16. V. Hovi and M. Varteva, Phys. Kondens. Materie 3, 305 (1965)
17. J. Pöyhönen, Ann. Acad. Sci. Fenn. VIA, No. 58 (1960)

18. K. Clusius, A. Kruis and W. Schanzer, Z. Anorg. Alleg. Chemie 236, 24 (1938)

19. A. Smith and D. Tollenaar, Z. Physik. Chemie 52B, 222 (1942)

20. A. Smith, G.J. Mueller and F.A. Kroger, Z. Physik. Chemie 38B, 177 (1938)

21. R.C. Plumb and D.F. Hornig, J. Chem. Phys. 23, 947 (1955)

22. E.L. Wagner and D.F. Hornig, J. Chem. Phys. 18, 296 (1950)

23. E.L. Wagner and D.F. Hornig, J. Chem. Phys. 18, 305 (1950)

24. N.E. Schumaker, Ph.D. Thesis, Massachusetts Institute of Technology, 1968

25. L.F.H. Bovey, J. Opt. Soc. Am. 41, 836 (1951)

26. I.M. Lifshitz, Advan. Phys. 13, 483 (1964)

27. E. Whalley and J.E. Bertie, J. Chem. Phys. 46, 1264 (1967)

28. C.W. Garland and N.E. Schumaker, J. Phys. Chem. Solids 28, 799 (1967)

29. L. Couture-Mathieu and J.P. Mathieu, J. Chim. Phys. 49, 226 (1952)

30. R.S. Krishnan, Proc. Ind. Acad. Sci. A26, 432 (1947)

31. R.S. Krishnan, Proc. Ind. Acad. Sci. A27, 321 (1948)

32. C.J.H. Schutte, Spectrochim. Acta 16, 1054 (1960)

33. A.M. Soldate, J. Am. Chem. Soc. 69, 987 (1947)

34. E.R. Peterson, Ph.D. Thesis, Washington State University, 1964

35. W.H. Stockmayer and C.C. Stephenson, J. Chem. Phys. 21, 1311 (1953)

36. H.L. Johnston and N.C. Hallet, J. Am. Chem. Soc. 75, 1467 (1953)

37. G.T. Furukawa, M.L. Reilly and J.H. Piccirelli, J. Res. Nat. Bur. Soc. 68A, 651 (1964)

38. S.C. Abrahams and J. Kalnajs, J. Chem. Phys. 22, 434 (1954)

39. N.R. McQuaker, B.Sc. Thesis, University of British Columbia, 1965

40. P.T. Ford and H.M. Powell, Acta Cryst. 7, 604 (1954)

41. C.C. Stephenson, D.W. Rice and W.H. Stockmayer, J. Chem. Phys. 23. 1960 (1955)

42. P.M. Harris and E.P. Meibohm, J. Am. Chem. Soc. 69, 1231 (147)

43. N.C. Hallet and H.L. Johnston, J. Am. Chem. Soc. 75, 1496 (1953)

44. H.A. Levy and S.W. Peterson, J. Chem. Phys. 21, 366 (1952)

45. G.L. Carlson, Spectrochim. Acta 24A 1519 (1968)

46. E.B. Wilson, Jr., J.C. Decius and P.C. Cross, Molecular Vibrations, McGraw-Hill Book Co., Inc., New York, N.Y., 1955.

47. R.W. Green and K.B. Harvey, to be published

48. G. Herzberg, Infrared and Raman Spectra, D. Van Nostrand Co., Inc., Princeton, N.J., 1945

49. S. Bhagavantum and T. Venkataryudu, Theory of Groups and Its' Application to Physical Problems, Andhra University, Waltair, 1951

50. R. Loudon, Advan. Phys. 13, 423 (1964)

51. M. Born and K. Huang, Dynamical Theory of Crystal Lattices, Oxford University Press, 1954

52. W. Cochran and R.A. Cowley, J. Phys. Chem. Solids, 23, 447 (1962)

53. R.H. Lyddane, R.G. Sachs and E. Teller, Phys. Rev. 59, 673 (1941)

54. H.C. Teh, B.N. Brockhouse and G.A. Dewitt, Phys. Lett. 29A, 694 (1969)

55. C. Kittel, Introduction to Solid State Physics, John Wiley and Sons Inc., New York, N.Y., 1968

56. R. Loudon and F.A. Johnson, Proc. Roy. Soc. 281A, 275 (1964)

57. J.L. Birman, Phys. Rev. 131, 1489 (1963)

58. C.H. Perry and R.P. Lowndes, J. Chem. Phys. 51, 3648 (1969)

59. C. Haas and D.F. Hornig, J. Chem. Phys. 26, 707 (1957)

60. B. Szigeti, Trans. Faraday Soc. 45, 155 (1949)

61. J.R. Durig and D.J. Antion, J. Chem. Phys. 51, 3639 (1969)

62. I.M. Lifshitz, Zh. Eksp. Teor. Fiz. 12, 117 137 (1942)

63. T. Nagamiya, Proc. Phys. Math. Soc. Japan 24, 137 (1942); 25, 540 (1943)

64. H.S. Gutowsky, G.E. Pake and R. Bersohn, J. Chem. Phys. 22, 643 (1954)

65. D.E. Woessner and B.S. Snowden, J. Phys. Chem. 71, 952 (1967)

66. D.E. Woessner and B.S. Snowden, J. Chem. Phys. 47, 378 (1967)

67. L. Niemelä and E. Ylinen, Ann. Acad. Sci. Fenn. VIA, No. 307 (1969)

68. R.W. Green, private communication

69. R.C. Wade, ed. Sodium Borohydride, A Manual of Techniques, Metal Hydrides Inc., 1958

70. Tung Tsang and T.C. Farrar, J. Chem. Phys. 50, 3498 (1969)

71. G.W. Ossman and J.W. McGrath, J. Chem. Phys. 47, 5452 (1967)

72. R.W.G. Wyckoff, Crystal Structures, Vol. 1, Interscience Publishers, Inc., New York, N.Y., 1963

73. J.E. Bertie and E. Whalley, J. Chem. Phys. 46, 1271 (1967)

74. E. Whalley and H.J. Labbé, J. Chem. Phys. 51, 3120 (1969)

75. T.C. Farrar, private communication